Ph.D. degree in Systems Medicine (curriculum in Human Genetics) European School of Molecular Medicine (SEMM)

University of Milan and University of Naples "Federico II"

Settore disciplinare: MED/04

Phenotypic and molecular characterization of a novel p63α knock-out mouse model

Gloria Urciuoli

CEINGE, Naples

Matricola n. R12426

Supervisor: **Prof. Caterina Missero CEINGE, Naples**

Internal Supervisor: **Prof. Brunella Franco TIGEM, Naples**

External Supervisor: **Prof. Marja Mikkola, University of Helsinki**

Academic Year 2021-2022

TABLE OF CONTENTS

LIST OF ABBREVIATIONS

AER Apical Ectodermal Ridge

DBD DNA binding domain

FGF Fibroblast Growth Factor

K14-Cre;p63α-/- K14-Cre;p63αfl/fl

OD Oligomerization domain

p63α-/- pCX-NLS-Cre;p63αfl/fl

p63α+/+ p63αfl/fl

SAM Sterile alpha-motif

TA Transactivation domain

TID Transcriptional inhibitory domain

FIGURES INDEX

ABSTRACT

The transcription factor p63, a p53 gene family member, plays a crucial role in embryonic development of stratified epithelia where it can function either as an activator or a repressor. In the epidermis, p63 is a master regulator of epidermal gene expression and is crucial for cell proliferation, cell adhesion and stratification. Here we describe a new p63α-/- mouse model in which we delete exon 13 leading to the expression of the p63β isoform. Newborn p63α-/- mice die soon after birth and are characterised by cleft palate and digit malformations but exhibit normal skin. Our study indicates that p63α and p63β are not interchangeable in palate and limb development during embryogenesis, whereas expression of either one allows normal skin development, laying the foundation for a better understanding of the contribution of each p63 isoforms to mouse development. Compared to previously generated p63 knock-out mice, morphological and molecular impairment in p63α-/- model are mainly caused by alterations in the expression of genes involved in cell-cell and cell-matrix interactions. Taken together, these novel findings shed light on the function of both the alpha and the beta isoforms, and indicate that p63α is specifically required for limb and palate development, whereas p63β can replace p63α in skin development and in the adulthood.

1. INTRODUCTION

1.1 p63 and its multiple functions in cell biology

The first connection of the body with its environment occurs through the skin. Histologically the skin appears as a multilayered tissue that is constantly renewed by epidermal stem cells, present in the basal layer of the epidermis, that undergo an asymmetric division to ensure a niche of stemness for renewal and, at the same time, differentiated keratinocytes that will form middle and upper layers of the skin. These latter layers (in order spinous, granular and cornified) are those who create the barrier that on one hand protects the organism from external stress and, on the other, avoid unregulated water loss keeping skin healthy. The tetrameric transcription factor p63, encoded by the TP63 gene in humans and Trp63 in mice, is a master regulator of epidermis development and it regulates a large plethora of biological processes fundamental for skin development and maintenance (1, 2). p63 belongs to the p53-family of transcription factors, comprising p53, p63 and p73 and shares a high degree of sequence similarity with p53 and p73. Accordingly, the family members share some target genes and regulate in a similar or opposite fashion the cell cycle and apoptosis depending on the isoforms being expressed in specific tissues (3). However, each family member has also specific function, which in the case of p63 is to establish and maintain the identity of cells in stratified epithelia and to regulate the balance between cell proliferation and differentiation. p63 expression in stratified epithelia is dependent on a cis-regulatory enhancer which is bounded by p63 itself generating an auto-regulating positive loop (4, 5). It is encoded by a 16-exons gene, located on chromosome 3q27-29 in human and on chromosome 16qB1 in mouse, and it is transcribed in two main classes regulated by different promoters: one, called TA, that has an acidic N- terminal domain corresponding to the p53 transactivation domain (TA), a DNA-binding domain (DBD) and an oligomerization domain (OD); the other, called ΔN, is shorter and contains an alternative smaller N-terminal domain. Two additional TAp63 have been identified in human: a longer N-terminal called TA*p63α and another N-terminal GATp63α, which is expressed in male germ line (6). Both classes of proteins can have alternative C-terminal domains due to differential splicing events the 3' of the RNA, generating at least five different isoforms for each class (α, β, γ, δ and ε) (7, 8) (Figure 1).

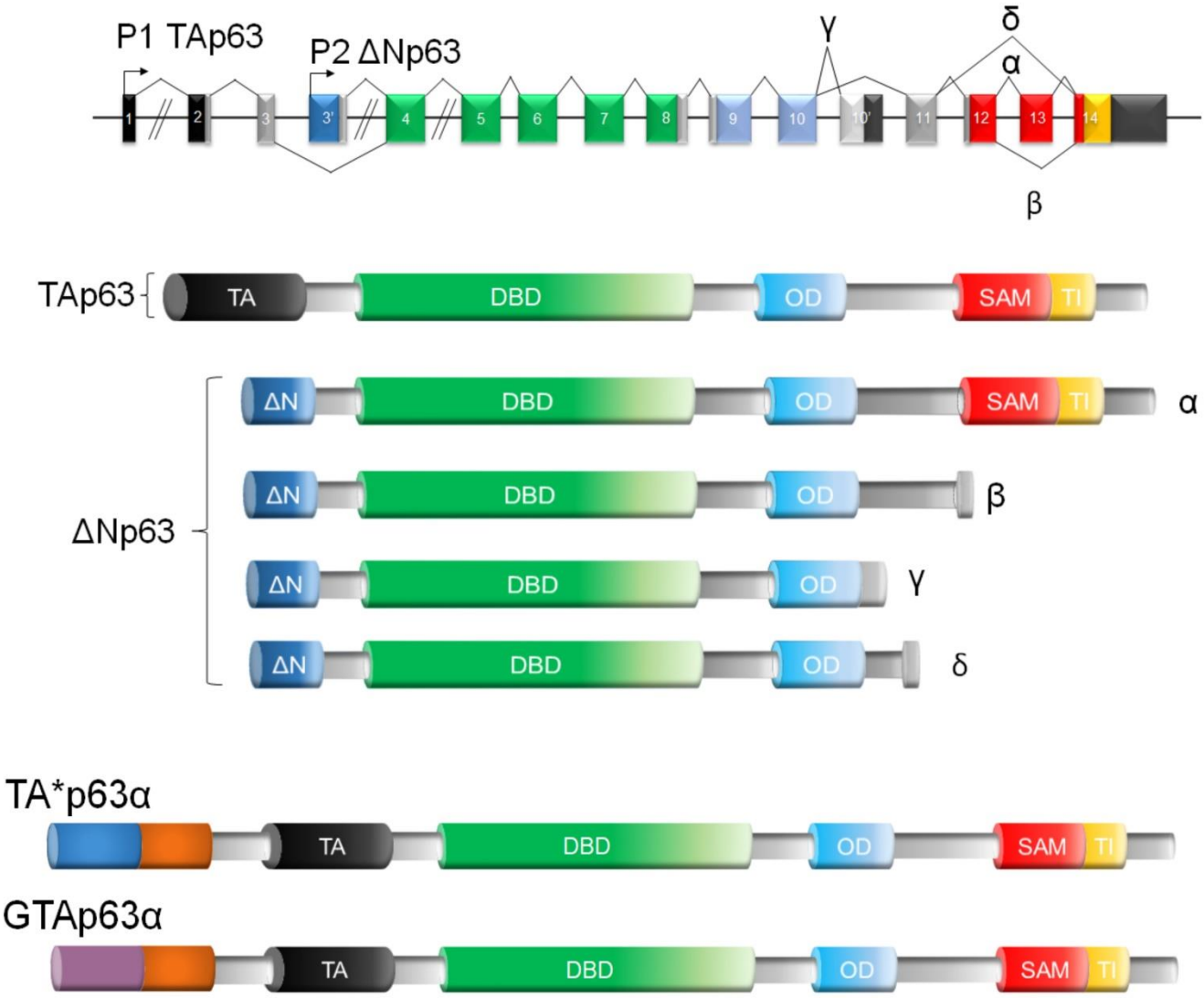

Figure 1: p63 gene and protein structure.

TAp63 gene structure with alternative splicing sites (Top panel). TAp63 protein and ΔNp63 different protein isoforms (Mid panels). Newly identified TA*p63 and GATp63 (Bottom panels). Transactivation domain (TA); DNA-binding domain (DBD); oligomerization domain (OD); Sterile alpha-motif (SAM); Trans-Inhibitory domain (TID).

Among the different protein isoforms, the p63α isoform is the longest and, include a Sterile alpha-motif (SAM) and a Trans-Inhibitory domain (TID) (9, 10). In particular, C-terminal TID domain is essential for the auto-inhibitory role exerted on the transactivation domain (TA) at the N-terminus inducing a conformational change in the p63 protein structure that leads to its closure and inactivation (11). This role is

crucial for preventing an improper activation of DNA damage response elicited by active TAp63 in oocytes (12, 13).

Each p63 variant exerts distinct roles that vary in different stages of embryonic development and in different tissues. During the early phases of embryonic development, p63 binds to regulatory elements of genes involved in neural cell fate. In the following stages of embryogenesis p63 acts as a pioneer factor, binding closed chromatin at ectodermal enhancers sites and allowing their opening to induce expression of genes that are involved in epidermal commitment and development (14, 15). The relevance of p63 in embryonic development has been primarily proven by knock-out experiments in mice. p63-null mice showed limb deficiency, underdeveloped skin with lack of an organized stratified epidermis, absence of skin-associated structure as hair-follicle, teeth and mammary glands, and cleft lip and palate. Mutant embryos had a single-layered epithelium at the distal tip of the outgrowing limb, indistinguishable from the surrounding ectoderm instead than forming the Apical Ectodermal Ridge (AER), a specialized stratified epithelium at the tip of the limb bud, essential for limb morphogenesis, and more specifically in proximodistal development. As a consequence, p63-null embryos at E15.5 lacked the hindlimbs and displayed truncated forelimbs with humerus and ulna, but without radius and autopod bones (16-19). Fibroblast growth factor 8 (FGF8) marks the AER and its deletion in early limb ectoderm causes a reduction in limb bud size and hypoplasia or aplasia of specific skeletal elements, such as aplasia of the radius and first digit with 100% penetrance in the forelimb, and often hypoplasia or absence of the humerus and second digit, with carpal bones variably fused and/or absent. Ectodermal Fgf8 signaling in turns is responsible for Fgf10 expression in the mesenchyme (20, 21). At E9.5-10, Fgf8 was weakly expressed in p63 mutant embryos as compared to wild-type, and its expression was lost at E10.5-11 (16). A similar defect in Msh homeobox 1 (Msx1) was observed, another marker of AER. In addition, both LIM homeobox transcription factor 1 beta (Lmx1b) and wingless-type MMTV integration site family, member 7A (Wnt7a) showed a more ventral spatial distribution than in the wild type, indicating a ventral shift in the dorsoventral boundary. In limb, p63 binds to enhancers that regulate Dlx5/6 genes expression. Human syndromes (such as Ectrodactyly–ectodermal dysplasia–cleft EEC and Split-Hand/Foot SHFM syndromes) in which p63 function is impaired, are characterized by a downregulation of Dlx5/6 expression levels. Moreover, a Dlx5/6 ablation in mice results in ectrodactyly as these genes are considered to be among the main actors of limb development (22, 23). It has been also demonstrated that the Fibroblast Growth Factor

Receptor 2, Fgfr2b, essential for Fgf10 and Fgf8 mesoderm-AER signaling loop in the outgrowing limb bud (24-26), is also a p63 direct target, as its expression is reduced in Ankyloblepharon-ectodermal defects-cleft lip/palate (AEC) syndrome in which p63 gene is mutated (27). It is known that among p63 different isoforms, ΔNp63γ and TAp63γ are the most abundantly expressed p63 proteins in the AER from early to later stages of limb development. In particular Fgfs signaling (specifically Fgf8 and Fgf4) are directly regulated by ΔNp63γ, whereas TAp63γ transactivates Jagged 2 (Jag2) which exerts a repressive role on limb formation (28). When p63 is specifically depleted in the AER, mutant mice lack the more distal limbal elements, the digits (28).

Regarding p63 function in palate development, it has been found that p63 directly regulates genes involved in epidermal and ectodermal development, cell adhesion and regulation of cell death and proliferation. Moreover, it plays a role in modulating Transforming growth factor beta (TGF-β) and WNT signaling pathways that remodel the cytoskeleton and are important in periderm formation that prevents premature fusion of opposite palatal shelves (29-32). In details, there is a large number of previously identified p63 target genes such as Interferon Regulatory Factor 6 (IRF6), IκB kinase α (CHUK or IKKα), Receptor-interacting serine-threonine kinase 4 (RIPK4), Stratifin (SFN), Grainyhead like transcription factor 3 (GRHL3) and Jagged 2 (JAG2) (30, 32-34) whose deletions lead to cleft palate similarly to p63-null mice as happen even for TGF3-β null mice (31). This fine regulation exerted by p63 in palate formation is essential to ensure the correct function of the periderm, a single layer of flattened cells that prevents premature and non-physiological fusion of juxtaposed epithelia in the whole embryo. Peridermal cells are high polarized as they express cell adhesion structures only in the basal portion of the cell, and this characteristic is essential for their proper function (31). When another p63 palatal target, Irf6, is mutated in mice cleft lip and palate occur (35, 36). Similarly to p63, Irf6 is required for the formation and maintenance of periderm (37).

In the epidermis, cells in which p63 has been depleted are only partially committed to the epidermal lineage and are unable to differentiate: the absence of a well-structured epidermis is amenable to a loss of proliferating cells in the basal layer of the ectodermal surfaces rather than alteration in differentiation (16, 17, 38-41). Indeed p63 exerts a different role in different developmental time windows: in tissues formation it induces cells to start stratification program, whereas in already formed skin, it is important for self-renewal of basal keratinocytes ensuring and maintaining their proliferative potential (42). When p63 is removed in mature tissues, the skin appears

hypoplastic, due to a reduction of proliferative capacity of p63-expressing cells, and exhibits defects in differentiation (43, 44). Moreover, when p63 is absent or non-functional in the epidermis this cause a detachment from the underling dermis due to the lack of cell-cell and cell-matrix junction proteins such as desmosome components (45, 46).

p63 has been found to act both as a transcriptional activator and as a repressor. The consensus sequence that makes p63 bind to regulatory elements with high affinity is composed of two different parts: the CA/TG motif that represents the core of the binding region and an AT-rich sequence that flank the core sequence at 5' and 3'. These flanking regions are the ones that mostly differ in the sequence from p53 consensus. Alterations in this motifs highly reduce the DNA binding ability of p63 (47).

Despite its similarity with p53, p63 is able to regulate a large number of p63 target genes that are not under p53 control (48). p63 operates as a pioneer factor, binding closed chromatin at enhancer regulatory elements and inducing chromatin opening to allow the expression of genes involved in epidermal commitment and development (14, 49). It is able to induce these changing in the chromatin architecture coordinating its function with CTCF, a genome organizer that delimits topologically associated domain (TAD) borders, defining the three-dimensional space of chromatin loops that put in closed contact regulatory elements such as enhancers with corresponding promoters (50). Furthermore, p63 has been found to be directly regulated by WNT/β-catenin pathway thus contributing to the regulation of self-renewal, differentiation, migration and apoptosis of epithelial cells (51). p63 has been involved in Notch signaling pathways by positively regulating Notch1 and Jag2, and therefore promoting the early steps of epidermal differentiation (19, 39, 52, 53). In turn Notch limits p63 expression in the differentiated upper layers contributing to determine the balance between basal cells self-renewal and their commitment to differentiation (53-56). Moreover, p63 induces cell cycle progression with different mechanisms, including repression of p53 target genes such as the microRNA miR34a and miR34b (57), and repression of CDKN1A, encoding for the cyclin-dependent kinase inhibitor $p21^{Cip1/Waf1}$ (58-60). p63 provides a stemness potential to cells by directly regulating a complex network of genes involved in differentiation, as already discussed Notch, WNT and TGF-β pathways, or in proliferation being part to the FGFs signaling through regulation of the Fibroblast growth factor receptor 2 (Fgfr2b). p63 can bind also to genes important for apoptosis and for the adhesion program. All this fine

regulation of cellular processes allows p63 to control the number of progenitor cells available in a determined tissue (27, 46, 56, 61).

1.2 TAp63 and ΔNp63 specific contribution

TA and ΔNp63 proteins, encoded by alternative transcripts, have different functions and localization, both in human and murine tissues. ΔN isoforms are the most abundant variants detected in regenerative, stratified squamous and transitional epithelia, and in primary keratinocytes. Their expression is more prominent in the basal progenitor cells where they promote clonogenicity and cell proliferation (8, 56, 62). ΔNp63α is the predominantly isoform found in ectodermal tissues, in skin and its appendages, and in thymus (63, 64). RNA-seq studies performed at E18.5, P0, P3 and 10 week-old murine skin show that among ΔNp63 isoforms, the ΔNp63α is the most abundant p63 protein detected, while lower levels of expression are observed for ΔNp63β and γ (65, 66). On the other hand, TA isoforms are expressed at very low levels in most tissues, but are required for female germ line cells to control DNA damage in oocytes (12, 67-69), in particular the TAp63α is important in regulating the number of oocytes produced as its deletion, with the induction of TAp63β, leads to female infertility in mice (12, 68). As previously indicated, the GATp63 protein has been detected in male germ line (70) and, similarly to TAp63, takes care of germ line quality control (6). In these tissues TAp63 proteins are all able to induce apoptosis, through the upregulation of death receptors, and in particular TAp63β shows stronger induction of apoptosis then TAp63α (71). Transactivation domains in the TAp63 are the N-terminal TAD (Activation Domain) and the Proline-rich domain present in the α, β and γ isoforms, whereas the C-terminus domains are not involved in the transactivation of target genes (72). TAp63α has an auto-regulatory effect on its own transactivation that seems to be important to keep itself inactive during cell cycle arrest, after oogenesis until ovulation in the female germ line, monitoring their essential genetic stability (11, 12). Moreover the TAp63 transcripts are important in skin aging and in the maintenance of stem cells potential in adult tissues, as mice knocked out for TAp63 aged prematurely and mutant cells show genomic instability and accumulate DNA damage (44, 73).

The N-terminal truncated p63 isoforms, are also involved in transcriptional regulation: ΔNp63 is able to bind and regulate p53 and p73 target genes and, directly, genes involved in metabolism, signaling pathways, cell cycle, proliferation and death, and in

cell adhesion (61, 74). During epidermal development and early in ectodermal differentiation, ΔNp63 isoforms are the main proteins expressed. They are required to commit ES cells to an epithelial cell fate enabling these cells to differentiate in squamous stratified tissues that express typical basal keratins (Krt5 and Krt14) (75, 76). The ΔNp63 promoter is found in an open chromatin conformation in developing epidermis and in keratinocytes, and p63 is able to positively regulate its own expression by binding to an enhancer element in intron 4 (77).

Mice depleted for ΔNp63 isoforms show alterations in limb development exhibiting absence of hindlimbs and truncated forelimbs similar to the p63-null mice, however they differ from these latter in the skin phenotype: ΔNp63-null mice show a disorganized and patched epidermis that is poorly stratified but is still able to terminally differentiate even if prematurely (78). Specific target genes of ΔNp63 are those whose function is part of the growing and differentiation process of the cell (79): extracellular matrix and cell-adhesion components, which ensure integrity of the interface between epidermis and dermis, as well as genes important in the formation of the spinous layer thus sustaining the epidermal terminal differentiation (80, 81). Among ΔNp63 variants, ΔNp63α is the most abundant in stratified epithelia and exerts a fundamental role in the asymmetric division of keratinocytes belonging to multilayered ectodermal tissues. Moreover, cell migration, proliferation and differentiation of corneal limbal epithelial cells has been found to be dependent on the expression of ΔNp63α that is induced by Keratinocytes growth factor (KGF) through the p38 pathway (82). ΔNp63α is also involved in the regulation of the cell cycle (57): it is induced in mitotic cells while its expression decreases during mitotic exit controlling premature release from mitosis (83). When ΔNp63α and β are depleted, $p21^{Cip1/Waf}$ levels increase and hypoproliferation of the epidermis is observed (60).

The p63α protein isoforms are the longest p63 isoforms, with the C-terminal region that includes all terminal exons and contains a poorly characterized sterile-α-motif (SAM). This α-isoform specific domain is organized in alpha-helices, typical of Transcription Factors (TFs) both activators or repressors, allowing protein-protein interactions and is essential to form homo- and heterodimers (84). In detail, p63 SAM domain is composed of five-helix bundle and it is codified by exon 13 and a small portion of exon 14 of the TP63 gene, and a post-SAM (PS) domain codified by exon 14. These two domains are absent in the β and other isoforms (C-terminal truncated) (85). In p63 C-terminus ablated mice, in which α and β isoforms are both knocked out, the skin is present but appears hypoplastic with ectodermal malformation and with a

reduced capacity of proliferation of the epidermal progenitor cells. Similar to p63-null mice, these mice die soon after birth but, differently from previous mouse models, they are mainly characterized by cleft palate. Moreover, these mutant mice show presence of both hindlimb and forelimb proximal bones while they lack more distal structures (as radius). When digits are present in some mutants, generally they are affected by syndactyly or ectrodactyly (86).

Table 1. Summary of p63 mutant mice

p63 mutant mouse	**Phenotype**	**References**
p63 -/- (p63-null mice)	• Absent or truncated limbs • Cleft lip and palate • Severely malformed skin and lack of ectodermal derivatives	Yang et al. 1999 (16) Mills et al. 1999 (17)
Msx2-Cre;p63Δ/fl (AER-specific p63 depletion)	• Hypoplasia of limbal autopod and distal zeugopod, absence of digits	Kawata et al. 2017 (28)
TAp63 knockout mice	• Normal embryonic development • No skin abnormalities • Reduced life span • Defective control of oocyte DNA damage	Suh et al. 2006 (12) Su et al. 2009 (73)
ΔNp63-null	• Absence of hindlimbs and truncated forelimbs	Romano et al. 2012 (78)

	• Disorganized and poorly stratified epidermis	
p63C-/- (Depletion of α and β isoforms)	• Lack of the radius and syndactyly or ectrodactyly of forelimbs; presence of only femur at hindlimbs • Cleft of secondary palate • Hypoplastic and thin epidermis with lack of hair follicles	Suzuki et al. 2015 (86)

1.3 p63 related human syndromes

In humans, mutations in the TP63 gene are dominant and lead to a variety of genetic syndromes which overall characteristics are ectodermal dysplasia, cleft lip/palate and limb malformations. These syndromes are distinguished by some specific features that correspond to mutations in specific protein domains with a genotype-phenotype correlation: the phenotype of each disorder is specific to the protein domain in which the mutation falls (87-89). Ectrodactyly ectodermal dysplasia-cleft syndrome 3 (EEC3, MIM: 604292) causing mutations are mainly clustered in the p63 DBD, impairing the protein ability to bind the DNA and regulate gene expression (90). EEC mutant keratinocytes show defects in epidermal differentiation and in the general chromatin landscape that is altered compared to healthy cells (91). EEC mutations falling in the DBD, cause a Disorder-to-Order transition in the protein structure that is reflected in an altered conformational behavior of its adjacent residues that generally blocks its binding to the genome while the protein still retains its normal nuclear localization. This structural alteration has a dominant-negative effect on the functionality of wild type proteins (88, 92-95). Limb-mammary syndrome (LMS, MIM: 603543) shows similar EEC phenotype, except for the ectodermal alterations

that are milder in LMS than in EEC patients. LMS is caused by frameshift mutations that alter the N-terminal or C-terminal sequence of p63 (87, 88). In Split hand/foot malformation-4 (SHFM4, MIM: 605289), patients are affected by limb malformations but lack a skin phenotype. SHFM is also associated with Dlx5 and Dlx6 gene mutations, whereas only in few cases the non-syndromic defect is caused by missense or nonsense mutations in the p63 gene that disrupts its DNA binding ability. In this case the p63 protein is no more able to induce gene transcription resulting in a failure in the stratification of the AER and the subsequent development of the limb, an alteration which occurs also in EEC (23, 88). Missense mutations clustered in the SAM and TID domains are responsible for Ankyloblepharon ectodermal defects-cleft lip/palate (AEC) (OMIM 106260) and for Rapp-Hodgkin Ectodermal Dysplasia (RHS) (OMIM 129400) syndromes (96). RHS phenotype is macroscopically similar to the EEC and AEC ones with patients affected by ectodermal dysplasia and hyperkeratosis of the palm but lack skin erosion. Microscopically they are characterized by cell-cell detachment in keratinocytes of the upper layers of the epidermis (97, 98). AEC patients are affected by several impairments such as: congenital ectodermal dysplasia, alopecia, scalp infections, dystrophic nails, hypodontia, Ankyloblepharon and cleft lip and/or cleft palate. Skin defects are likely due to an alteration of cell-cell junction complex, such as hemi-desmosomes, and to cell-cell detachment due to reduce expression of desmosome components (45, 46). Some missense mutations in the SAM domain led to the substitution of important amino acids that are predicted to be involved in p63 protein-protein interactions (94). To study the role of p63 in the etiogenesis of AEC syndrome, a mouse model has been generated. AEC mutant mice are affected by severe skin erosions, similarly to human patients, that result from abnormality in the basal membrane and alterations in the differentiation and proliferation programs of the suprabasal cells that impair general skin integrity. p63 is not transcriptionally active even in heterozygosity (45, 99, 100). Its impaired function leads to a downregulation of FGFs signaling thus reducing the epidermis progenitor cells capacity to proliferate and preserve the stem cell compartment of the skin (27). In molecular details, AEC associated mutations led to a destabilization of the thermodynamic 3D structure of p63 protein that exposes hydrophobic residues making the protein prone to the aggregation. The protein aggregates, present also in keratinocytes of the KI mouse model of AEC, are likely to trap other proteins including p63 wild-type itself, impairing its ability to bind the DNA and/or transactivate target genes, thus acting as a dominant negative on wild type p63 function (100). AEC mutants are still able to bind the DNA (95) but are not able to

transactivate target promoters such as the CDKN1A one (9). It is possible that alterations in this domain impair ΔNp63α interactions with a wide range of proteins involved in many roles such as chaperones, heterogeneous ribonucleoproteins acting in metabolism and transport of mRNAs. To date symptoms in young patients are treated with generic wound care and novel targeted treatment are highly desirable.

2. MATERIALS & METHODS

2.1 Generation of the conditional knock-out p63α mutant mice

The exon 13 of p63 gene, flanked by two Lox sites, was inserted into the p63 locus in E14TG2a (129/Ola) ES cells by homologous recombination. Twenty-four hours after electroporation ES cells were selected with 100 μg/ml G418 (Thermo Fisher Scientific) for 7 days. Neo-resistant ES clones were screened at 5' and 3' for the correct insertion in the p63 endogenous locus by PCR analysis using the TaKaRa LA Taq® DNA Polymerase (Clontech) with an oligonucleotide annealing in the neomycin cassette and in the genomic DNA (5'Arm Forward and Reverse; 3'Arm Forward and Reverse). The homologous recombination event was also confirmed by Southern blotting. Genomic DNA was digested with HindIII and analyzed with a probe located inside the neomycin cassette. An ES positive clone was injected into C57BL/6 blastocysts and the obtained chimeric mice were tested for germline transmission by breeding with C57BL/6 females. Offspring was genotyped for germline transmission of the p63 wild-type and Exon13-flox allele by PCR using tail genomic DNA and specific primers (p63cond-ko screen F, R1 and R2). The neomycin cassette was removed by breeding the first generation of heterozygous mice with transgenic mice carrying the Flip recombinase. Mouse genotyping was performed by PCR with the p63cond-ko screen F, R1 and R2 and CMV-Cre oligonucleotide primers.

Primers	**Sequence**
5'arm	Fw: GCTGCTGCTTTGTGGATGTGTGGTTT RV: ACTTTCTCGGCAGGAGCAAGGTGAGA
3' arm	Fw: ATGGCTTCTGAGGCGGAAAGAACCAG Rv: AAGCCCCATGAAATGACACGACAGAAT
P63condkoscreen	Fw: ATCAGGCAGGAGAGCAGAAA Fw2: GTCACAGGCCAGCATTACAAAG Rv2: AGGATCAGGTTGCTGCAAGT
CMV-Cre	Fw: GGCAGTAAAAACTATCCAGCAACA Rv: TAACATTCTCCCACCGTCAGTA

2.2 Primary keratinocytes, cell cultures and viral preparations

Newborn mice were placed in petri dishes with ice and inserted in an ice bucket. After 30-45' newborn mice were washed twice with 70% ethanol and twice with milliQ water to remove ethanol completely. Using sterile scissor and tweezers, mice tails and limbs were amputated; tails were used for genotyping, then skin was carefully separated from the rest of the viscera and flattened in an empty 6 well dish with the dermis facing down. Two ml of Dispase solution (0.5mg Dispase- GIBCO, Na-bicarbonate 0.75%, Hepes 10mM, Antibiotic-Antimycotic in HBSS) were added to each well and incubated o/n at 4 °C. The next day epidermis was separated from the dermis and placed in a 100mm Petri dish in 2ml (for each epidermis) of Trypsin 0.0625% -EDTA 1mM minced with tweezers and scissors for max 3-5' until it was reduced in very small fragments. The solution was then incubated at 37°C for 5-8 minutes. Trypsin solution was then inactivated with DMEM+10% FBS and filtered by applying it to cell strainer (BD Falcon 352350, 70µm) in order to remove floating particles. Alternatively, after dermis separation, the epidermis was placed on 500 µL of Accutase (EuroClone ECB30560) with the basal layer downward and incubated for 20 minutes at room temperature. After incubation the epidermis was gently shacked in 2 mL of fresh 4% of chelated serum in LCM medium supplemented with 2.5 ng/mL of human recombinant EGF (Corning® Epidermal Growth Factor 354052) to separate single cells, then sequential washes of 2mL each of medium were performed to remove residual cells detached reaching 6-8mL of final volume. In both dissociation methods cells were subsequently span for 5 minutes at 1000 rpm and were plated onto collagen coated (HBSS with 10mg BSA, 20mM HEPES pH6.5, 300ug/mL PureCol ultra-pure) dishes ($2x10^6$ cells/ml) and incubated at 34°C, 8% CO_2.

HEK293T, used to produce lenti- and retrovirus, were grown in Dulbecco's Modified Eagle Medium (DMEM) and 10% FBS (Euroclone).

Human Fibroblast (HDF) and BJ Human Fibroblast (BJ-HDF) were kindly provided by Dr. Davide Cacchiarelli and were cultured in DMEM/ F12 supplied with 10% FBS.

HEK293T, HDF and BJ-HDF cell lines were growth at 37°C in a humidified atmosphere of 5% (vol/vol) of CO_2 in air.

2.3 Retroviral preparation

High-titer retroviruses were produced in HEK293T cells by transient co-transfection of pBABE p63 constructs or pMXs-KLF4 plasmid and amphotropic viral envelope plasmid (pAmpho) in the presence of 30ul of Lipofectamine 2000 (Thermo Fisher Scientific), according to the manufacturer's instructions. Cell supernatants containing the retroviruses were collected 48 hours after transfection, then fresh medium was added and collected again 72 hours after transfection. Finally, the retrovirus preparation was filtered using 0.45μm filters to remove cell debris.

2.4 Lentiviral preparation and cell infection

HEK293T cells were co-transfected with viral packaging plasmids (1.5ug of Plp1, 1.5ug of Plp2 and 1ug of Plp-Vsvg) and 2ug our plasmid of interest using Lipofectamine2000 (Thermo Fisher Scientific) and incubated O/N at 37°C. After 48 hours virus particles were collected. HDF-BJ cells were infected with lentivirus for 2 hours. Two days after infection, cells were selected with 1 μg/ml of puromycin for 3 days.

2.5 Adenoviral infection

Mouse primary keratinocytes were infected after 4-5 days of plating, when they reached confluence and differentiated. Adenovirus carrying the GFP or the Cre-recombinase (provided by OKAIROS srl, CEINGE) at MOI 100 were diluted in 250μL, for 12-well, of non-supplemented LCM. After 2 hours of infection, supplemented medium (4% of chelex serum and 2.5 ng/mL of hEGF) was added to plates and cells were incubated O/N at 34°C with 8% of CO_2.

2.6 RNA extraction, RT-PCR and Real-time RT-PCR

Total RNA was extracted from HDF, mouse primary keratinocytes or mouse epidermis using TRIZOL reagent (Invitrogen). cDNA was synthesized using SuperScript Vilo (Invitrogen). Two-step real-time reverse transcription RT-PCR was performed using the SYBR Green PCR master mix in an ABI PRISM 7500 (Applied Biosystems). Levels of the target genes were quantified using specific oligonucleotide primers and normalized for Actin (ß-actin) for mouse samples and for RPLP0 for

human cells. Total RNA used to perform RNA-seq on E12.5 hindlimbs and E14.5 palates was extracted following the Quick-RNA MicroPrep Kit protocol (R1050 Zymo Research) while total RNA from P2 mKer and from E18.5 epidermis was extracted using the RNeasy Plus Micro Kit (Qiagen).

Target gene	**Real-Time Oligos sequence**
Total Trp63	Fw: AGCACCAGCACCTACTTCAGAAAC Rv: CATTCCTGAAGCAGGCTGAAAG
Trp63 β	Fw: CATTGTCAGGATTTGGCAAGTC Rv: GCTGCCTGTGGTCCAGGAT
Trp63α	Fw: ACTCTCCATGCCCTCCAC Rv: GAGCAGCCCAACCTTGCT
Actin	Fw: CTAAGGCCAACCGTGAAAAGAT Rv: GCCTGGATGGCTACGTACATG
DSP	Fw: TGCGAGCAGAGCTCATCGT Rv: CGAGTCAGTTGTATTCCATCTCCAT
K14	Fw: GGATGACTTCCGCACCAAGT Rv: TCCACACTCATGCGCAGGT
IRF6	Fw: ACCAAGTCCCCAGGAGCTCT Rv: TGAAGGCAGGAAGAAGACAGC
RPLP0	Fw: GACGGATTACACCTTCCCACTT Rv: GGCAGATGGATCAGCCAAGA

On total RNA, extracted from E18.5 epidermis, was used to perform RT-PCR to detect p63β and p63δ isoforms using specific β and δ primers. RT-PCR products were run on a 1.5% of agarose gel. DNA marker: GeneRuler 1Kb DNA ladder (Thermo Scientific).

Target Gene	**RT-PCR Oligos sequence**
Trp63β	Fw: CTGCAGCATTGTCAGGATTTGG Rv: AATCATTCCACTCGTCACGGG
Trp63δ	Fw: GGAGCCAACAGATTTGGCAAGTC Rv: CGACGAGAATCCATGTCAAAGTT

2.7 Sanger sequencing

DNA of RT-PCR product from p63β amplification band was extracted from agarose gel using QIAquick Gel Extraction Kit (28704 Qiagen) and templates were sequenced by the DNA Lab facility at CEINGE.

2.8 Western blot

For immunoblotting of cultured human and mouse cells, they were lysed in sample buffer (10% glycerol, 0.01% Bromophenol Blue, 0.0625 M Tris-HCl pH 6.8, 3% SDS, 5% ßmercaptoethanol) supplemented with protease and phosphatase inhibitors. For immunoblotting of epidermal extracts, isolated epidermis was fast frozen in dry ice and then homogenized with a tissue lyser in SDS lysis buffer (0.125M Tris pH6.8, 6%SDS) supplemented with phosphatase and protease inhibitors. Proteins were run on a denaturing SDS-PAGE gel and subsequently transferred to Immobilon-P transfer membranes (Millipore) probed with primary antibodies and detected by chemiluminescence (ECL, GE Healthcare Life Sciences; Clarity- Biorad). Antibodies used for immunoblotting were: p63tot (EPR570, Abcam); β-actin (sc69879, Santa Cruz Biotechnology); anti-Keratin 6A (PRB-169P Biolegend); anti-Keratin 14 (PRB-155P Biolegend); anti-Keratin 15 (a gift from Langbein); anti-Vinculin (Sigma V4505). Secondary antibodies used were: goat anti-Mouse IgG HRP Conjugate (ImmunoReagents GtxMu-003-DHRPX); mouse anti-Rabbit igG HRP (Cell Signaling BK7074S); anti-Guinea Pig (JIR 106-001-003); donkey anti-Goat IgG-HRP (Santa Cruz sc-2020).

2.9 BrdU assay

E13.5 pregnant mice were peritoneally injected with 1.5mg of 5-bromo-2′-deoxy-uridine (BrdU 000103 Life Technologies)/ 25gr of weight per female for 2 hours. Then mice were sacrificed to collect embryos for subsequent histological analysis performed in collaboration with Jill Dixon laboratory (Faculty of Biology, Medicine & Health, Manchester Academic Health Sciences Centre, University of Manchester, UK).

2.10 Histology and Immunostaining

Dorsal skin, embryo palates and whole embryo were dissected, fixed in 4% paraformaldehyde (PFA) and embedded in paraffin. 7 and 5 μm sections were stained with Hematoxylin and Eosin (H&E), Hematoxylin and Alcian Blue, for mouse heads, or used for immunofluorescence according to standard methods. Immunofluorescence on cells: cells were fixed in 4% paraformaldehyde for 30 min at 37° C and permeabilized with 0.1% Triton PBS for one hour at room temperature. Cells were then incubated at room temperature for two hours with primary antibodies in 0.1% triton 100X and 5% FBS in PBS. For paraffin sections, permeabilization for antigen retrieval was performed by microwaving samples in 0.01 M citrate buffer at pH 6.0.

Fluorescent signals were monitored under a Zeiss Axioskop2 plus image microscope and a Zeiss Apotome 2.0 provided by the Advanced Light Microscopy (ALM) Facility at CEINGE. Macroscopic photos obtained using a stereomicroscope (Leica M205FA) provided by the Advanced Light Microscopy (ALM) Facility at CEINGE.

The following antibodies were used: p63tot (4a4 Abcam and EPR5701 Abcam); p63α (ab53093, Abcam); anti-Keratin 6A (PRB-169P Biolegend); anti-Keratin 14 (PRB-155P Biolegend); anti-Keratin 15 (a gift from Lutz Langbein, DKFZ, Heidelberg); anti-Keratin 5 (PRB-160P, Biolegend); E-cadherin (610181 BD, Bioscience), anti-Ki67 (16667 Abcam); anti-BrdU, anti-Krt17, anti-p63, anti-Krt14 immunofluorescence on palates were performed in collaboration with Jill Dixon laboratory. pH3 and TUNEL staining on limb bud sections were performed in collaboration with Maria A. Ros laboratory.

The following secondary antibodies were used for immunofluorescence staining: Alexa Fluor ® 488 goat anti-mouse (Invitrogen); Alexa Fluor ® 594 goat anti-rabbit (Invitrogen); Alexa Fluor ® 488 goat anti-rabbit; Biotinylated anti-mouse IgG (BA-2000, Vector Laboratories); Biotinylated anti-rabbit IgG (BA-1000, Vector Laboratories); Streptavidin Cy3-conjugate (Sigma S-6402).

2.11 Alizarin and Alcian staining

For skeletal staining embryos were eviscerated, limbs were dissected, and the skin removed, then limbs were fixed in 90% ethanol for 7 days and then in 100% acetone for additional 2 days at room temperature. Specimens were incubated in Alcian Blue Solution (2mg of Alcian Blue dissolved in 80% ethanol and 20% Glacial Acetic Acid

solution) for 3 days at room temperature. Limbs were subsequently rehydrated by immersing them sequentially in 70% Ethanol, 40% Ethanol and 15% Ethanol for 3 hours and then rinsed in water. Specimens were kept in 1% KOH for 4 hours at room temperature, then incubated in Alizarin Red S Solution (1mg of Alizarin Red S dissolved in 1% KOH solution) for 2 days. After bones staining, specimens were incubated in 1% KOH Solution for 3 hours for several times followed by clearing in a series of 0.8% KOH/20% glycerol,0.5% KOH/50% glycerol and 0.2% KOH/80% glycerol for 3-5 days each. After complete clearing, specimens were stored in 100% glycerol.

2.12 Macroscopic pictures

Macroscopic photos were obtained using a stereomicroscope (Leica M205FA).

2.13 RNA-seq and bioinformatics analysis

Libraries were prepared, converted to cDNA, and sequenced by using the Illumina HiSeq2000 next generation sequencer at TIGEM. Raw data were processed and filtered for average count >5 and FDR> 0.05 or FDR>0.01. Metascape and David tools were used to perform Gene Ontology analysis.

2.14 Wound Healing Assay

General anesthesia of mice was induced by 5% Isoflurane in 100% O_2 and subsequently maintained using 3% Isoflurane. The back skin was shaved, thoroughly cleaned, and disinfected prior the surgery using antibacterial soap solution and 75% EtOH solution. Two circular full-thickness excisional wounds of 6 mm of diameter were generated on the lower back skin of each animal, one on each side of the dorsal skin, 1 cm from the back midline and roughly 2 cm apart from each other. At the day of sample collection (day 3 and day 7 from wound), animals were euthanized using CO_2 and skin samples were excised post-mortem, fixed in a buffered 4% formaldehyde solution at 4 °C overnight for samples to be embedded in paraffin. Paraffin blocks were processed into sections of 7 μm. Morphometric analysis was performed on 7 μm sections obtained from the middle of D3 and D7 wounds and stained with H&E. Measurements of wound closure, distance between wound border HFs (contraction

assessment), and length of newly formed wound epithelium (re-epithelialization) were analyzed using ImageJ. Wound area was determined for each wound by quantification of wound area based on pictures taken from day 0 to day 10 post surgery. The area at different time points after wounding were then reported to the original area value at day 0 for each wound.

2.15 Conversion assay of HDF-BJ to iKCs with retrovirus

100.000 neonatal nHDF or HDF-BJ were plated in 12 well plate and co-infected, the day after plating, with two retroviruses carrying p63 and KLF4 (101) in the presence of 8 μg/mL Polybrene. Cells were incubated in the retrovirus mix for 2 hr at 37°C. The next day a second infection was performed. Cells were then passed into one 6-well plate and one 12-well plate. Infected cells were selected using 2 μg/ml puromycin 48 hr after the second infection, changing medium supplemented with puromycin every other day, until the uninfected control cells died (48 hr after the start of selection). Cells were changed with supplemented DMEM medium every day for a week and then on alternate days. HDF-to-iKCs conversion was stopped 15 days after the first infection and assessed by RT-qPCR and Western Blot and IF analysis.

2.16 Plasmids

Human ΔNP63α, ΔNP63β were cloned, by Christian Osterburg in the laboratory of V. Dötsch of the Goethe University of Frankfurt, in pBABE vector on the BamHI site to perform conversion assay from HDF-BJ to iKC with retrovirus.

2.17 Skin permeability assay

Skin permeability of embryos at E17.5 and E18.5 was investigated by toluidine blue dye penetration assay. Briefly, small pieces of the embryo tails were cut for genotyping. Embryos were then gently rinsed and rehydrated in PBS and immersed in 25%, 50%, 75%, and 100% methanol for 2 minute each step. After PBS, embryos were placed in filtered 0.1% for E18.5 and 0.0125% for E17.5 toluidine blue solution for 10 minutes at 4 °C. After staining, pups were rinsed with PBS and photographed using a stereomicroscope (Leica M205FA). The TEWL was measured on back skin at E18.5

and back and ventral skin at E17.5 with a Tewameter (TM NANO; Courage and Khazaka).

2.18 ChIP-seq and bioinformatic analysis

For ChIP-seq analysis, 2 million mouse keratinocytes isolated from P0 epidermis of two mutant and two wild-type littermate were cross-linked with 1% formaldehyde for 10 min at 37°C, washed in PBS and resuspended in SDS lysis buffer (50 mM Tris-HCl at pH 8.1, 10 mM EDTA, 1% SDS) and sonicated (BioRuptor High Power 60 sec ON 90 sec OFF for 45 minutes in ice) in order to obtain chromatin fragment lengths of 100–1000 bp. Chromatin was diluted in ChIP dilution buffer (16.7mM Tris-HCl at pH 8.1, 167 mM NaCl, 1.2 mM EDTA, 1.1% Triton X-100, 0.01% SDS) and incubated overnight at 4°C with specific antibodies (anti-p63 EPR570, Abcam; 1mg protein: 1ug antibody) conjugated with Dynabeads® Protein A and G (ThermoFisher Scientific). Immunoprecipitated samples were washed with Low salt buffer (0.1% SDS, 1% Triton X-100, 2mM EDTA, 20mM Tris-Hcl pH 8.1, 150 mM NaCl) High salt buffer (0.1% SDS, 1% Triton X-100, 2mM EDTA, 20mM Tris-Hcl pH 8.1, 500mM NaCl) and LiCl Immune complex wash buffer (10mM Tris-Hcl pH 8.1, 0.25 M LiCl, 1 mM EDTA, 1% Na deoxycholate, 1% NP-40) and twice with TE buffer. After immunoprecipitation, DNA was eluted in 1% SDS plus 0.1 M $NaHCO_3$, purified with QiaQuick columns (ThermoFisher Scientific) and quantified using Qubit assay (Invitrogen). Immunoprecipitated DNA was used as template for a preliminary quality-control qPCR and for library construction of Illumina sequencing. All qPCRs were performed with SYBR Select Master mix (Applied Biosystems) on a 7900 Real-Time PCR system (Applied Biosystems). All 50-bp sequence reads were uniquely mapped to the mouse genome NCBI Dec.2011 (GRCm38/mm10) using bwa 0.6.1 with standard parameters. p63 ChIP-seq datasets were normalized to the same sequencing depth by randomly removing aligned reads. Duplicated reads were removed before normalization. Peak recognition for p63 ChIP-seq was performed using MACS2, an updated version of MACS, that is specifically designed to process mixed signal types (https://github.com/taoliu/MACS) with default settings and a P-value threshold of 1E-9 using a genomic DNA as background control. Peaks were mapped to RefSeq genes, downloaded from UCSC Genome Browser (mm10), to determine genomic location of the p63 binding sites. p63 target sequences were then analysed with MEME, STREME, TomTom and CentriMo tools (https://meme-suite.org/meme/). Associated genes resulting from the ChIP-seq were intersected with

data from RNA-seq performed on P0 epidermis with Cerca.Vert tool and Metascape and David analysis were performed on p63 direct targets. Venn Diagrams drawing was performed using Bioinformatics & Evolutionary Genomics web tool.

2.19 Whole-mount RNA in situ hybridization and in situ hybridization

Embryos were fixed in 4% PFA overnight at 4°C, dehydrated in methanol overnight at −20°C, rehydrated through a methanol/PBS series, washed in PBS, then treated with proteinase K for 20 min (10 μg/ml−1), washed in PBS, fixed for 30 min in 4% PFA at room temperature and then pre-hybridized at 65°C for 2 h (50% formamide/50% 2× SSC). Antisense DIG-labelled (Roche) mRNA probes (1 μg) were added in 1 ml of hybridization buffer (50% formamide/50% 2× SSC) at 65°C overnight. Embryos were washed twice in hybridization buffer, twice in 50:50 hybridization buffer: MAB buffer and then twice in MAB buffer, before being transferred to blocking buffer (2% blocking reagent 20% lamb serum in MAB buffer) for 2 hours at room temperature. Embryos were transferred to blocking buffer containing anti-digoxigenin antibody (Roche 1:2000) at 4°C overnight, then washed in MAB buffer overnight before being transferred to NTM buffer containing NBT (Promega, S3771)/BCIP (Roche, 16 853 423). For in situ hybridization on paraffin sections permeabilization was performed by incubation in PK (10 μg/ml) for 7.5 min at room temperature. Sections were post-fixed with 4% PFA, followed by an acetylation step to reduce background signal. Both in whole mount and tissue sections, hybridization was performed using *in vitro* transcribed digoxigenin-labelled antisense RNA probes, at 65°C ON. After washing, tissue sections were incubated with alkaline phosphatase-conjugated anti-digoxigenin antibody (Roche, 16 646 821) ON at 4°C and detection reactions were performed with NBT (Promega, S3771)/BCIP (Roche, 16 853 423). mRNA distribution visualized using a LeicaMZ16F microscope.

Probes used were Shh, Fgf8, Dusp6, Wnt7a kindly provided by A. Joyner (Sloan-Kettering Institute, New York, USA), G. Martin (University of California at San Francisco, San Francisco, USA), B. Robert (Institute Pasteur, Paris, France), U. Ruther (Heinrich-Heine-University, Düsseldorf, Germany) and C. Tabin (Harvard Medical School, Boston, USA).

Probes	Sequences
Lmx1b	Fw: GGATCGCTTTCTGATGAGG Rv: GATGTCATCATTCCTTCCATTCG

2.20 Preparation of samples for RNA-seq on E10.5 limb ectoderm-mesoderm separation

Forelimbs of embryos at E10.5 embryonic stage were collected in ice-cold PBS and distal Apical Ectodermal Ridge region was carefully dissected. Then, to separate the ectoderm and the mesoderm components, the dissected bands of distal tissue were subject to mild digestion in 0.25% trypsin-EDTA on ice. After a quick wash in cold PBS + 10% FBS, the separation of the two limb components was completed in cold PBS with the help of fine forceps. For each replicate ectoderm samples came from 2 forelimbs of 4 wild-type and 4 mutants. RNA was extracted using Quick-RNA MicroPrep Kit protocol (R1050 Zymo Research) and samples analyzed by 3'DGE sequencing at Next Generation Diagnostics srl (Pozzuoli, Italy).

3. RESULTS

3.1 Generation and characterizations of the p63α conditional knock- out mouse

To determine the function of the p63α isoform in embryogenesis and in adult stratified epithelia, we generated a conditional p63α knock-out mouse model by deleting exon 13, which is specific for the p63α isoform. This strategy led to the robust expression of the p63β isoform that intrinsically lacks exon 13 (Figure 2), and is physiologically expressed in wild-type epidermis albeit at much lower level than p63α (66).

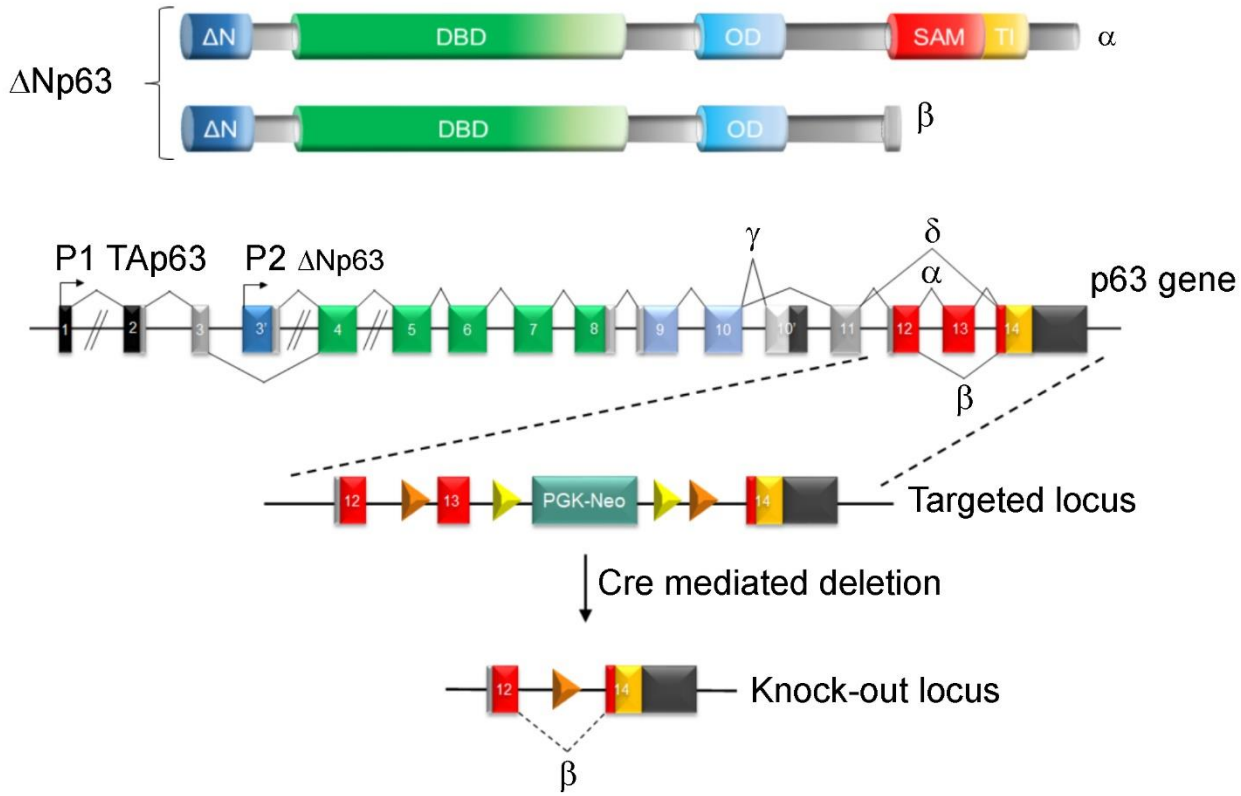

Figure 2. p63 gene structure and genome editing startegy.

Upper panel: ΔNp63α and ΔNp63β protein isoforms. Lower panel: p63 gene structure and strategy used to generate an inducible p63α-/- mouse model. LoxP sites flanking the wild type exon 13 were inserted together with a neomycin resistance cassette flanked by FRT loci that was subsequently removed. DBD: DNA Binding Domain; OD: Oligomerization Domain; SAM: Sterile Alpha Motif; TI: Trans-Inhibitory; PKG-NEO: phosphoglycerate kinase I (PGK) promoter, neomycin resistance gene (NEO) cassette.

In human and mouse, p63 is essential for palate, limb and skin development (1, 3, 18, 88, 89, 91). To establish the function of p63α in embryonic development, p63α fl/fl mice were crossed with pCX-NLS-Cre mice that ubiquitously express the Cre

recombinase starting from early stages of embryonic development (69). Proper exon 13 deletion was confirmed at the RNA and protein levels in mouse primary p63α fl/fl keratinocytes infected with an adenovirus carrying the Cre recombinase (Ad-Cre) or a Green Fluorescent Protein (Ad-GFP) as control (Figure 3A-B).

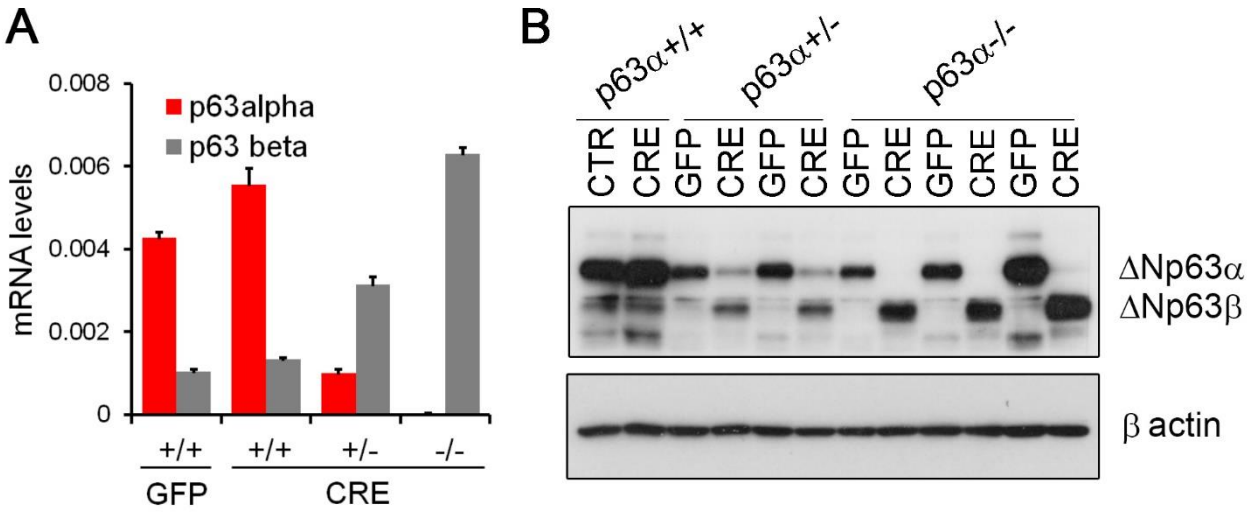

Figure 3. Confirming exon 13 deletion *in vitro*.

A) Real Time RT-PCR performed on mouse primary keratinocytes isolated from wild type and mutant epidermis and infected with adeno-Cre (Ad-Cre) or adeno-GFP (Ad-GFP) as control. B) Western Blot analysis performed on proteins extracted from Adeno-infected mKer.

The pCX-NLS-Cre;p63α+/fl mouse was subsequently crossed with p63αfl/fl (hereafter named p63α+/+) to obtain pCX-NLS-Cre;p63αfl/fl (hereafter named p63α-/-). Homozygous p63α-/- mutants were obtained at nearly Mendelian ratio (23.2% p63α-/-; 56.5% p63α +/-; 20.3% p63α +/+; n=306), and exhibited cleft palate and fully penetrant limb malformations, whereas the skin was indistinguishable from the wild-type one (Figure 4A-B). p63α-/- newborn mice died within few hours after birth. Limb malformations consisted of ectrodactyly and syndactyly of both forelimbs and hindlimbs (Figure 4C),

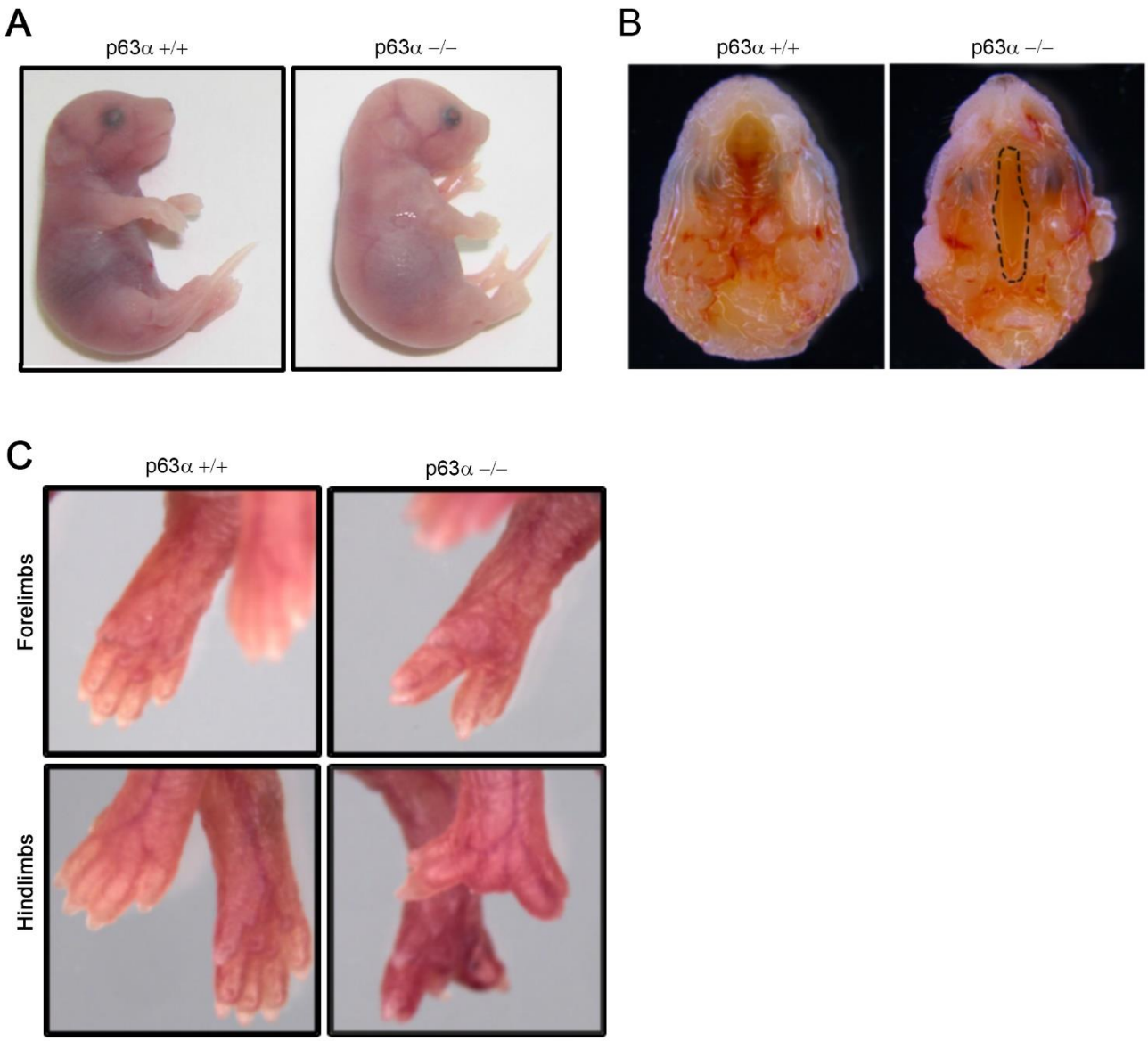

Figure 4. Macroscopic phenotype.

A) Limb malformations and macroscopically healthy skin in mutant embryos at birth (P0). A wild type littermate is shown as control. B) Cleft palate in p63α-/- mutants at E18.5. Dashed line delimits the palate malformation. C) p63α-/- newborn mice display severe limb malformations. with syndactyly in the forelimbs (top panel) and ectrodactyly and syndactyly in the hindlimbs (bottom panel).

with supernumerary phalanges especially of the forelimbs only in a few cases (Figure 5).

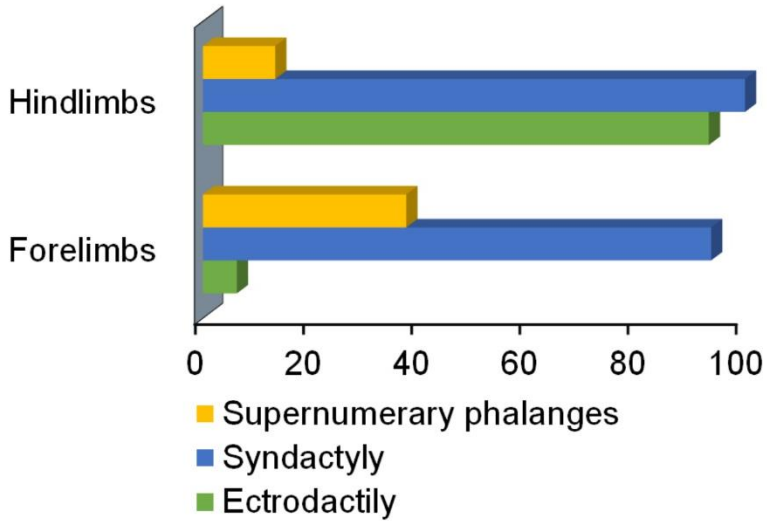

Figure 5. Limb malformations statistics.

Statistics of the limb malformations detected in mutant embryos at E.18.5 and P0 (n=16).

Immunofluorescence staining of p63α-/- epidermis at P0 with antibodies raised against the α-specific carboxyl terminal domain confirmed the absence of the p63α protein. However, using pan-p63 antibody recognising all p63 isoforms, p63 expression was comparable to the one seen in control epidermis, albeit it appears to be more restricted to the basal layer than the wild type counterpart (Figure 6).

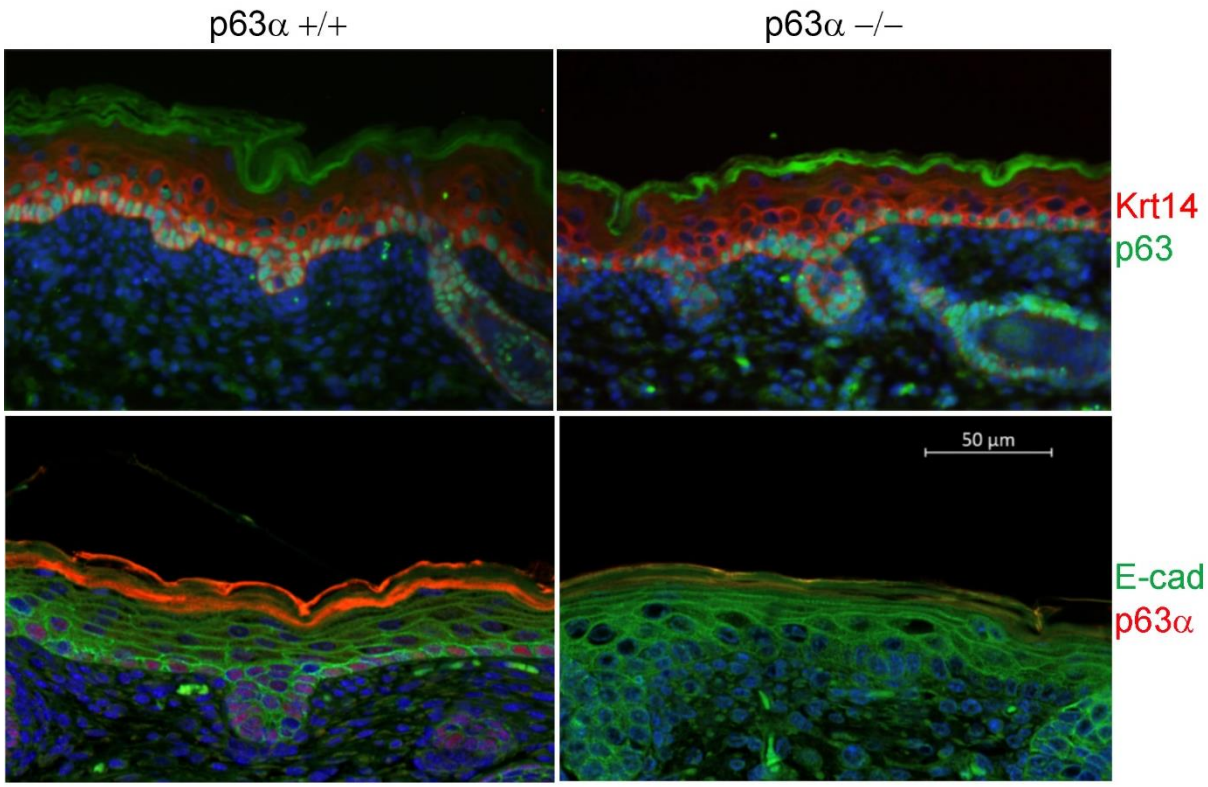

Figure 6. p63α ablation and p63β expression in mutant skin.

Immunofluorescence staining with p63 (in green) and Keratin 14 (Krt14; in red). A pan-p63 antibody shows a comparable signal among wild-type and mutant skin confirming that p63β is expressed in place of p63α (top panel); when mutant skin is stained with a specific p63α isoform antibody, it is appreciable the lack of p63α in the basal layer of p63α-/- mouse epidermis compared to wild-type (bottom panel).

Immunoblot analysis revealed a complete absence of the ΔNp63α protein with a concomitant induction of a lower molecular weight protein, corresponding to the size of the ΔNp63β (Figure 7).

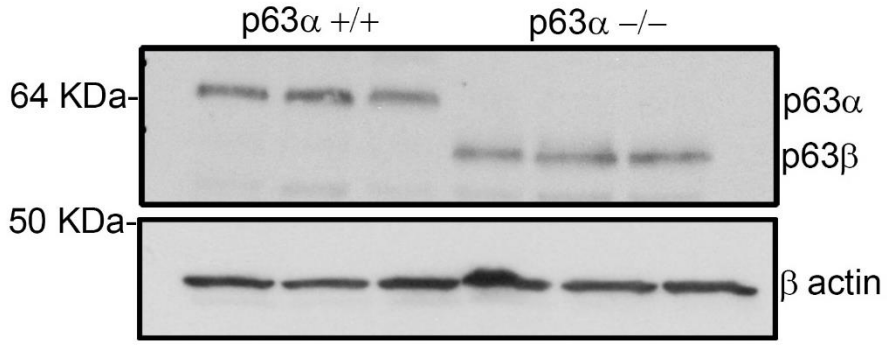

Figure 7. p63α ablation and p63β expression in mutant epidermis protein extracts.

Proteins collected from E18.5 epidermis of four p63α+/+ and four p63α-/- embryos and blotted with a pan-p63 antibody showing a complete absence of the p63α isoform and the concomitant induction of p63β in mutants.

RT-qPCR performed using specific oligonucleotide primers that distinguish p63β from p63α, confirmed the accumulation of p63β mRNA in the p63α-/- epidermis (Figure 8).

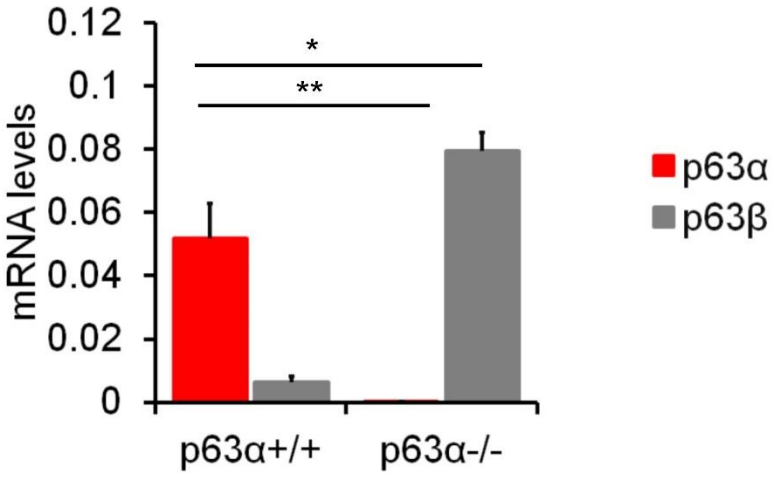

Figure 8. p63α ablation and p63β expression in mutant epidermis RNA extracts.

Real Time RT-PCR performed on RNA extracted from E18.5 epidermis of four wild type and four p63α-/- embryos. *p-value<0.05; **p-value<0.005.

In contrast, similar to the control and in line with previous reports (66), p63δ isoform lacking both exon 12 and exon 13 was expressed at very low levels (Figure 9).

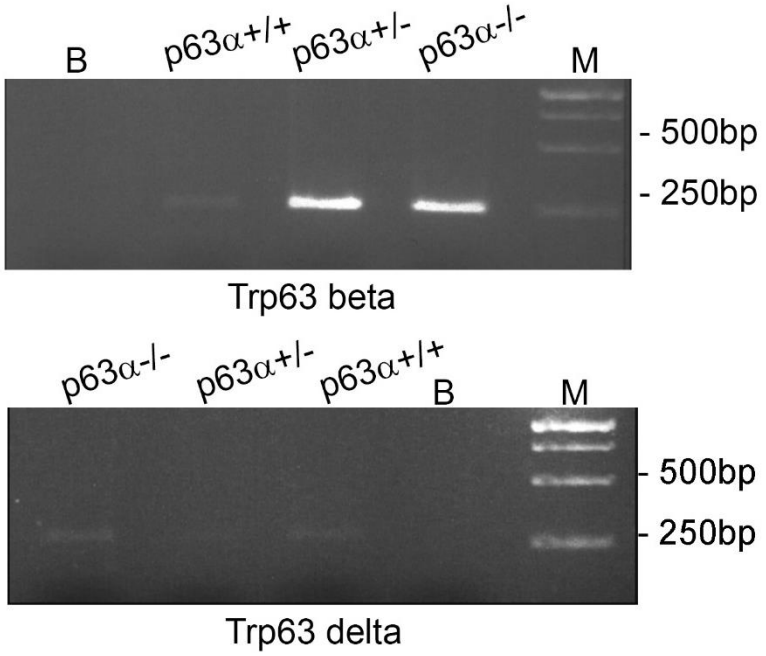

Figure 9. No aberrant splicing isoforms are detected.

RT-PCR on mouse epidermis showing the presence of wild type p63β isoform (top panel) and wild type p63δ isoform (bottom panel) in p63α +/+, p63α +/- and p63α-/- mice (M: marker; B: blank).

To ensure that no other isoforms were aberrantly generated as a consequence of exon 13 deletion, sequencing of the RT-PCR product spanning from exon 11 to exon 14 that include the mRNA regions encoding the α, β and δ p63 proteins, detected only the p63β and no other splicing isoforms (Figure 10).

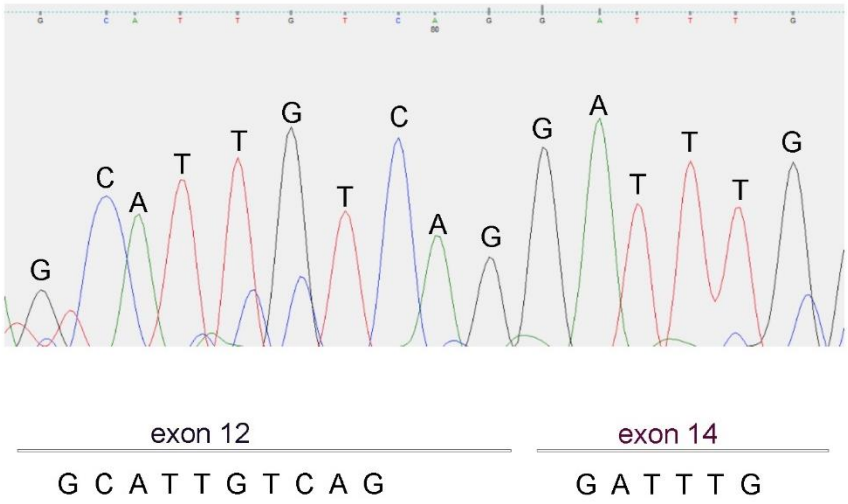

Figure 10. p63β wild type sequence expressed in mutants.

Electropherogram showing the sequencing of the RT-PCR band in Figure 9 (top panel) corresponding to p63β.

3.2 p63α deletion causes severe craniofacial malformations

p63α-/- mutant mice displayed a fully penetrant wide cleft of the secondary palate without involvement of the lip/primary palate or other cranial or mandibular malformations (Figure 4B). To probe into the cleft palate phenotype, histological analysis of the palatal shelves during embryonic development was performed at E13.5, E14.5, E15.5 (Figure 11). At E13.5, mutant palatal shelves pointed downwards on either side of the tongue similarly to their wild-type littermates, wheras at E14.5 palatal shelves were elevated both in wild-type and mutant, but the latter failed to meet in the midline appearing widely spaced compared to the wild-type. Consistently, at E15.5 palate fusion was completed and the midline had disappeared in the wild-type embryos, whereas mutant palates failed to fuse (Figure 11). Differently from p63-null mice that exhibited only a rudimentary palate process at E13.5 (102), p63α-/- and p63α +/+ embryos are characterised by similar palatal shelves size (31, 103), in all three embryonic stages analysed. However at E13.5 we observed an abnormal fusion between the epithelia of maxillary and mandibular processes in the mutant embryos likely causing a delay in the elevation of palatal shelves (Figure 11 dashed box in the upper panel) as previously observed in p63-transcriptonal target mutants (Irf6, IKKα, Ripk4, Sfn, Grhl3 and Jag2) (30, 32-34) and in the Tgf3β -/- model (31).

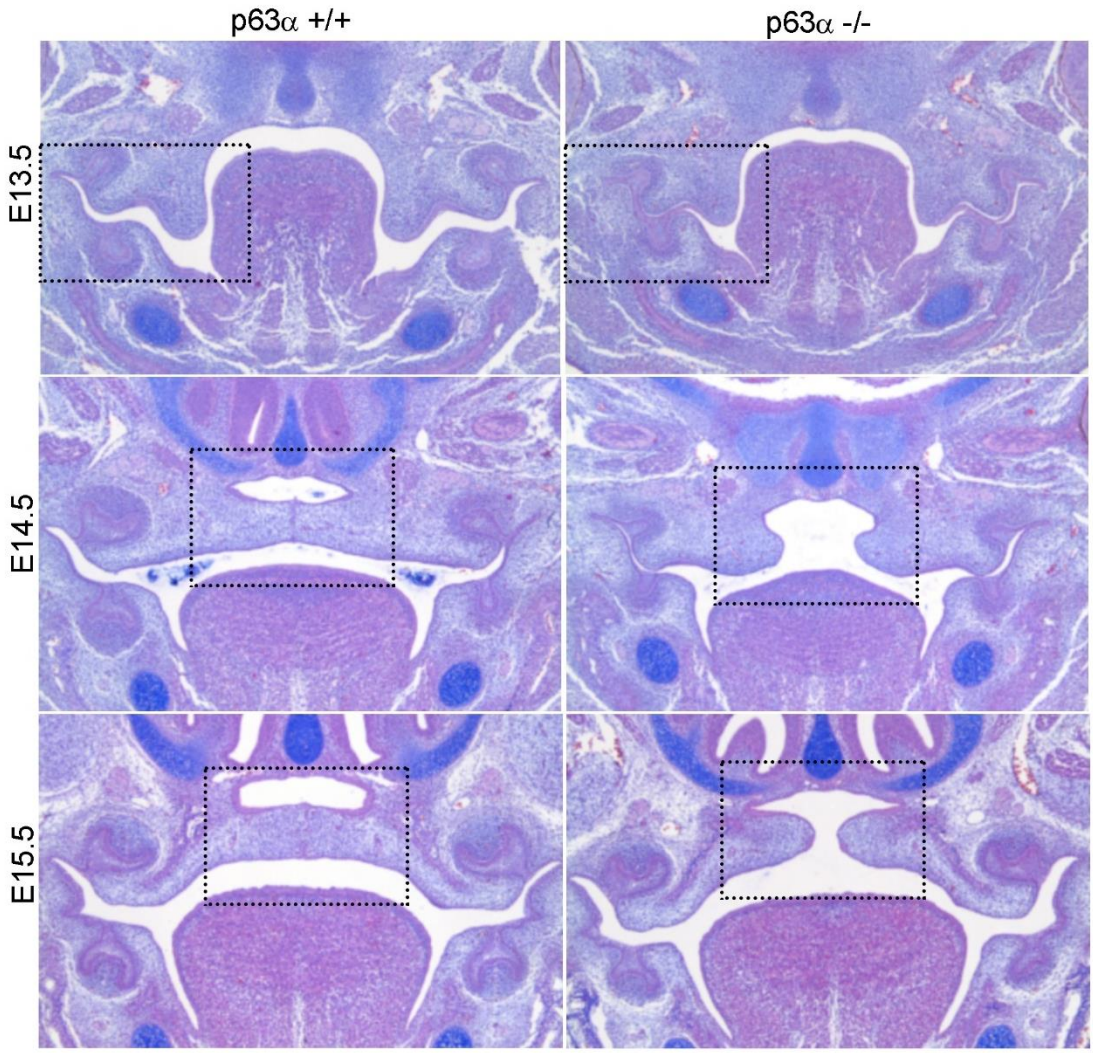

Figure 11. Comparison of wild type and mutant palatal elevation and fusion process.

Hematoxylin and Alcian Blue staining of wild type and p63α-/- mouse heads showing the presence of cleft of the secondary palate in p63α-/- mice. At E15.5 when palatal shelves meet at the midline, mutant palates fail to fuse. Dashed lines indicate the defect observed in mutants in comparison to the wild types. (Performed in collaboration with Jill Dixon)

Staining for Keratin 14 (Krt14), a marker of the basal epithelium, revealed that mutant p63α-/- palates showed no alterations that directly involved epithelial cells at E13.5, while total p63 staining confirmed the upregulation in mutants of p63 itself (Figure 12A). During palate development, and more generally in the epithelial tissues of the entire embryo, starting from E9 to E17, a protective epithelial layer called periderm, prevents premature adhesion between opposing epithelia that should remain spatially separated (30, 32). Given the previously observed fusion between mandibular and maxillary epithelia, we verified whether in mutant palate periderm underwent alterations, performing an immunofluorescence analysis on E14.5 wild-type and

mutant mice. We used antibodies against Keratin 14 (Krt14) to mark the basal epithelium, and Keratin 17 (Krt17), a marker for the periderm. This analysis demonstrated that differently from p63-null palate, in p63α-/- mouse palate the periderm was present, but it showed some regions in which the Krt17 signal invaded the basal layer mingling with the Krt14 signal (Figure 12B). Moreover, while wild type periderm appears as a single-cell layer of flattened cells with highly polarized tight junctions expression (30), in p63α-/- palate, peridermal cells showed an altered morphology, more rounded than flat (Figure 12B). In addition, we found that mutant tongue had a spotted and lower expression of Krt17 compared to the wild type (Figure 12C). BrdU analysis on E13.5 palatal shelves excluded a reduction, in p63-expressing cells, of the proliferation as the cause of the observed defect (Figure 12D).

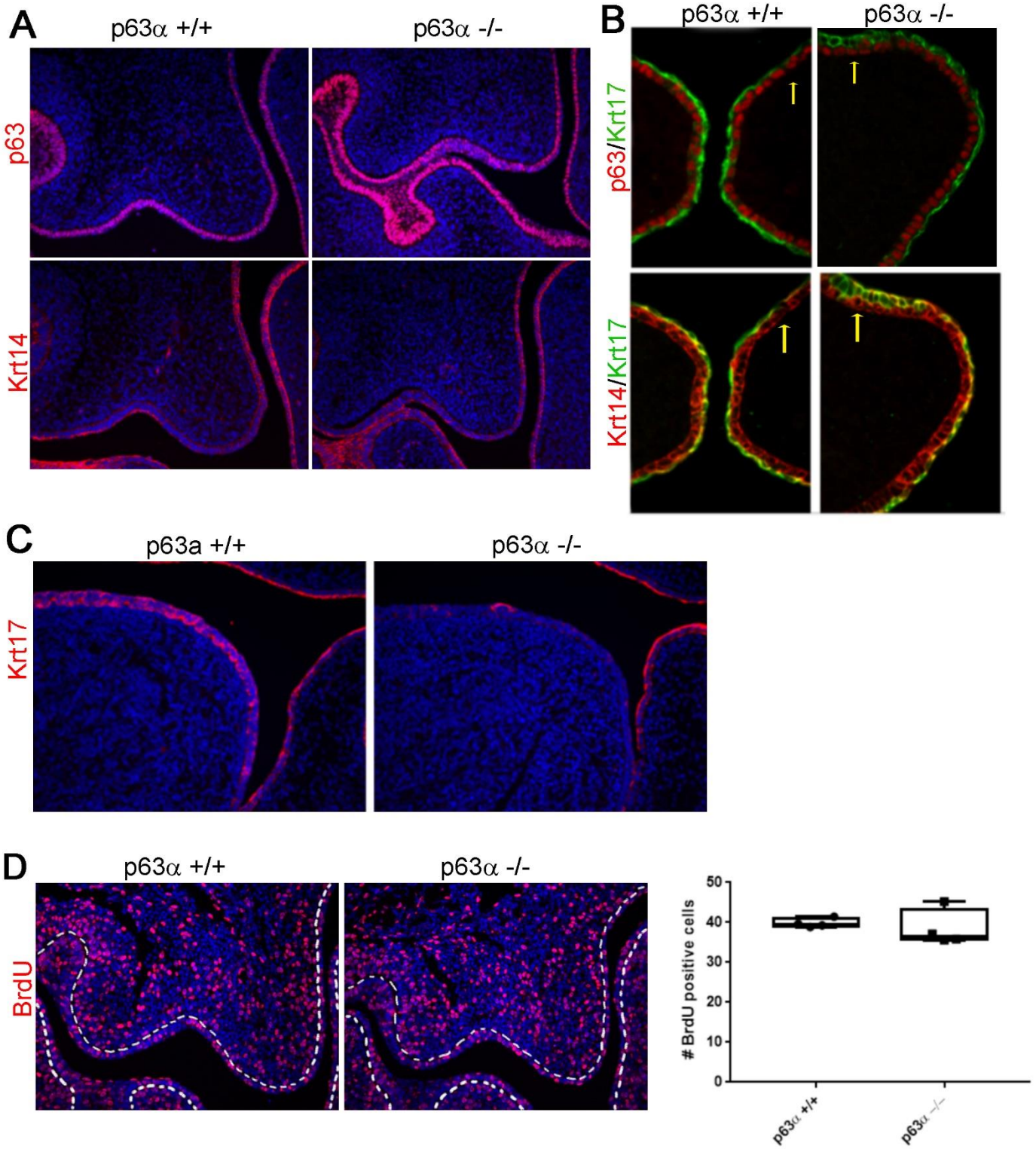

Figure 12. Immunofluorescence analysis of wild type and mutant palatal and tongue epithelia.

A) Immunofluorescence analysis on E13.5 wild type and mutant palates stained for total p63 and Krt14 showing the fusion between the epithelia of maxillary and mandibular processes in mutant embryos. B) Immunofluorescence analysis on E14.5 wild type and mutant palates stained for p63 (red) and Krt17 (green) (top panel), and for Krt14 (red) and Krt17 (green) (bottom panel). The periderm was less organized in the mutant palatal shelves, in which cuboid peridermal cells intermingled with Krt14 positive cells (yellow arrows). C) Immunofluorescence analysis on E14.5 wild type and mutant tongues stained for Krt17 (red) showing only few peridermal cells in p63α-/- embryos. D) BrdU staining on

E13.5 wild type and mutant palatal shelves; dashed white lines delimit the epithelial layers in which BrdU positive cells were counted. Quantification of BrdU positive cells in p63α +/+ and p63α-/- (n=4) (right panel). (Performed in collaboration with Jill Dixon).

To identify the key molecular pathways being altered in mutant palates, we performed a transcriptomic analysis on RNA samples extracted from mouse palatal tissues obtained from E14.5 p63α-/- and wild type embryos. We observed an up-regulation of some *bona fide* target genes of p63 (such as Notch1, Trp73, Znf750 and Trp63 itself), some involved in periderm development, such as Grhl3, and more generally, the Gene Ontology (GO) analysis revealed an enrichment for genes that regulate the epidermis development program such as Cdh3, Krt10, Krt5, Trp63, Dsp, Krt14, Dsc3, Dsg2 and Dsg3 (Figure 13A-B). Among them, Dsp, Dsc3, Dsg2 and Dsg3 are desmosome genes, involved in cell-cell junction. Among the downregulated genes, significant enrichment was observed in genes involved in the general process of blood vessel development. The switch from p63α to p63β expression seems to impair the cell-cell adhesion program and the extracellular matrix organization (Figure 13B).

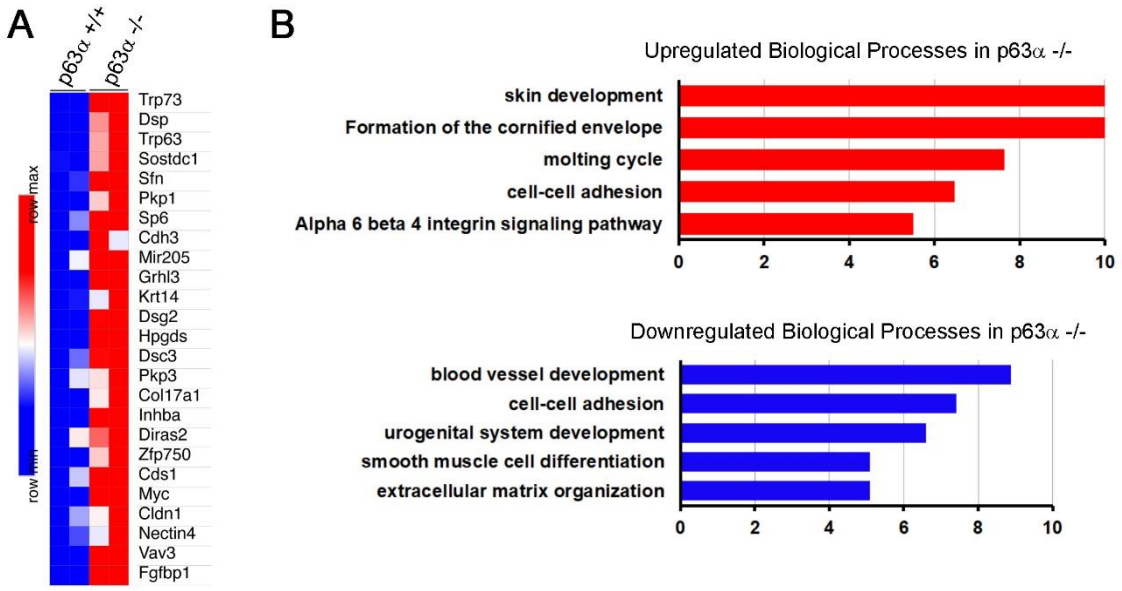

Figure 13. Palates RNA-seq analysis.

A) Heatmap showing relevant and known p63-targets upregulated in p63α-/- on E14.5 palates (n=4). B) Metascape analysis on E14.5 palates RNA-seq data showing differentially regulated Biological Processes of the most statistically significant genes.

3.3 p63α deletion causes severe limb malformations

To characterize the limb alterations observed in the p63α-/- mice, we first verified that p63α and p63β showed expression levels comparable to those observed in the skin where p63β expresses in place of p63α (Figure 14).

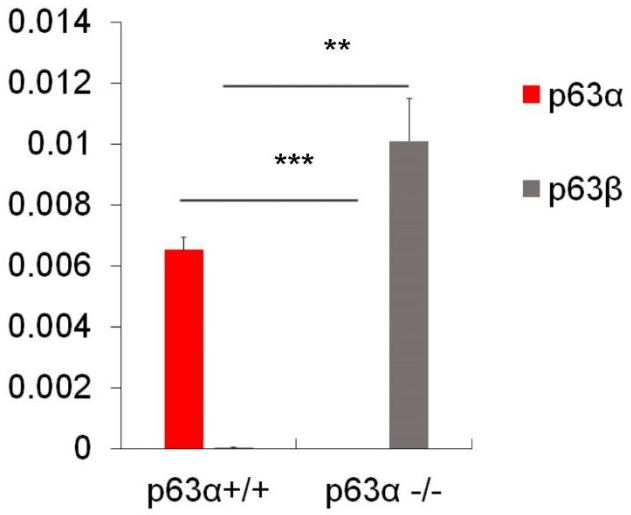

Figure 14. p63α ablation and p63β expression in mutant limb RNA extracts.

Real Time RT-PCR performed on RNA extracted from E12.5 hindlimbs of four wild type and four p63α-/- embryos. The absence of p63α and the induction of p63β in mutant limbs is statistically significant.

Then we focused on digit formation process starting from mid stages of limb development (E13.5) until the end of the process at E15.5 (Figure 15). At E13.5, when interdigit apoptosis has not yet occurred, we observed a clear and reproducible alteration of the distal end of the forelimbs with a split hand like phenotype, whereas hindlimbs were even more severely affected (Figure 15). By E15.5 mutant forelimbs displayed established syndactyly, whereas hindlimbs had signs of both syndactyly and ectrodactyly (Figure 15) with more rare cases of polydactyly in both limbs (Figure 5).

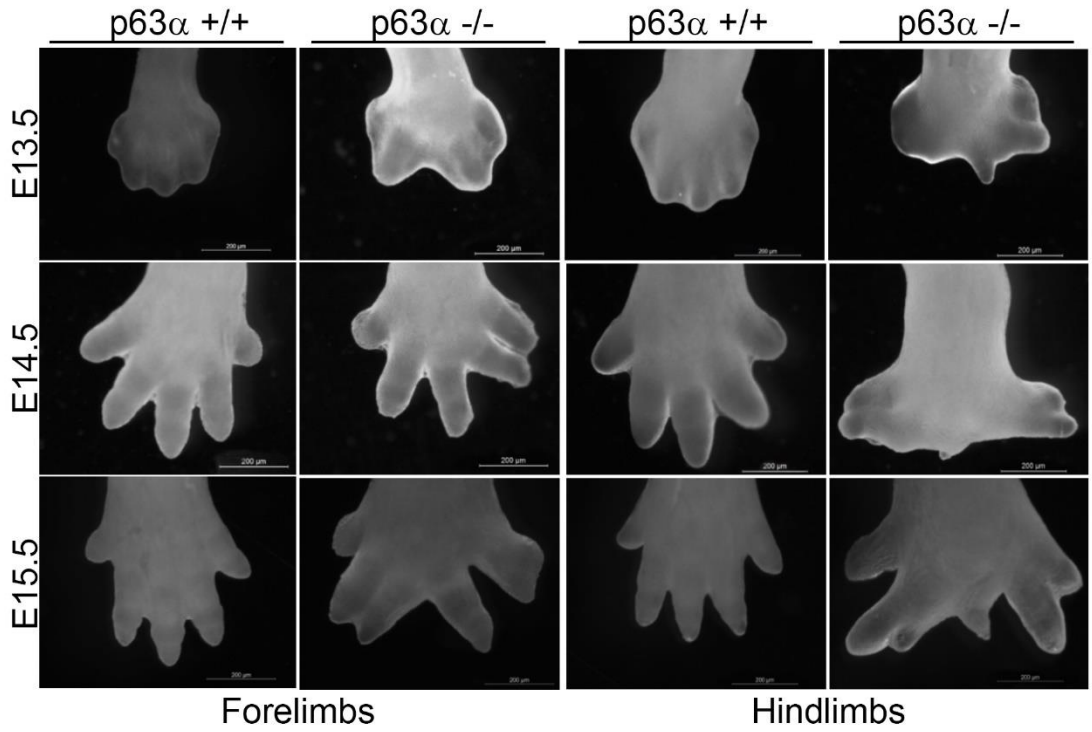

Figure 15. Macroscopic limb phenotype.

Morphological malformations of limbs are appreciable early in development starting from E13.5 to E15.5. Hindlimbs show a more severe phenotype compared to forelimbs.

To observe general alterations in limb skeletal structure and to verify that syndactyly observed was due to digital bone fusion, we performed Alcian-Alizarin staining at E18.5 limbs in wild type and p63α-/- embryos. This analysis revealed normal development of the humerus/femur ulna/tibia and radius/fibula in p63α-/- mice. In contrast, digit malformations were observed in 100% of mutant mice: forelimbs appeared misaligned most likely due to soft tissue syndactyly in 100% of mutants (39, n=39), with altered morphology and extra portion of distal digits found in 25.6% of cases (10, n=39) and only one case of ectrodactyly; whereas in hindlimbs we observed more severe alterations including ectrodactyly in 97.4% of mutants (37, n=38), bone and soft-tissue syndactyly in 97.4% (37, n=38) and more rarely polydactyly with extra-numerary phalanges, 7.9% of mutants (3, n=38) (Figure 16).

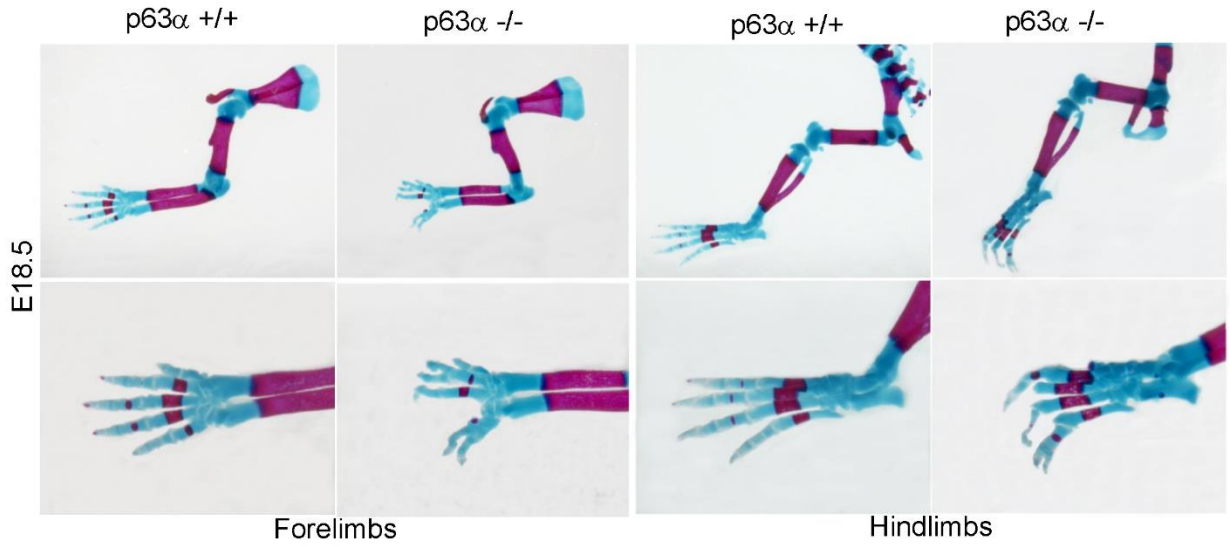

Figure 16. Forelimb and hindlimb bones appearance.

Alcian and Alizarin staining of p63α-/- and wild-type mice limbs at E18.5, shows mainly ectrodactyly of hindlimbs and syndactyly, through soft tissue fusion, of forelimbs in mutant mouse but a normal development of stylopod and zeugopod.

To understand which of the fundamental signalling pathways acting in limb development may be impaired in p63α-/- mice, we performed several RNA In Situ Hybridization (ISH) to verify if some of the players involved in limb development, such as Fgf8, Shh and Dlx5/6 genes, retained not only a physiological level of expression but also showed their specific and proper expression domains. At E10.5 ISH on whole embryos and on fore- and hindlimbs for Fgf8 together with Shh confirmed the expected presence of an AER-signalling defect in mutant embryos: the density of Fgf8 signal in AER cells is much lower and spotted and absent in the central portion compared to the control (Figure 17A). Consistent with an impairment of the Fgf8 signalling in the AER, mutant limb buds exhibited a strong downregulation of the expression of Dusp6, a reporter of the general Fgf signalling, in the mesoderm compared to wild type (Figure 17B). Given the split-hand phenotype similarity between p63α-/- and Dlx5/6 -/- mutants, and that Dlx5/6 are known to be p63 target genes (23), we performed ISH for Dlx6: at this stage the wild type embryos poorly expressed Dlx6 in the AER, whereas no expression could be detected in the mutant (Figure 17B). Moreover, the hybridization for Fgf8 and Shh in paraffin-embedded tissue sections of E10.5 limb buds showed a reduced stratification of the AER both in

mutant fore- and hindlimbs (Figure 17C) suggesting that the switch of p63 isoform prevents AER stratification. Performing a TUNEL staining on same sections we demonstrated that there was no significant difference in the number of apoptotic cells in the distal and proximal portion of the forelimb bud between mutant and controls (Figure 17D).

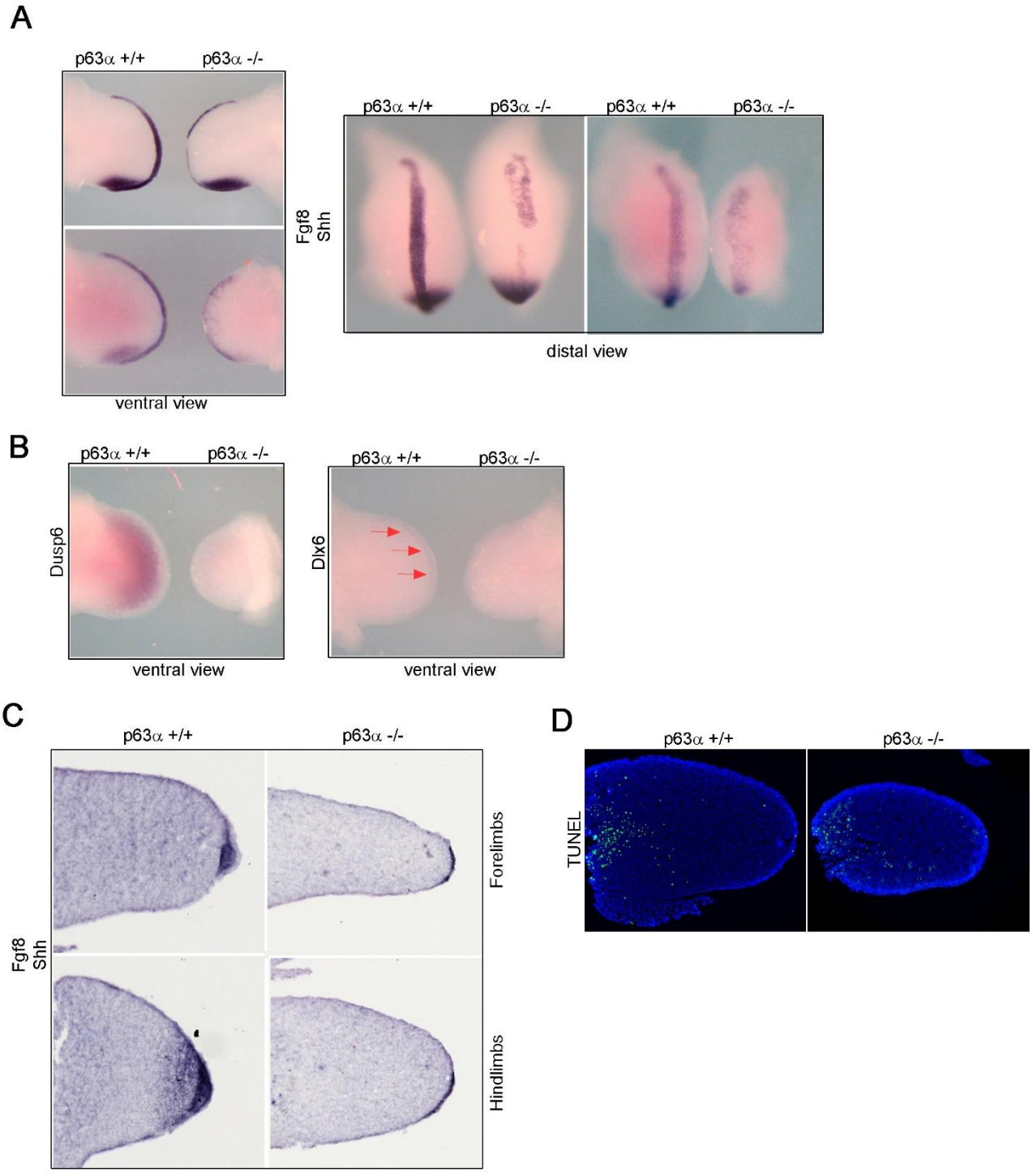

Figure 17. Molecular analysis of key limb development pathways on E10.5 limb buds.

A) RNA In-Situ Hybridization on wild type and mutant forelimbs at E10.5 using Fgf8 and Shh probes (ventral view on left panel and distal view on right panel). B) RNA In-Situ Hybridization on wild type and mutant forelimbs at E10.5 using Dusp6 (left panel) and Dlx6 (red arrows, right panel) probes. C) RNA ISH on paraffin-embedded sections of wild type and mutant forelimbs and hindlimbs at E10.5 for Fgf8 and Shh detection showing the AER epithelium appearance: stratified in p63α +/+ and flattened in p63α-/-. D) TUNEL staining showing cell apoptosis on paraffin-embedded sections of wild type and mutant distal forelimbs buds at E10.5, revealing no significant differences at this stage compared with the controls. (Performed in collaboration with Maria Angeles Ros Lasierra).

To understand further the key molecular pathways being altered by p63α ablation in limb development, we used the same approach, as for E10.5, for E11.5 wild type and mutant embryos. Whole Mount In Situ Hybridization (WMISH) was performed on mutant and control embryos proving that, also at this developmental stage, the Fgf8 signalling was impaired exhibiting a lower and dotted expression in mutant forelimbs compared to wild type. A stronger Fgf8 downregulation was observed in the hindlimbs consistent with the more severe phenotype found (Figure 18A). Among the p63 target genes, Dlx5 and Dlx6, were characterized by a lower level of expression in p63α-/- than in wild type even at this embryonic stage although their expression was low also in the wild type compared to E10.5 (Figure 18B). In contrast, Engrailed 1 (En1) that is essential for ventral patterning spatially regulating Wnt7a expression (104), is totally absent both in the mutant forelimbs and hindlimbs (Figure 18C). Lmbx1 (LIM homeobox transcription factor 1 beta), a downstream target of Wnt7a (105), was still detectable in mutant limb buds showing the same and correctly localized expression domains observed in the wild type (Figure 18D). Moreover, ISH on tissue sections for Fgf8 confirmed the previously flattening of the AER already found at E10.5. Detection of Sp6, that differently from En1 regulates the ventral patterning of limbs starting from E9.5, acting downstream of the Wnt-βCat signalling pathway and upstream of Fgf8, appeared to be unmodified in mutant limbs (Figure 18E). To investigate on changes in proliferation and cell death in the distal mesenchyme, controlling the pool of autopod progenitors that carry on the correct formation of distal limb elements, we first performed immunofluorescence analysis on E11.5 paraffin-embedded sections of limb buds using an anti-pH3 antibody that marks cycling cells in late G2 and mitosis: there was a clear decrease in proliferation, as expected, in the mutant distal limb

mesoderm reflecting the progressive loss of Fgf8-driving signal coming from the AER, where, contrariwise, proliferation is physiologically very low or absent (Figure 18F). Cell death was evaluated performing a TUNEL assay showing at this stage, no differences in the number of apoptotic cells between p63α +/+ and p63α-/- limbs in particular in the distal area (Figure 18F).

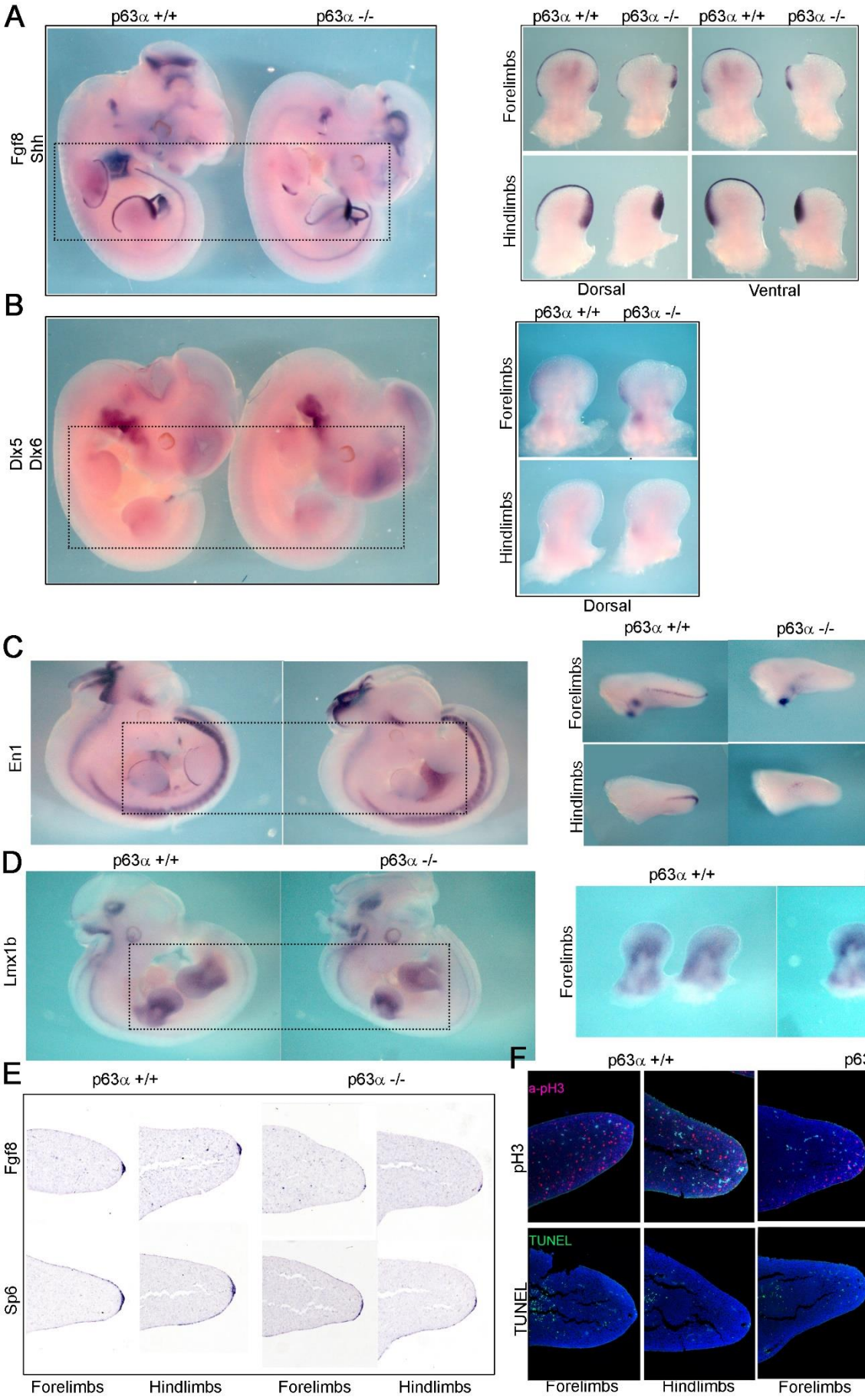
A
p63α +/+
p63α -/-
Fgf8
Shh
p63α +/+
p63α -/-
p63α +/+
p63α -/-
Forelimbs
Hindlimbs
Dorsal
Ventral
B
Dlx5
Dlx6
p63α +/+
p63α -/-
Forelimbs
Hindlimbs
Dorsal
C
En1
p63α +/+
p63α -/-
Forelimbs
Hindlimbs
D
Lmx1b
p63α +/+
p63α -/-
p63α +/+
p63α -/-
Forelimbs
E
p63α +/+
p63α -/-
Fgf8
Sp6
Forelimbs
Hindlimbs
Forelimbs
Hindlimbs
F
p63α +/+
p63α -/-
a-pH3
pH3
TUNEL
TUNEL
Forelimbs
Hindlimbs
Forelimbs
Hindlimbs

Figure 18. Molecular analysis of key limb development pathways on E11.5 limb buds. A) Whole Mount In Situ Hybridization (WMISH) for Fgf8 and Shh (left panel) RNA probes on E11.5 wild type and mutant embryos; details of E11.5 limb bud (dashed box) with Fgf8 and Shh detection on dorsal and ventral view (right panel). B) WMISH for Dlx5 and Dlx6 (left panel) RNA probes on E11.5 wild type and mutant embryos; details of E11.5 limb bud (dashed box) with Dlx5 and Dlx6 detection on dorsal view (right panel) showing their characteristic domains of expression. E) RNA In-Situ Hybridization on paraffin-embedded sections of wild type and mutant forelimbs and hindlimbs at E11.5 for Fgf8 (top of the panel) and Shh (bottom of the panel) detection showing the AER epithelium appearance: polystratified in p63α +/+ and flattened in p63α-/-. F) Immunofluorescent staining using antibodies for phospho-Histone H3 (pH3) showing a reduction of proliferating cells in mutant paraffin-embedded fore- and hindlimbs at E11.5 (top panels) compared to wild type; and TUNEL staining indicating a reduction in the number of apoptotic cells in mutant paraffin-embedded fore- and hindlimbs at E11.5 compared to control. (Performed in collaboration with Maria Angeles Ros Lasierra).

To get an overview on the molecular pathways involved in limb development being altered by p63α ablation, we performed RNA-seq analysis on RNA isolated from E12.5 embryo hindlimbs. Data were filtered for pValue < 0.05 resulting in 214 differentially expressed genes (DEGs) (Figure 19A), including Krt15 and Gjb5, two p63 target genes. Metascape analysis revealed that they are mainly involved in forelimb morphogenesis, tissue morphogenesis and positive regulation of cell junction assembly (Figure 19B; Figure 19C). This latter biological process is similarly altered in mutant palates. In addition, the RNA-seq confirmed the impairment in En1 expression, already observed by ISH.

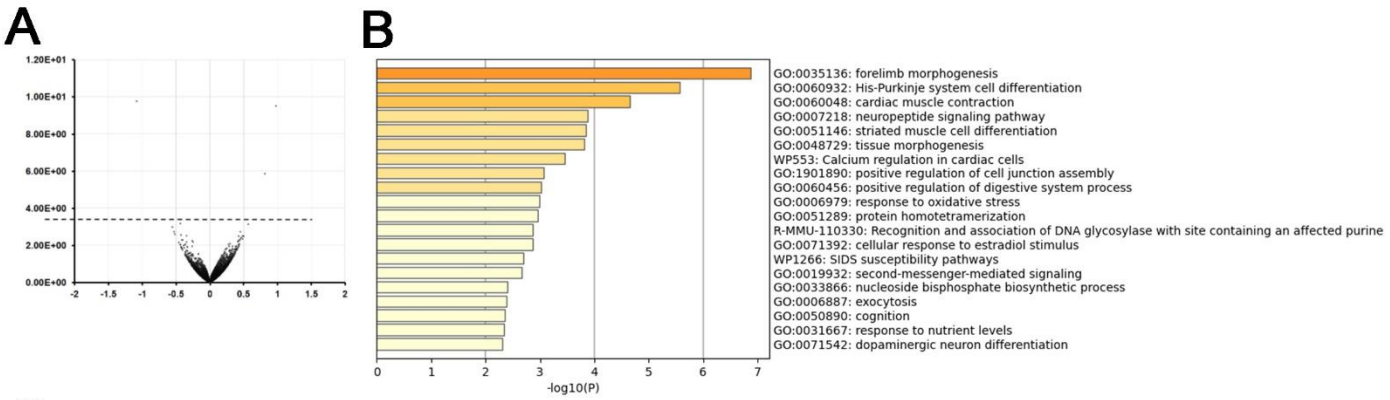

C

Biological processes	LogP	Symbols
forelimb morphogenesis	-6.878470694	En1,Fmn1,Hoxa11,Msx2,Aldh1a2,Tbx5,Rspo2,Barx1,Nr2f1,Hoxb5,Irx3,Nbl1,Nkx2-5,Pax1,Sfrp1,Wt1,Dnah5,Alx1,Egfr,Gjb5,Gjb6,Hyal1,Nfe2,Nsdhl,Tcf21,Cdk6
limb morphogenesis	-3.741872952	En1,Fmn1,Hoxa11,Msx2,Aldh1a2,Tbx5,Alx1,Rspo2
mesenchyme development	-2.908387788	Msx2,Nkx2-5,Pax1,Aldh1a2,Sfrp1,Tbx5,Tcf21,Wt1,Alx1
morphogenesis of an epithelium	-3.61333281	Egfr,Fmn1,Hoxa11,Irx3,Msx2,Nkx2-5,Aldh1a2,Sfrp1,Tbx5,Tcf21,Wt1,Brsk2,Esrp1,Alx1,Rspo2
branching morphogenesis of an epithelial tube	-2.127444963	Hoxa11,Msx2,Tcf21,Wt1,Esrp1,Rspo2
positive regulation of cell junction assembly	-3.0719215	Fmn1,Irx3,Tbx5,Adgrl2,Adgrb3,Lrtm1,Lrfn4,Gjb6,Nrxn3,Cntnap1
response to oxidative stress	-2.98861516	Chrna4,Egfr,Hyal1,Pdk2,Ucp2,Rgs14,Ngb,Thg1l,Meak7,Prkaa2,Nox1

Figure 19. Hindlimb RNA-seq analysis.

A) Volcano plot of E12.5 hindlimbs RNA-seq results (n=4). B) Metascape analysis on 214 DEGs filtered for p-value < 0.05 C) Biological processes and genes involved in determined biological processes resulted from Metascape analysis.

3.4 p63α deletion has a mild effect on skin development and differentiation *in vivo*

p63 -/- mice are characterized by impaired skin development, loss of epidermal stratification and differentiation and poorly adherent basal cells (16, 17, 106). Similarly, in the p63ΔC -/- mice skin appeared severely eroded with a hypoplastic and thin epidermis with a concomitant lack of hair follicles (86). In contrast, p63α-/- newborn mice had no macroscopic alteration of the skin, and analysis of hematoxylin and eosin staining on p63α-/- mice skin sections at P0 revealed a normal development of the epidermal layers (Figure 20).

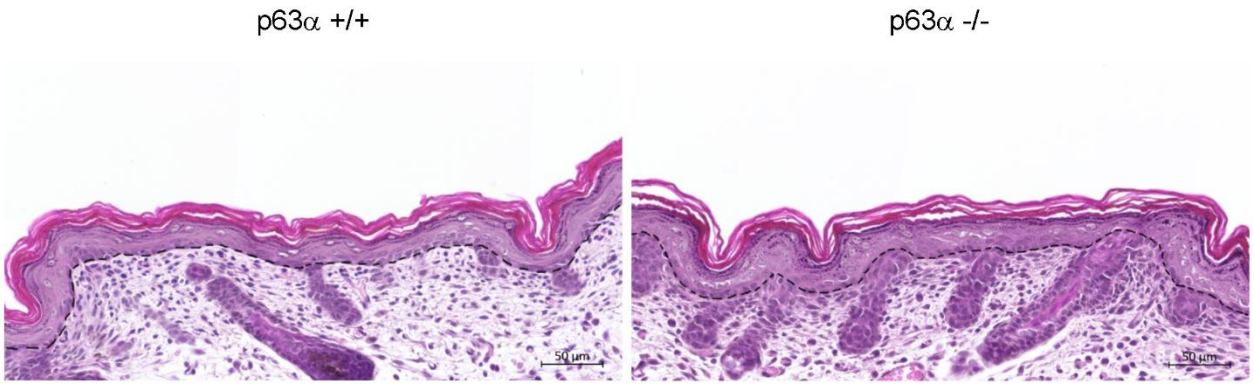

Figure 20. Wild type and mutant epidermal appearance and thickness.

Hematoxylin and Eosin staining on paraffin sections showing a normal skin thickness of mutant skin at P0. Dashed lines delimit the basal layer of the epidermis.

To characterize the presence of possible molecular alterations in the mutant epidermis, we performed an RNA-seq analysis on E18.5 p63α-/- embryos epidermis. To define the differentially expressed genes (DEGs) in p63α-/- mice compared to wild type mice, we identified the downregulated and the upregulated genes upon p63α-/- filtering for an FDR ≤ 0.01 (Figure 21A). The Gene Ontology (GO) analysis on upregulated genes, showed an enrichment for processes associated with morphogenesis of an epithelium and keratinocytes differentiation, while the downregulated genes are mainly enriched in processes such as negative regulation of cell differentiation and extracellular matrix organization (Figure 21B-C). In particular among downregulated genes, we found one of the most statistically significantly affected gene was Krt15, that was similarly decreased in mutant limbs, confirming that it may be a p63α specific target gene.

Moreover, the upregulation of Krt6a confirmed a general alteration of the differentiation program (Figure 21B).

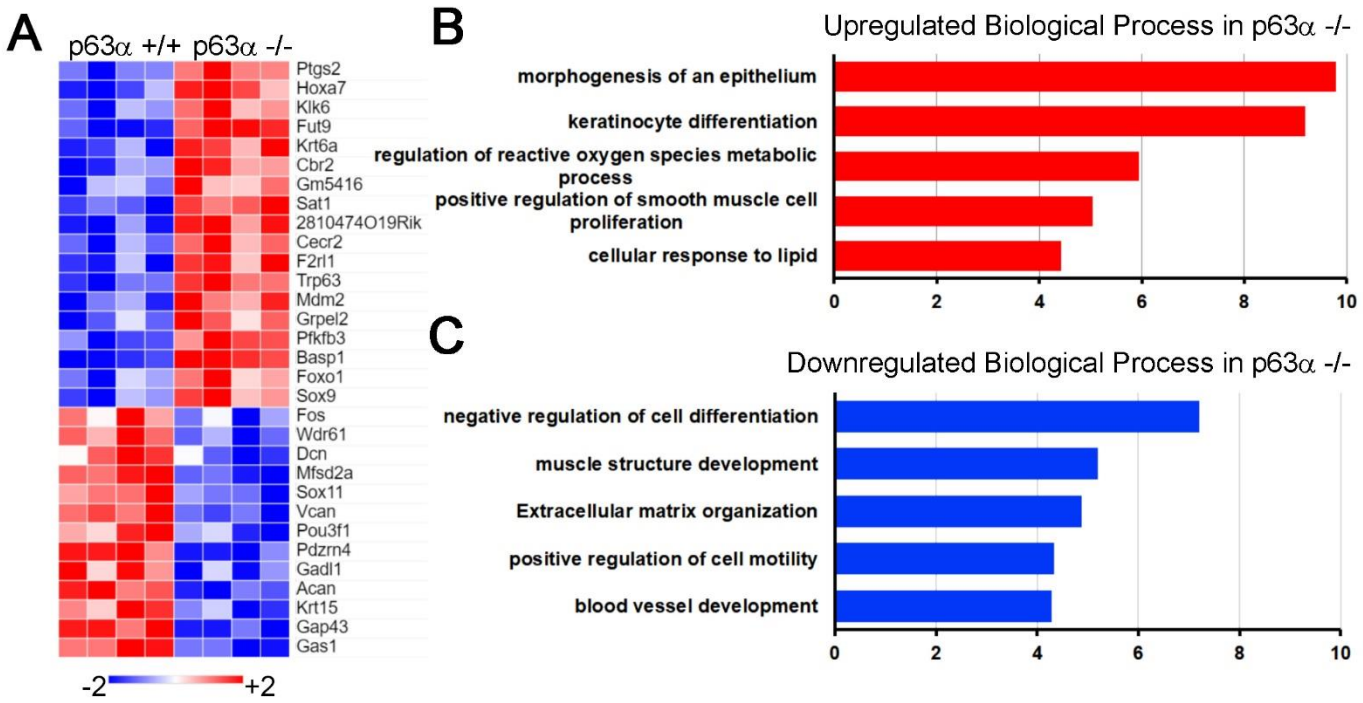

Figure 21. Epidermis RNA-seq analysis.

Differentially expressed genes resulted from the RNA-seq performed on mutant and wild-type P0 epidermis filtered for FDR ≤ 0.01 (n=4). A) Heatmap showing relevant upregulated and downregulated genes in p63α-/- resulted from RNA-seq results on E18.5 epidermis (n=4). B-C) Gene Ontology analysis performed on upregulated and downregulated genes resulting from the RNA-seq.

We next tested the alteration in epidermal cell differentiation at the protein level. Immunofluorescence staining for the basal cell layer marker Krt14 showed that the maintenance program of the basal layer cells was not altered in mutant mice compared to controls (Figure 22). In contrast, as we expected from gene expression profiling, Krt15, which also expressed in the basal layer of the epidermis, was strongly downregulated in mutant epidermis, whereas Krt6a was ectopically expressed in the upper differentiated layers, while in wild type is physiologically expressed only in the hair follicle, thus confirming a mild alteration of the keratinocyte differentiation program (Figure 22).

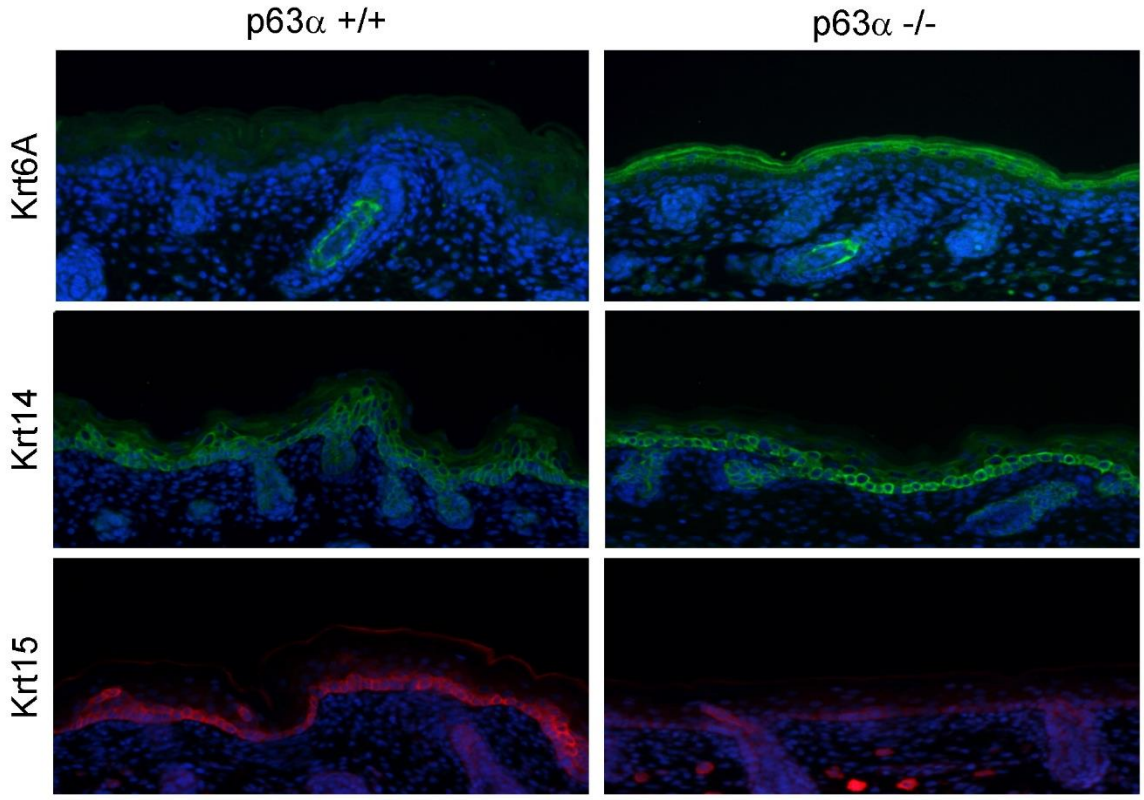

Figure 22. Mutant altered expression, resulted from RNA-seq in epidermis, of epidermal markers *in vivo*.

Immunofluorescence analysis on paraffin sections of P0 skin confirmed the induction of Keratin6 (Krt6A) and inhibition of Keratin15 (Krt15) compared to Wild Type skin observed in RNA-seq analysis, whereas a mostly normal Keratin14 (Krt14) expression.

These results were also confirmed by western blotting performed on P0 mouse epidermis (Figure 23).

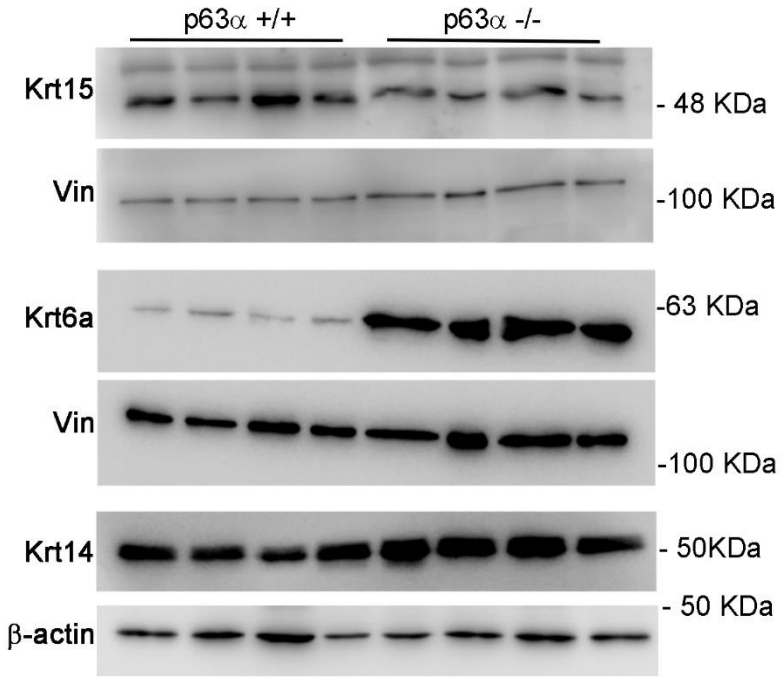

Figure 23. Validation of epidermis RNA-seq results in wild type and mutant protein extracts.

Proteins extract collected from four wild type and four p63 -/- epidermis were processed for immunoblotting analysis to confirm results from RNA-seq on P0 epidermis. Similarly, to what was observed in the immunofluorescence, Krt14 had similar levels of expression in mutants compared to controls, whereas Krt6a was induced and Krt15 was inhibited in mutants. Vinculin (Vin) and β-actin were used to normalize samples.

Next, we tested whether the switch between p63α and p63β had any effects on cell proliferation. by immunostaining cells for the proliferative marker Ki67. The total amount of Ki67-positive cells in p63α-/- skin sections was comparable to wild type skin, thus indicating that cell proliferation is not significantly affected *in vivo* by the switch between p63α and p63β (Figure 24).

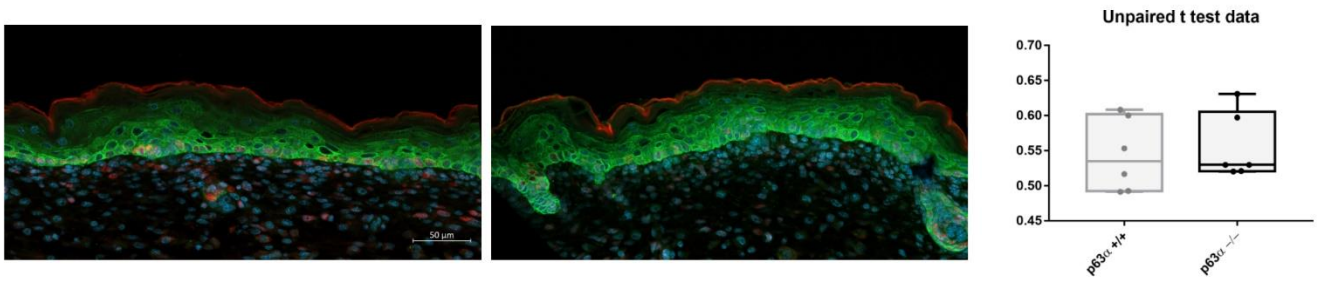

Figure 24. Basal keratinocytes proliferation is not altered in mutant epidermis. Immunofluorescence for Ki67 (red) and E-cad (green) on P0 mutant and wild type epidermis showing no alteration in the proliferation rate of basal keratinocytes. Quantification of Ki67-positive cells in the basal layer of the epidermis (right panel).

Taken together these findings support the hypothesis that the switch between the p63α and p63β isoforms does not affect drastically epidermal development, or epidermal differentiation or the stratification program. Therefore, p63β isoform can in part replace the p63α function and transactivate genes relevant for epidermal commitment during late embryogenesis.

3.5 Mutant embryos show a delay in the formation of the epidermal barrier

To test the functionality of the skin barrier during the last stages of embryonic development, we measured Transepidermal Water Loss (TEWL) and we stained epidermis with and Toluidine Blue in E17.5 and E18.5 mutant and wild type embryos. An impairment in the permeability of the epidermal barrier was detected only in the ventral portion of the skin at E17.5, indicating a mild delay in the formation of a functional skin. At E18.5, the mutant skin was impermeable as in control mice (Figure 25A and B).

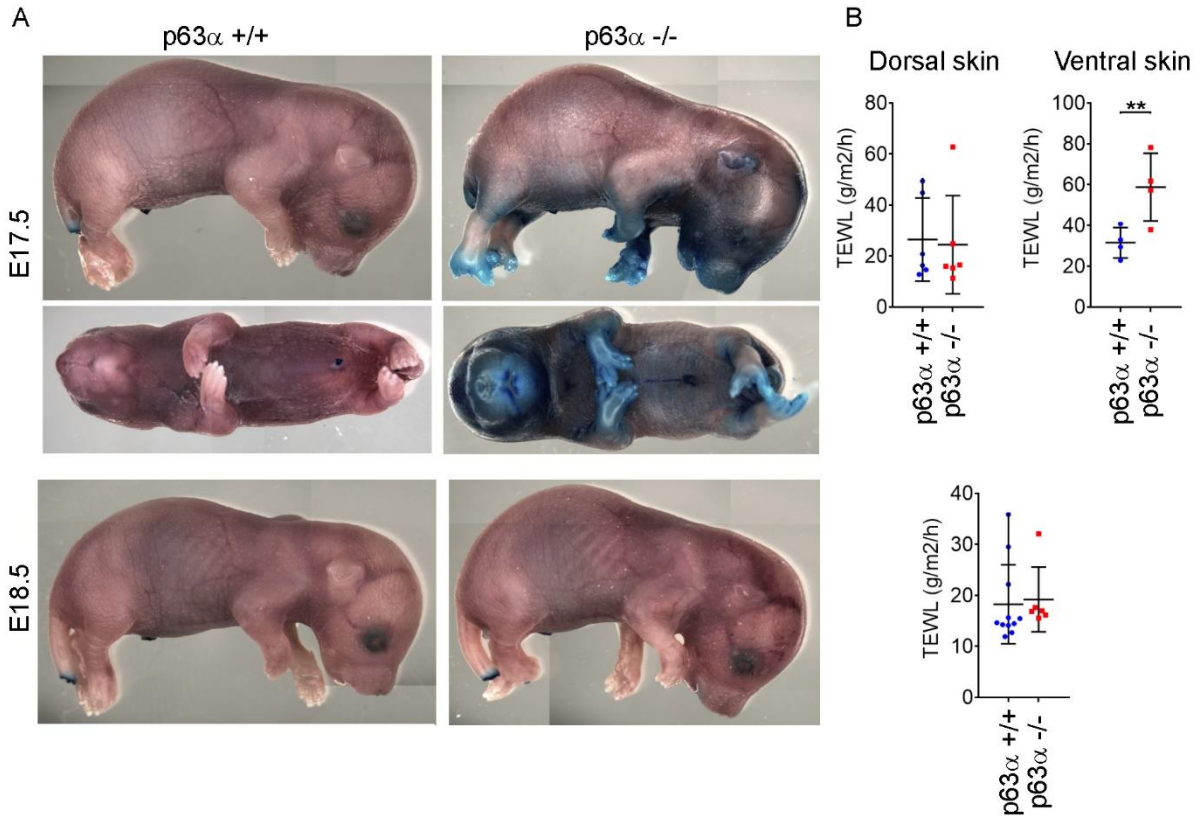

Figure 25. Delayed skin barrier formation in mutants.

A) Toluidine Blue staining. Top panel: E17.5 embryos lateral and ventral skin view; bottom panel: E18.5 embryos. B) TEWL Assay. Top panel left: E17.5 embryos dorsal skin measurement; right: E17.5 embryos ventral skin measurement. Bottom panel: E18.5 embryos dorsal skin measurement.

3.6 p63a deletion does not affect the skin homeostasis after birth

To better characterized the effect of the p63α loss and concomitant induction of p63β in epidermal homeostasis during postnatal development, we crossed the p63α fl/fl mouse already generated with a Krt14-Cre knock-in mouse model (107), in order to obtain a Krt14-Cre;p63α-/- mouse in which the *Cre recombinase* is under the control of a Keratin 14 (Krt14) promoter that is active starting from E17.5 day of embryonic development in stratified epithelia only. At birth, Krt14-Cre;p63α-/- mice were healthy and did not show any limbs or palates malformations as expected. Moreover, skin and its appendages were indistinguishable from the wild type in the adult life (Figure 26).

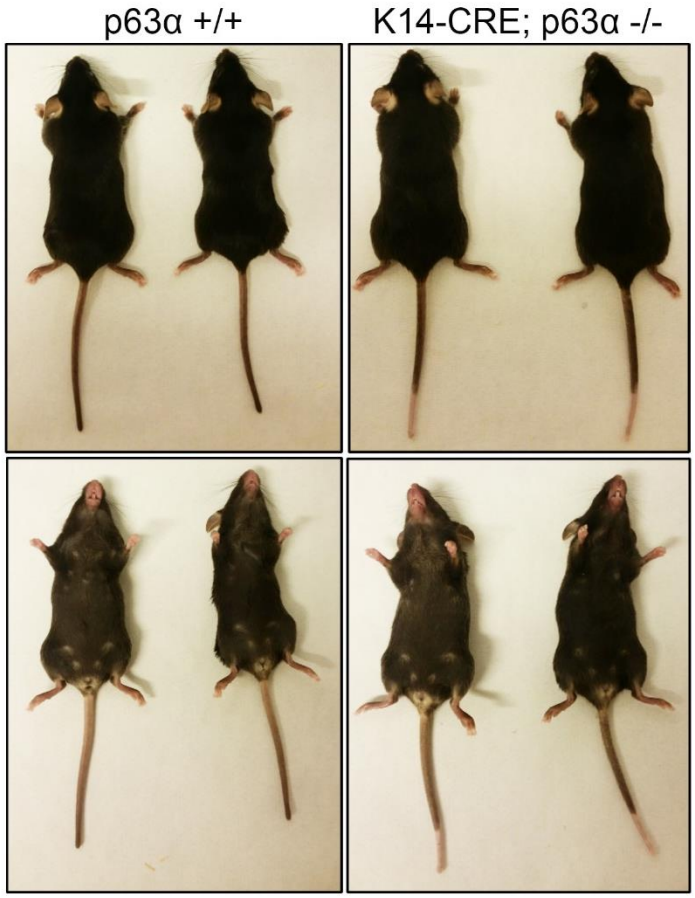

Figure 26. Macroscopic phenotype of Krt14-Cre;p63α-/- mice.

Two months adult Krt14-Cre;p63α-/- showed no skin phenotype compared to wild type.

Similarly, at the histological level skin showed no morphological alterations (Figure 27).

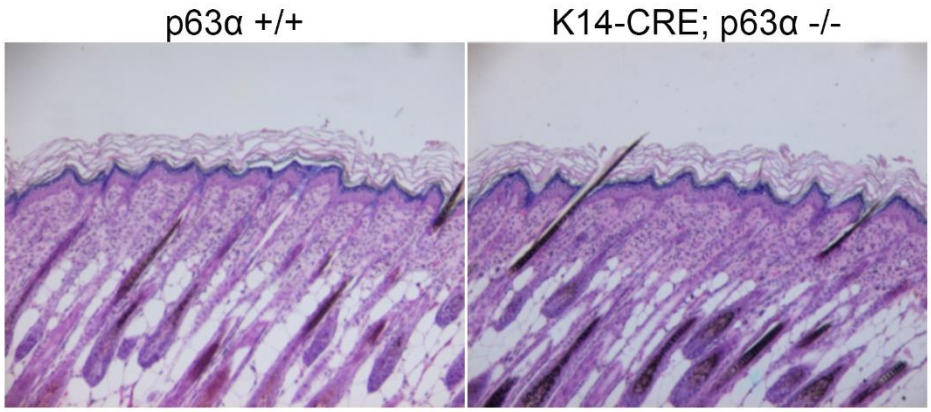

Figure 27. Wild type and mutant epidermis appearance.

Hematoxylin and Eosin staining of wild type and mutant skin section at P5 postnatal day, revealed no morphological differences between them.

Western blot analysis showed the same induction of p63β in K14-Cre;p63α-/- mouse epidermis compared to control as we already observed in p63α-/- mouse (Figure 28).

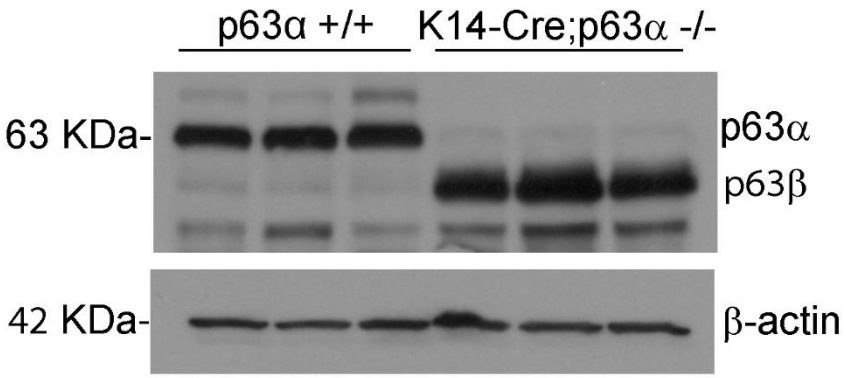

Figure 28. p63α ablation and p63β expression in mutant Krt14-Cre;p63α-/- epidermis protein extracts.

Immunoblotting of proteins extract from P5 skin of Krt14-Cre;p63α-/-mouse and wild type, using a p63 antibody confirmed the expression of p63β-isoform in mutant skin in place of p63α. β-actin was used to normalize samples.

Immunostaining on P0 dorsal skin sections with p63 total and p63α antibodies confirmed the p63α-specific ablation with the concomitant induction of the p63β isoform that we had demonstrated by western blot (Figure 29).

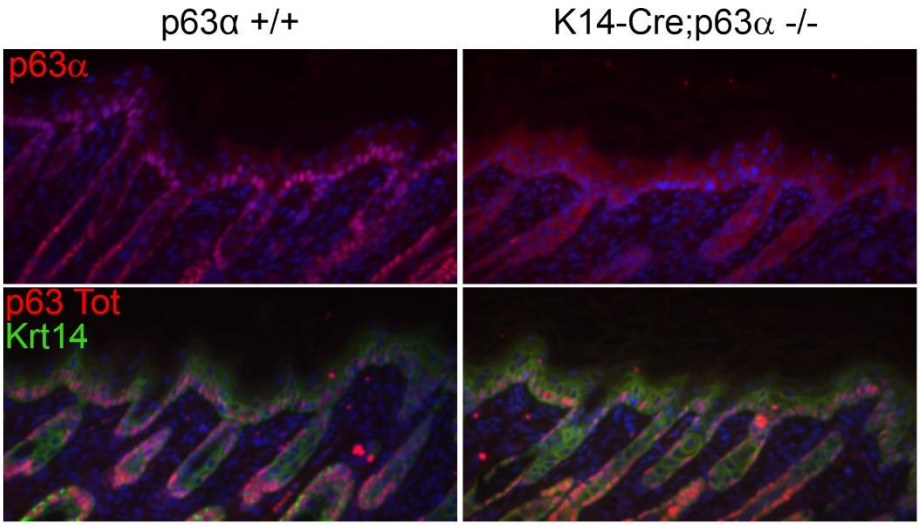

Figure 29. p63α ablation and p63β expression in mutant Krt14-Cre;p63α-/- skin.

Immunofluorescence analysis, using a p63α-specific (red) and a total p63 antibodies (red), of wild type and Krt14-Cre;p63α-/- skin sections confirmed the absence of p63α isoform in Krt14-Cre;p63α-/- mice compared to controls (top panel), while total p63 is revealed in both, wild type and Krt14-Cre;p63α-/- respectively due to the presence of p63β in mutant skin; anti-Krt14 (green) antibody was used to mark the basal layer (bottom panel).

Absence of skin differentiation and cell proliferation defects were observed also verifying the expression of, respectively, Krt6 and Ki67 markers by immunofluorescence analysis on dorsal skin sections at P5 of Krt14-Cre;p63α-/- and control mice. p63α and p63β expressing cells were equally proliferating (Figure 30).

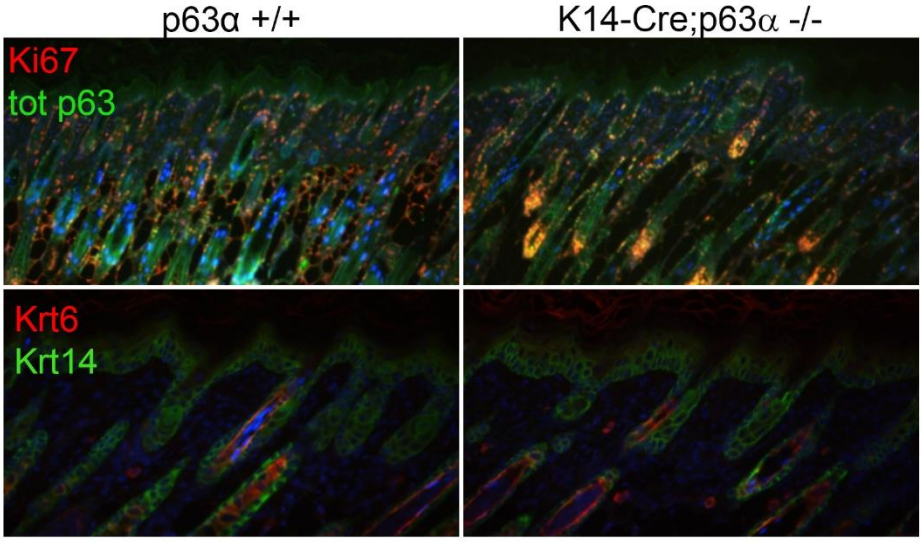

Figure 30. Mutant skin exhibited no alteration in differentiation and proliferation.

Immunofluorescence analysis on P5 skin section using antibodies against Ki67 (red) and total p63 (green), revealed that there is no alteration of Ki67 expression in Krt14-Cre;p63α-/- mice compared to control and also showed that the β isoform is expressed in mutant skin in place of p63α (top panel). Immunofluorescence staining with specific antibodies against Krt6 (red) and Krt14 (green) showed a normal expression of Krt6 in the hair follicles of Krt14-Cre;p63α-/- mice at P5 indicating no alteration of the differentiation program. Krt14 is expressed, as in wild type, in the basal layer of epidermis.

To get deeper insights into the understanding of what was happening at a molecular level and to investigate if any genes had an altered expression pattern at least *in vitro*, we collected mouse keratinocytes from P2 Krt14-Cre;p63α-/- mouse epidermis and grown them to confluence and full maturation for seven days. Subsequently, their RNA was collected and RNA-seq was performed. Transcriptomic analysis confirmed no significant alterations even in cell culture in the absence of any homeostatic signals derived from fibroblasts (data not shown). To test the long-term effect of the deletion of p63α in the skin, Krt14-Cre;p63α-/- and wild type females were kept up to one and half year, however no macroscopic differences were visible between mutant and control littermates (data not shown).

To test the effect of the switch between p63α p63ß under stressful conditions after non physiological stimuli such as *in vivo* injury, we performed wound healing assay on 2 months old control and Krt14-Cre;p63α-/- females. Macroscopic measurements and morphometric analysis of wounds did not show any significant difference in the mean wound size at day 3 (D3) as well as at day 7 (D7) after injury (Figure 31A-B).

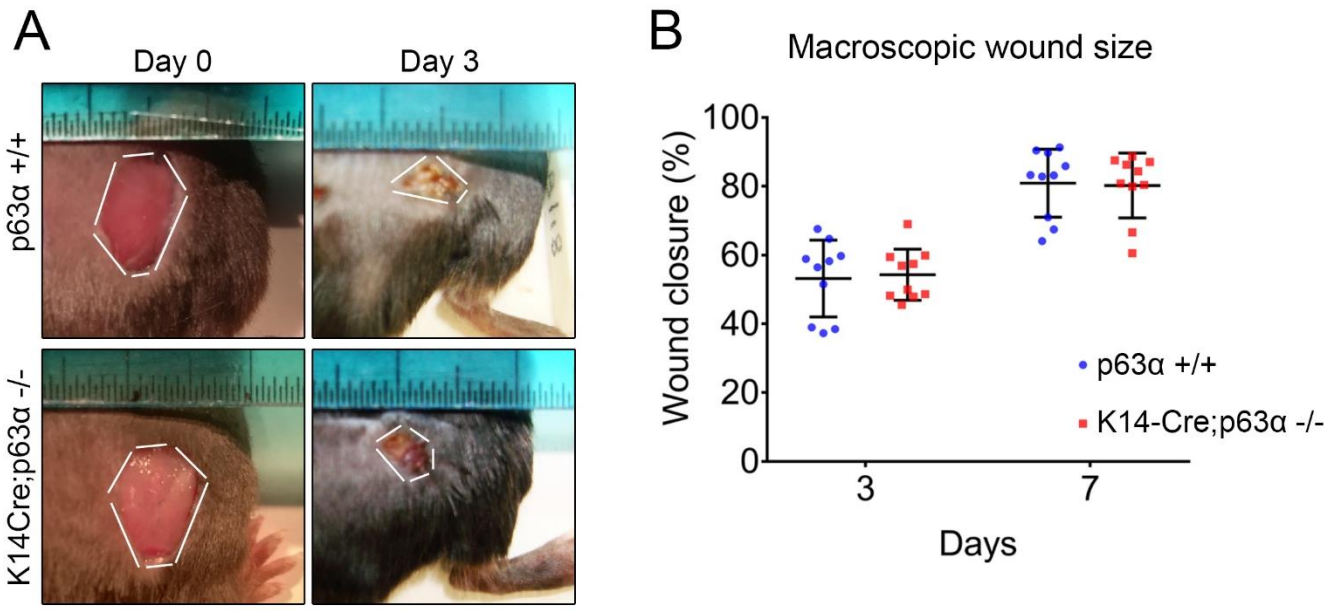

Figure 31. Krt14-Cre;p63α-/- mutants showed no alteration in stemness, migration and healing *in vivo*.

A) Representative macroscopic illustration of wound healing size in p63α +/+ and Krt14-Cre; p63α-/- animals at D0 (day of wound) and D3 (three days after wound). B) Longitudinal macroscopic quantification of individual wound areas at D3 and D7 (seven days after wound) in p63α +/+ and Krt14-Cre;p63α-/- mice in relation to their respective initial size at D0. Data show no significant difference in wound closure both at D3 and D7. (Performed in collaboration with Stefano Sol)

Moreover, we carried out morphometric analyses of histological wound sections stained for Hematoxilyn and Eosin at day 3 and day 7 after wounding (Figure 32A-B). Quantification of the distance of newly formed epidermis covering the wound revealed no difference in wound closure in Krt14-Cre;p63α-/- and control mice at the same time

point (Figure 32C). Likewise, in the absence of p63α isoform, the length of wound closure, the re-epithelization process and the wound width remained unchanged in Krt14-Cre;p63α-/- mutants compared to wild types, suggesting that the substitution of the p63α isoform with p63β isoform did not affect the global wound healing program *in vivo* (Figure 32D-E).

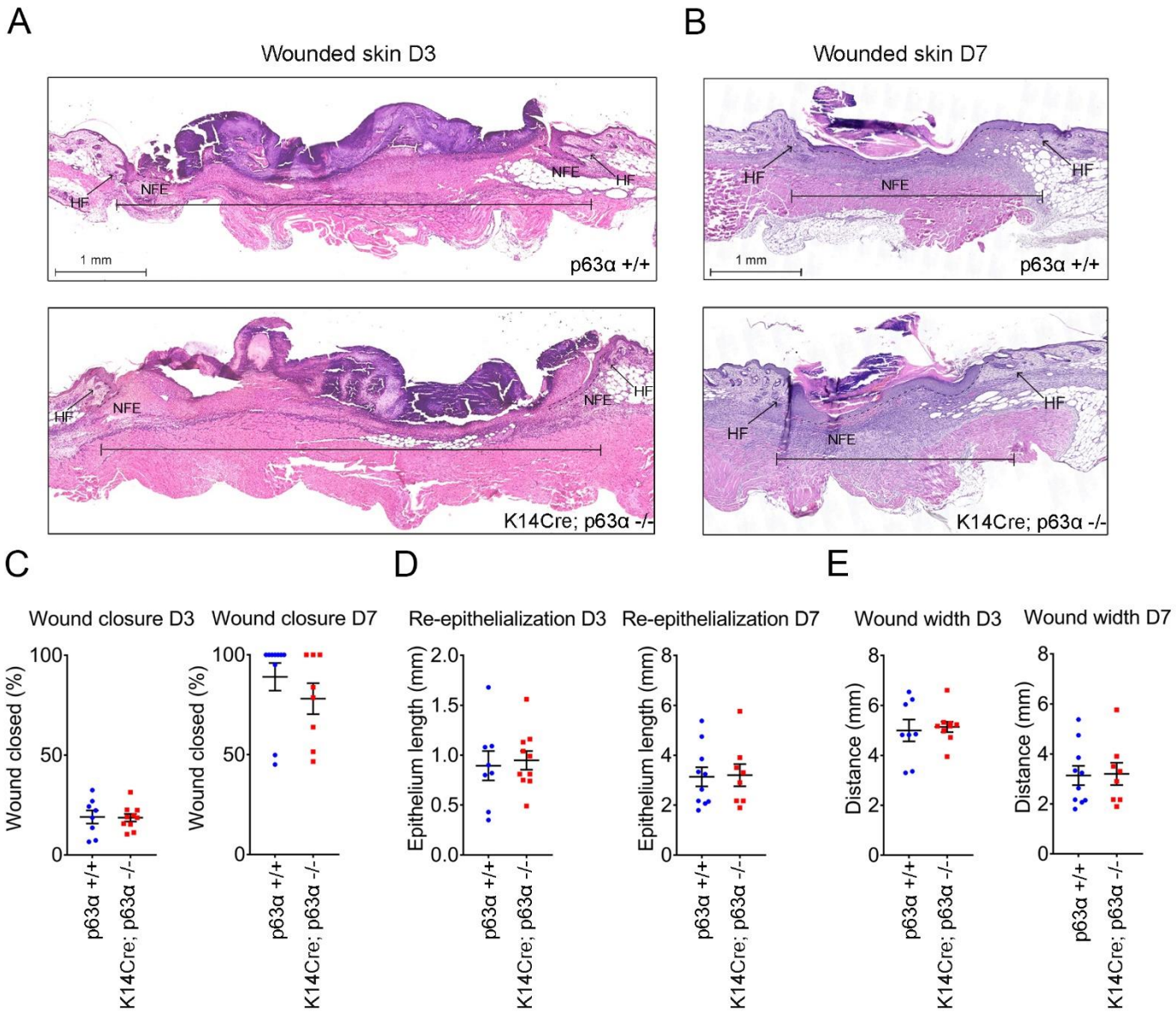

Figure 32. Analysis of *in vivo* Wound healing.

A-B). H&E-stained sections of p63α +/+ and Krt14-Cre; p63α-/- D3 and D7 wounds. NFE: newly formed epithelium; HF: healing front. C) Morphometric analysis of percentage of wound closure (length of newly formed epithelium (NFE)/length of NFE + length of gap between edges of wound epithelium × 100). D) Morphometric analysis of re-epithelialization (length of NFE expressed in millimetres (mm)). E) Morphometric analysis of wound width (distance between wound border HFs (black line in A and B) expressed in millimetres (mm). Scale bars, 1 mm. (Performed in collaboration with Stefano Sol)

In sum, these findings demonstrated that p63β isoform is able, at least after birth and in adulthood, to replace α isoform function without any effects on skin health when it is depleted in stratified epithelia specifically.

3.7 p63β is able to induce epidermal commitment

ΔNp63 is a transcriptional activator for many epidermal genes, and at the same time it can act as a repressor for some non-epidermal genes. Moreover, p63 plays an essential role in regulating enhancer landscape bounding specific keratinocytes enhancer sequences that are nucleosome-enriched in cells where p63 is not expressed (91). It has been previously demonstrated that p63, in concert with Krüppel like factor 4 (KLF4), one of the Yamanaka's factors, is required for inducing an epidermal cell fate and to convert human dermal fibroblast (HDF) that do not express any endogenous p63, into Keratinocytes like cells (iKC) with the consequent expression of typical keratinocyte markers (KRT14, KRT5, DSP, DSC3 etc.) (101, 108). In order to investigate further into the role that ΔNp63β isoform has in the epidermal commitment and skin development in human cells, we tested the ability of the p63β isoform to induce cell conversion of HDF into iKC, using a previously reported protocol (100, 101). In particular, we overexpressed ΔNp63α (as control) or ΔNp63β in HDF in combination with KLF4 either in primary dermal fibroblast (hHDFn) or in an immortalized cell line (HDF-BJ). Ten days after infection and selection with puromycin, morphological changes closely resembling primary keratinocytes were observed in both p63α and p63β infected cells compared to non-infected ones (Figure 33 upper panels). iKCs displayed a more rounded shape and formed colonies similarly to primary keratinocytes grown in culture, in contrast to non-converted cells that retained the typical fibroblast shape characterized by large, flat and elongated cell body with a flat and oval nucleus. Immunofluorescence (Figure 33 mid and bottom panels) and western blot analysis showed that, upon the overexpression of the beta isoform, typical keratinocyte differentiated markers, such as Krt14 and Krt5, were expressed as in p63α expressing fibroblasts (Figure 34A-B).

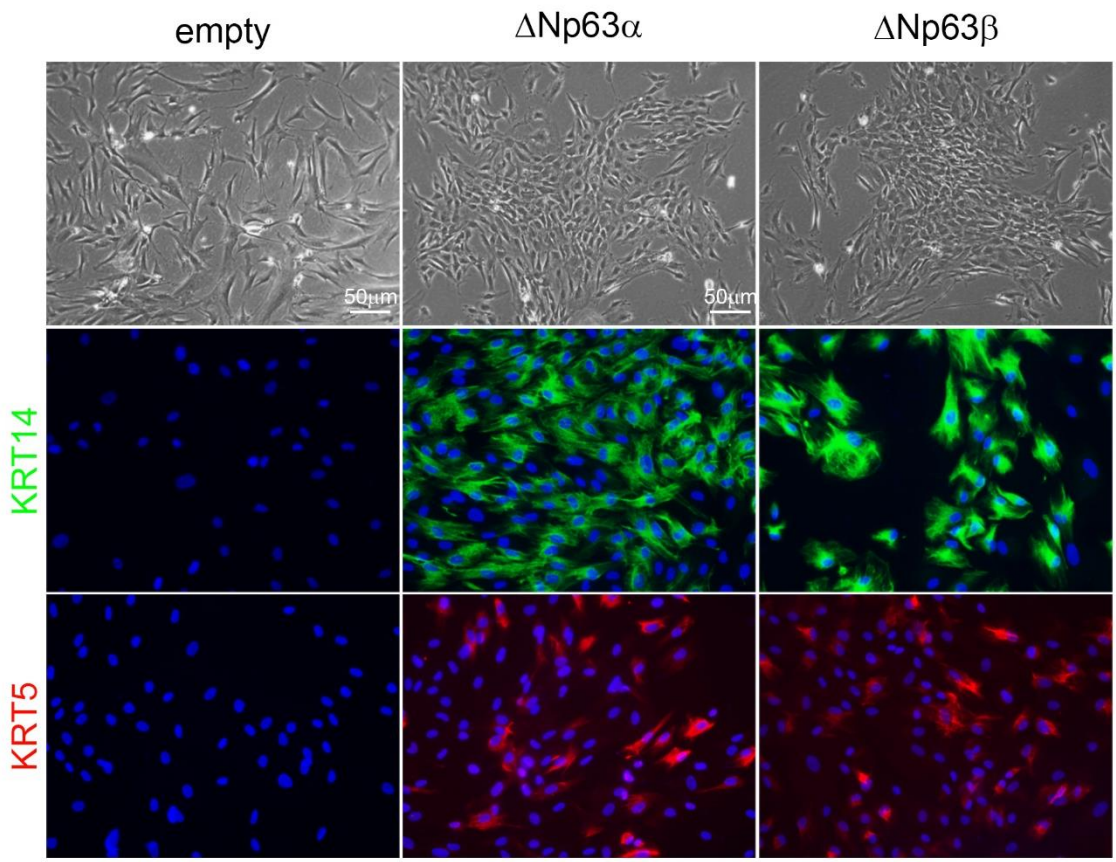

Figure 33. ΔNp63β is able to induce conversion of fibroblast to keratinocytes-like cells *in vitro*. Representative bright field images (top) and immunofluorescence staining using KRT14 and KRT5 specific antibodies (mid and bottom) of converted human fibroblast overexpressing ΔNp63α or ΔNp63β. (Performed in collaboration with Marco Ferniani)

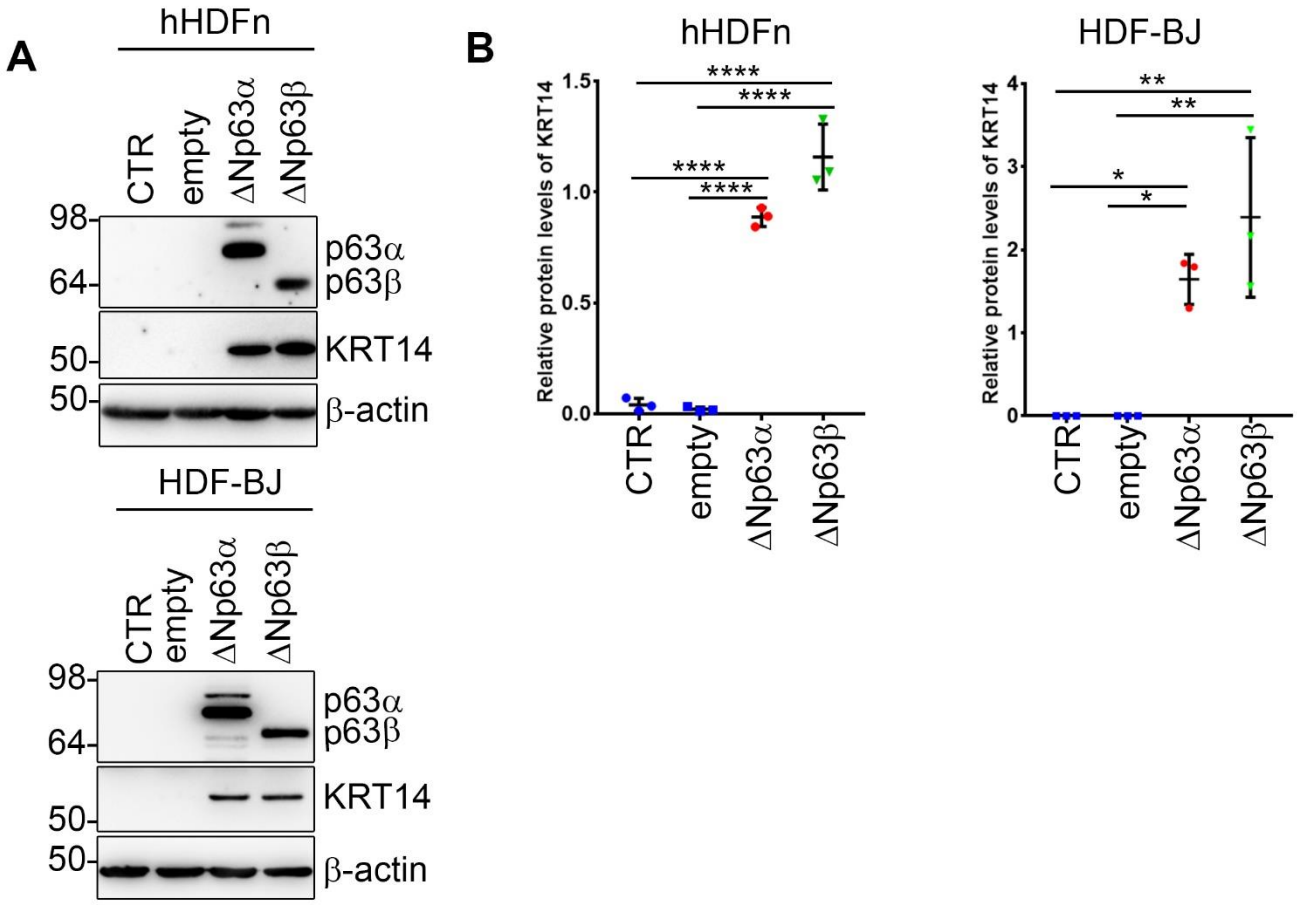

Figure 34. ΔNp63β induce KRT14 expression similarly to ΔNp63α *in vitro*.

A) Western blot on dermal fibroblast (hHDFn upper panel, HDF-BJ lower panel) converted into iKC to identify protein expression of KRT14 upon the transfection of the two different p63 isoforms. B) Relative protein quantification of KRT14 western blot signal showed in A. (Performed in collaboration with Marco Ferniani)

Furthermore, Real Time RT-qPCR analysis of the expression level of two other well characterized p63 target genes, Desmoplakin (DSP) and interferon regulatory factor 6 (IRF6) by Real Time RT-qPCR, showed that ΔNp63β was able to induce the expression of both target at levels compared to ΔNp63α (Fig 35).

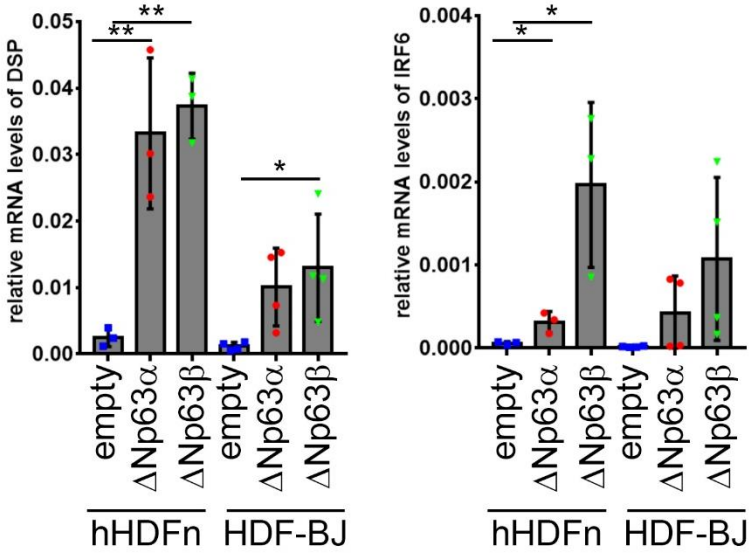

Figure 35. ΔNp63β induce the expression of two p63α known targets.

Real Time RT-qPCR for DSP and IRF6 mRNA expression upon the transfection of ΔNp63α or ΔNp63β constructs. (Performed in collaboration with Marco Ferniani)

Taken together these data demonstrate that ΔNp63β is able to induce epidermal commitment regulating a morphological reorganization and expression of typical epithelial markers similarly to ΔNp63α.

3.8 p63α and p63β bind to different genomic sequences and to a small subset of differentially regulated genes

To explore further the genomic regulatory network differentially generated by p63α and p63β, we performed ChIP-seq analysis using pan-p63 antibodies on primary keratinocytes isolated from P0 epidermis of two wild type and two NLS-Cre;p63α-/- mice. Data analysed on pooled samples, were filtered for Fold of Enrichment (FoE) >7, -LOG10(qvalue) (FDR) >20 resulting in 6473 binding regions for wild type and 12631 for p63α-/- keratinocytes. On these selected regions a genomic region-gene association using GREAT (version 4.0.4) (basal plus extension settings) was performed resulting in 6160 genes associated with p63 binding regions in wild type and 9521 genes for p63α-/-. Among them 5829 genes were associated with binding regions in both wild type and p63α-/-, 3692 mainly in p63α-/- and 331 mainly in wild type (Figure 36A). Gene Ontology analysis indicated that among the most statistically significant Biological Processes regulated by genes bound by both p63β and p63α were epidermis development, hair cycle, hair follicle development, cell junction organization and keratynocyte differention (Figure 36B). To better understand which genes were bound and, in particular, directly regulated in their expression by both and only p63α and p63β, we compared the data obtained from GREAT analysis with genes changing in the RNA-seq performed in E18.5 epidermis (FDR < 0.05). 252 genes that significantly changed in the RNA-seq were in common with wild type ChIP-seq and 330 with ChIP-seq performed in the p63α-/- (Figure 36C).

A

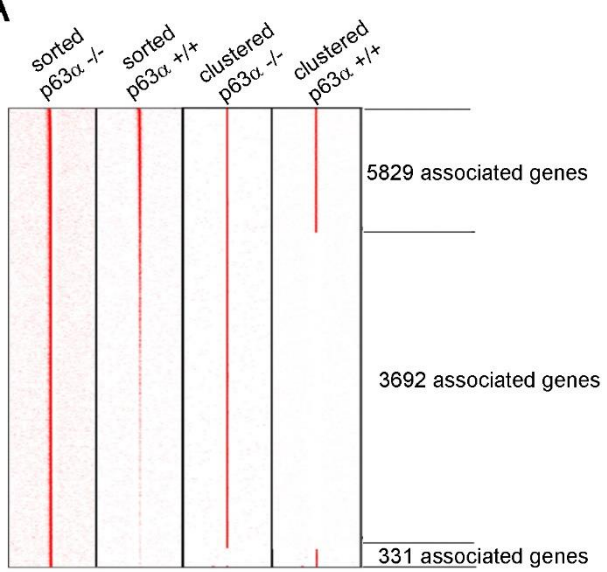

B

Genes associated with p63α -/-

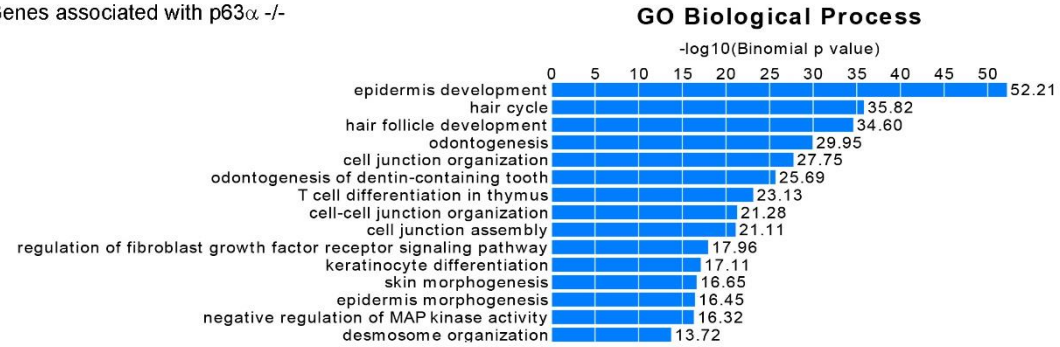

Genes associated with p63α +/+

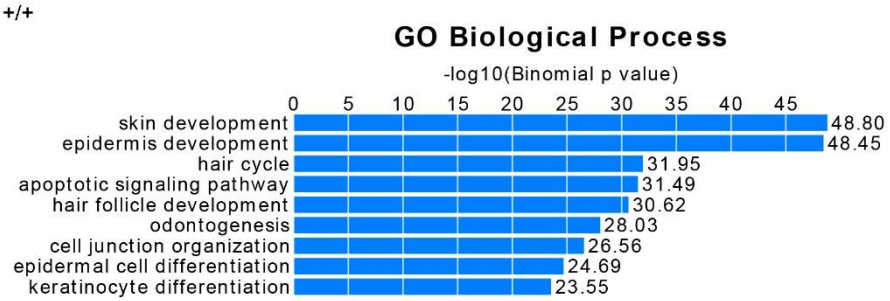

C

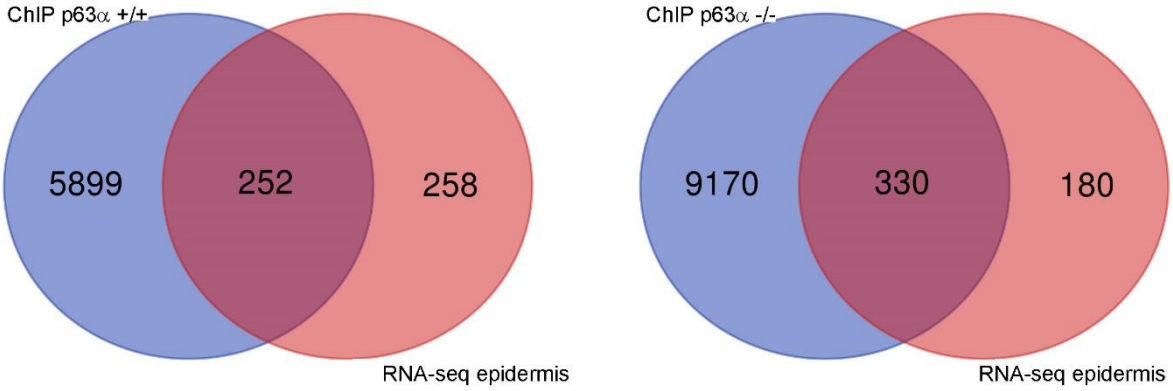

Figure 36. p63 ChIP-seq analysis.

A) Graphic rappresentation of differentially bound genomic regions by p63α and p63β. On the right number of regions associated with genes in both p63α +/+ and and p63-/- epidermis. B) GREAT Gene Function Annotation of associated genes resulted from p63-/- (top panel) and p63α +/+ (bottom panel) ChIP-seq. C) Venn Diagram showing comparative analysis between the p63 ChIP-seq performed in P0 mouse epidermis and the RNA-seq performed on E18.5 epidermis to identify directly bound and regulated genes.

Among them only 3 genes resulted to be directly bound and regulated by p63α (Sphk1, Tnf and Klk9), whereas 81 genes were unique targets of p63β, and 249 genes were bound and regulated by both variants (Figure 37A). In particular Sphk1 and Klk9 were downregulated, whereas Tnf upregulated indicating that for the first two genes p63β was not able to compensate the absence of p63α isoform and for Klk9 it allowed and induced its expression more than p63α did. Moreover genes differetially regulated and bound by both isoforms are mainly involved in the regulation of the MAPK cascade, extracellular matrix organization, skin development and positive regulation of cell death (Figure 37B). To get further on the role that p63β exerts in specifically regulating the gene network landscape in the epidermis, we investigated on the biological processes that involved the 81 genes direct targets of beta only. Among them 15 genes were upregulated and 66 were downregulated. Performing a Gene Ontology analysis on these differentially regulated p63β targtet genes, it resulted that among upregulated genes there were no particularly significant processes, whereas among downregulated we found enrichment in process such as extracellular matrix organization, positive regulation of cell migration, regulation of cell substrate adhesion and extracellular matrix assembly (Figure 37C), thus partially confirming that probably mutant keratinocytes were characterized by an impairment in the general migration program that is exerted by a constant renewal of cell-matrix and cell-cell interactions. We then analyzed the top 1000 peaks, sorted by Pile Up, enriched in ChIP-seq from p63 wild-type and p63α-/- keratinocytes, or those present in both, taking into consideration the peak summits +/- 50bp, to find differences in DNA binding motifs (Figure 37D). This analysis allowed the identification of a p53/p63/p73 and Smad3 motifs in all three categories. Motifs enriched in ChIP-seq derived from p63 mutant keratinocytes included Klf5 and Klf16 (Figure 37E).

A

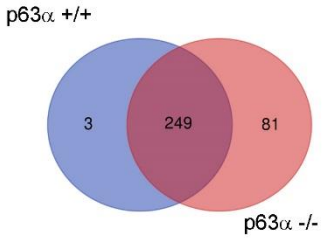
p63α +/+
3
249
81
p63α -/-

B

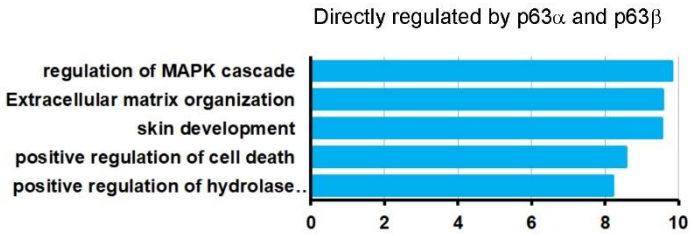
Directly regulated by p63α and p63β
regulation of MAPK cascade
Extracellular matrix organization
skin development
positive regulation of cell death
positive regulation of hydrolase..
0
2
4
6
8
10

C

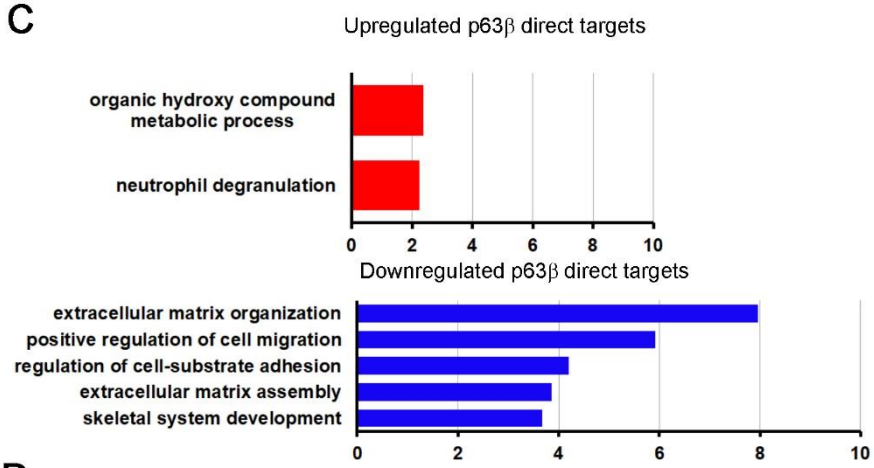
Upregulated p63β direct targets
organic hydroxy compound metabolic process
neutrophil degranulation
0
2
4
6
8
10
Downregulated p63β direct targets
extracellular matrix organization
positive regulation of cell migration
regulation of cell-substrate adhesion
extracellular matrix assembly
skeletal system development
0
2
4
6
8
10

D

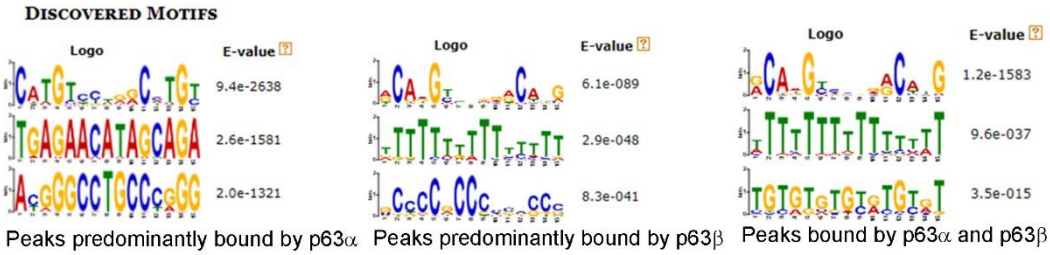
DISCOVERED MOTIFS
Logo
E-value
9.4e-2638
2.6e-1581
2.0e-1321
Peaks predominantly bound by p63α
Logo
E-value
6.1e-089
2.9e-048
8.3e-041
Peaks predominantly bound by p63β
Logo
E-value
1.2e-1583
9.6e-037
3.5e-015
Peaks bound by p63α and p63β

E

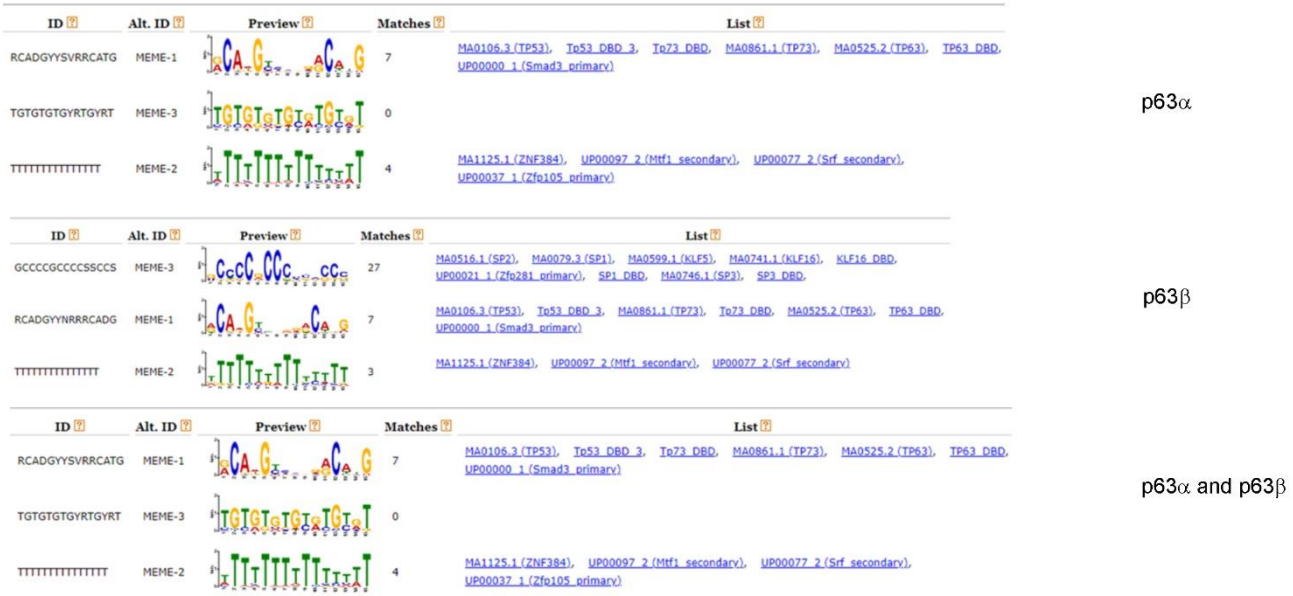
ID
Alt. ID
Preview
Matches
List
RCADGYYSVRRCATG
MEME-1
7
MA0106.3 (TP53), Tp53_DBD_3, Tp73_DBD, MA0861.1 (TP73), MA0525.2 (TP63), TP63_DBD, UP00000_1 (Smad3_primary)
TGTGTGTGYRTGYRT
MEME-3
0
TTTTTTTTTTTTTTT
MEME-2
4
MA1125.1 (ZNF384), UP00097_2 (Mtf1_secondary), UP00077_2 (Srf_secondary), UP00037_1 (Zfp105_primary)
p63α
ID
Alt. ID
Preview
Matches
List
GCCCCGCCCCSSCCS
MEME-3
27
MA0516.1 (SP2), MA0079.3 (SP1), MA0599.1 (KLF5), MA0741.1 (KLF16), KLF16_DBD, UP00021_1 (Zfp281_primary), SP1_DBD, MA0746.1 (SP3), SP3_DBD,
RCADGYYNRRRCADG
MEME-1
7
MA0106.3 (TP53), Tp53_DBD_3, MA0861.1 (TP73), Tp73_DBD, MA0525.2 (TP63), TP63_DBD, UP00000_1 (Smad3_primary)
TTTTTTTTTTTTTTT
MEME-2
3
MA1125.1 (ZNF384), UP00097_2 (Mtf1_secondary), UP00077_2 (Srf_secondary)
p63β
ID
Alt. ID
Preview
Matches
List
RCADGYYSVRRCATG
MEME-1
7
MA0106.3 (TP53), Tp53_DBD_3, Tp73_DBD, MA0861.1 (TP73), MA0525.2 (TP63), TP63_DBD, UP00000_1 (Smad3_primary)
TGTGTGTGYRTGYRT
MEME-3
0
TTTTTTTTTTTTTTT
MEME-2
4
MA1125.1 (ZNF384), UP00097_2 (Mtf1_secondary), UP00077_2 (Srf_secondary), UP00037_1 (Zfp105_primary)
p63α and p63β

Figure 37. Putative p63α and p63β direct targets and consensus sequence identification.

A)Venn diagram showing intersected genes among p63α and p63β directly regulated genes. B) Gene Ontology analysis performed on direct target genes differentially regulated from both p63α and p63β. C) Gene Ontology analysis performed on upregulated (top panel) and downregulated (bottom panel) direct target genes of p63β resulted from the intersection between mKer ChIP-seq and RNA-seq in epidermis. D) Motif-based sequence analysis (MEME) of top 1000 p63α (left panel), p63β (mid panel) and both p63α and p63β (right panel) peaks. D) TomTom analysis, a tool used to identify known binding motifs, performed on motifs discovered from previous MEME analysis for p63α (top panel), p63β (mid panel) and both p63α and p63β (bottom panel).

3.9 Direct p63α targets loss can partially explain the etiogenesis of limb and skin phenotype observed in p63α-/- mouse model

To identify specific p63α direct target genes involved in the etiogenesis of already known limb or skin diseases, we performed EnrichR analysis (Orphanet and OMIM sections) on ChIP-seq data intersected with RNA-seq results from E12.5 limbs and epidermis to identify genes that could be directly involved in the development of the mutant phenotype observed in our model. First, we analysed genes resulting from the intersection between p63α +/+ or p63α-/- ChIP-seq and RNA-seq in hindlimbs. Among p63α +/+ specific direct targets expressed in the Apical Ectodermal Ridge (AER) during embryogenesis (109), we found statistically significant results for Engrailed 1 (En1) and Secreted frizzled-related protein 1 (Sfrp1) both involved in Split hand-split foot-deafness syndrome (SHFM) (Figure 38A). As previously observed from ISH and RNA-seq analysis, in p63α-/- limbs En1 is downregulated, and similarly to mouse models of En1 loss of function (104, 110-113), malformations resulted in truncation or fusion of digits, in some cases involving bone fusion, even with a variability in which digits and bones were fused. Sfrp1 is also known to be a Wnt antagonist that regulates the anteroposterior (AP) pattern in murine limb development. Deletion of Sfrp1 in mice do not lead to a relevant digit phenotype because of its functional redundancy with Sfrp2 during embryonic development (114).

The same approach was used to investigate on p63α direct targets in epidermis that can cause the mild alterations found in p63α-/- epidermis. Among direct target genes of p63α +/+ and p63α-/- in the epidermis, Laminin subunit gamma-2 (Lamc2), Laminin subunit alpha-3 (Lama3), Laminin subunit beta-3 (Lamb3) and Collagen alpha-1(XVII) chain (Col17a1) were found to be upregulated in p63α-/- epidermis and significantly involved in the etiogenesis of Epidermolysis Bullosa (Figure 38B-C); in affected patients common signs of the disease are blistering and alterations in cell adhesion (115-117). This latter process was found to be impaired in p63α-/- mice from RNA-seq analysis in epidermis, in particular Laminin genes are already known to be involved in keratinocyte migration and their structural organization (118-120) wheras Col17a1 is important for epidermal development (121) and adhesion between cells and with the matrix (117, 122).

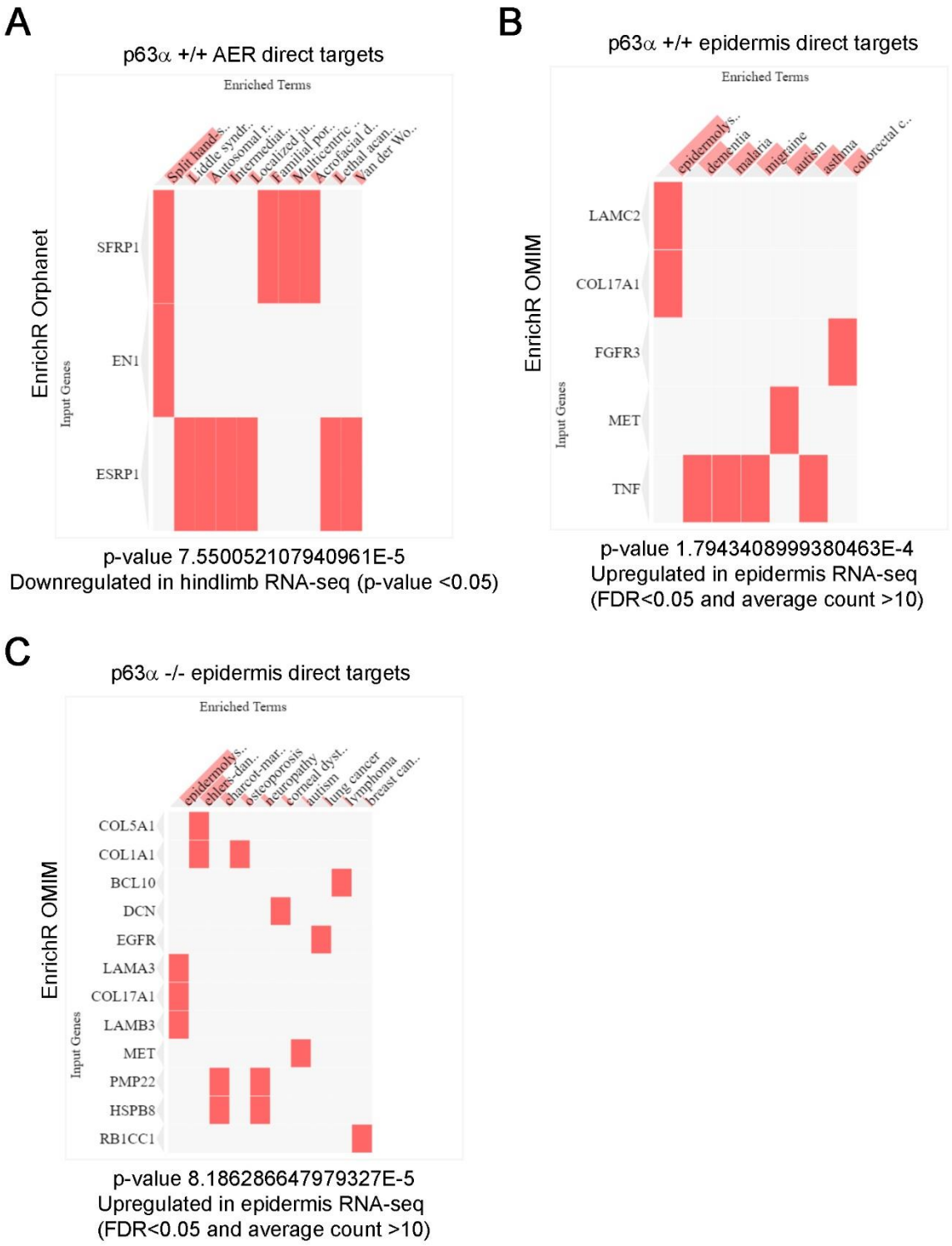

Figure 38. EnrichR analysis on putative p63β direct targets.

A) EnrichR analysis in Orphanet section on p63a +/+ direct target expressed in the Apical Ectodermal Ridge. B) EnrichR analysis in OMIM section on p63a +/+ direct target expressed in the epidermis. C) EnrichR analysis in OMIM sectio on p63a -/- direct target expressed in the epidermis.

4. DISCUSSION

The role of p63 and, more specifically, of the ΔNp63 isoform in stratified epithelia has been extensively characterized. In contrast, the specific functions of the C-terminal isoforms are less understood. By far the most abundant isoform in the epidermis is the ΔNp63α. Importantly, mutations in the C-terminal domain, unique to the p63α, can cause severe skin erosions typically found in AEC syndrome patients and mice (27, 45). To better understand the specific contribution of the p63α isoform in development, we generated the p63α knock-out mouse. Differently from other previously generated p63 deficient mice, the strategy we used of exon 13 deletion led to the expression of only p63β in place of p63α, with an overall similar amount of p63 total protein being expressed, leaving also p63γ isoforms unaltered. This mouse model revealed the p63α isoform is pivotal for the early stages of mouse embryonic development: in particular it is essential for proper digits formation whereas it is dispensable for development of the proximal limb structures, and ensures the correct fusion and closure of the palatal shelves avoiding cleft-palate. In the skin, but also in limbs and palates, deletion of p63α does not affect cell proliferation. Keratinocyte differentiation and cell adhesion program seem to be mildy affected as the p63β is able to upregulate cytoskeletal and cell-junction genes possibly causing an impairment in cell-cell and cell-matrix adhesion thus interfering with migration and leading to a delay in skin barrier formation and periderm migration.

To specifically support this latter hypotesis, it is important to know that during palate and limb development, and more generally in tissue development of the entire embryo, starting from E9 to E17, the periderm, composed of a single layer of flattened cells, prevents premature adhesion between opposing epithelia avoiding pathological adhesions between differentiating epithelial tissues that should remain spatially separated (30, 32, 123). Its specific characteristic is the expression of cell-cell adhesion complex molecules, in particular tight junction proteins, strongly expressed and polarized on the basolateral side and absent apically. This aspect, together with a proper morphology, is essential, when the periderm has completed its task, to ensure its removal from the underlying differentiated epithelium through active migration (30). In this work, mutant palatal peridermal cells acquire a more rounded morphology and, moreover, RNA-seq performed in palatal shelves and limbs displayed an upregulation not only of epidermal cell-cell adhesion molecules such as Dsp, Dsc3 and Dsg2 but, interestingly, also of Grhl3, while in mutant skin its expression is not

altered. Grhl3 is an important transcription factor involved in development, migration and correct formation of the epithelial barrier. It is a downstream target of Irf6 signalling and when its function is impaired cleft-palate and digits syndactyly occur (34, 124). Together these transcriptomic results can at least partially explain the phenotypical malformation observed in p63α-/- model.

Our hypothesis is that the cleft palate may be due to a failure of the periderm in its non-adhesive function caused by an altered cell morphology and in the ability of cell to migrate from the basal layer outwards, caused by overexpression of desmosomes that interfere with the migration program making it slower. These two aspects could lead to non-physiological tissues fusion between jaws that delay the complex series of events that lead to palate juxtaposition and their fusion may be impaired by a persistence of the periderm in the midline epithelial seam (MES) when it must migrate out enabling fusion and preventing cleft palate. It is already known that p63 is involved in the formation of a functional periderm and in its essential maintenance, it regulates cell adhesion network repressing the formation of tight junction in palatal epithelia; moreover its degradation, induced by Tgfβ3, in the medial edge epithelia (MEE) of the palatal shelves, is fundamental to ensure a correct periderm migration out of the midline epithelial seam (MES) (31). In p63α-/- palatal tissues it is possible to observe an induction of p63 itself; this aspect can add to an overall obstruction of shelves fusion. Generally, the migration process carried out by a fine regulation of the cell-cell and cell-matrix adhesion programs could be altered in part by an abnormal expression of adhesion component and migration regulators in mutant periderm and in the basal layer of the p63α-/- palatal epithelia.

Looking at digit alterations, it is already known that p63 is essential in limb development as its total depletion leads to complete absence of fore- and hindlimb structures with a drastic decrease of limbal progression main drivers such as Shh and Fgf8 (16, 17). Moreover, when p63 is specifically deleted in the AER, distal limbal elements do not develop (28). Here, we show that p63β can replace the α function in the formation of stylopode and zeugopode structures but for proper digit development p63α is strictly necessary. Indeed, our data show that p63β can support Shh expression and partially sustain Fgf8 signalling, that in part is still carried on by ΔNp63γ (28), even if at slightly lower levels and with a dotted localization domain. The switch of p63α with p63β seems to have no effect on the apoptosis. Moreover, we observed an absence of Dusp6 RNA in p63α-/- limbal mesoderm; this protein is normally induced by FGF signalling and inhibits phosphorylation of ERK (phosphor-ERK) (125). Its

decrease in mutants could be partially due to an absence of Fgfr2b, already proved to be a p63 direct target gene (27), that alters the response to Fgf8 signalling and, thus, may result in a general upregulation of phospho-ERK in the mesoderm leading to activation of genes that induce cytoskeletal protein expression probably altering their morphology and also their proliferation program. From E11.5 ISH results and transcriptomic analysis at E12.5 in hindlimbs coupled with ChIPseq, we demonstrated that En1 is a direct target of p63α in the AER. Accordingly, it is known to be essential for ventral patterning spatially regulating Wnt7a expression (104), En1 -/- mice show syndactyly and/or polydactyly in both fore- and hindlimbs (126, 127) similarly to p63α-/- reported malformations.

On skin development and general health, we did not observe a pathological phenotype. TEWL and Toluidine blue data from ventral skin indicate that there is a persistence of non-differentiated epidermis in mutants at E17.5 which resolves at E18.5. This phenotype could be partially explained by a slower migration in mutant periderm at E17.5 when it must disappear, from dorsal to ventral, leaving an underlying well-differentiated epidermis. This hypothesis could be supported by epidermal RNA-seq results that show an overexpression of tight junction components that, as happen in palate and limbs, could slow down the general process of migration of p63α-/- peridermal cells and, at E18.5, when the periderm has finished its migration, it has enough time to disappears in both mutants and wild types leaving a complete functional skin barrier.

To explain possible distinct functions exerted by p63α and p63β, here we demonstrate that when p63α is depleted during late embryogenesis, at E17.5, no limbs, palate or skin phenotype is observed, also at a molecular level. This absence of malformations can be in part undestood if we start from the assumption that at this developmental stage, the periderm has already completed its task without encountering obstacles. Moreover, looking at the ability of both isoforms to bind the DNA, it is clear that similarly to p63α, p63β is able to carry out an almost proper epidermal keratinocytes differentiation program binding many DNA regulatory elements that are also bound by p63α. This is possible because they share the same DNA binding domain but what differs between them is the absence of the SAM and TID domains in the p63β protein. This can lead to the hypotesis that, if there will be a difference between them, at least during embrionic development, it is not ascribable to a different genome binding landscape, but, more likely, it could be due to a difference in the interaction patterns with co-factors that are important for the transcriptional activation or repression of p63

target genes. In this perspective, the SAM and TID domains present in the p63α isoform, and their protein-protein interactions, are primarly necessary and non-replaceable in early stages of mouse embryo formation. When embryonic development is completed, p63β is able to substitute p63α function thanks to its ability to bind many similar regulatory elements in keratinocytes.

5. REFERENCES

1. Pozzi S, Zambelli F, Merico D, Pavesi G, Robert A, Maltere P, et al. Transcriptional network of p63 in human keratinocytes. *PloS one.* 2009;4(3):e5008.
2. Soares E, and Zhou H. Master regulatory role of p63 in epidermal development and disease. *Cellular and molecular life sciences : CMLS.* 2018;75(7):1179-90.
3. Dohn M, Zhang S, and Chen X. p63alpha and DeltaNp63alpha can induce cell cycle arrest and apoptosis and differentially regulate p53 target genes. *Oncogene.* 2001;20(25):3193-205.
4. Antonini D, Rossi B, Han R, Minichiello A, Di Palma T, Corrado M, et al. An autoregulatory loop directs the tissue-specific expression of p63 through a long-range evolutionarily conserved enhancer. *Molecular and cellular biology.* 2006;26(8):3308-18.
5. Antonini D, Sirico A, Aberdam E, Ambrosio R, Campanile C, Fagoonee S, et al. A composite enhancer regulates p63 gene expression in epidermal morphogenesis and in keratinocyte differentiation by multiple mechanisms. *Nucleic acids research.* 2015;43(2):862-74.
6. Pitzius S, Osterburg C, Gebel J, Tascher G, Schafer B, Zhou H, et al. TA*p63 and GTAp63 achieve tighter transcriptional regulation in quality control by converting an inhibitory element into an additional transactivation domain. *Cell death & disease.* 2019;10(10):686.
7. Mangiulli M, Valletti A, Caratozzolo MF, Tullo A, Sbisa E, Pesole G, et al. Identification and functional characterization of two new transcriptional variants of the human p63 gene. *Nucleic acids research.* 2009;37(18):6092-104.
8. Yang A, Kaghad M, Wang Y, Gillett E, Fleming MD, Dotsch V, et al. p63, a p53 homolog at 3q27-29, encodes multiple products with transactivating, death-inducing, and dominant-negative activities. *Molecular cell.* 1998;2(3):305-16.
9. Ghioni P, Bolognese F, Duijf PH, Van Bokhoven H, Mantovani R, and Guerrini L. Complex transcriptional effects of p63 isoforms: identification of novel activation and repression domains. *Molecular and cellular biology.* 2002;22(24):8659-68.
10. Serber Z, Lai HC, Yang A, Ou HD, Sigal MS, Kelly AE, et al. A C-terminal inhibitory domain controls the activity of p63 by an intramolecular mechanism. *Molecular and cellular biology.* 2002;22(24):8601-11.
11. Straub WE, Weber TA, Schafer B, Candi E, Durst F, Ou HD, et al. The C-terminus of p63 contains multiple regulatory elements with different functions. *Cell death & disease.* 2010;1:e5.
12. Suh EK, Yang A, Kettenbach A, Bamberger C, Michaelis AH, Zhu Z, et al. p63 protects the female germ line during meiotic arrest. *Nature.* 2006;444(7119):624-8.
13. Kerr JB, Hutt KJ, Michalak EM, Cook M, Vandenberg CJ, Liew SH, et al. DNA damage-induced primordial follicle oocyte apoptosis and loss of fertility require TAp63-mediated induction of Puma and Noxa. *Molecular cell.* 2012;48(3):343-52.
14. Santos-Pereira JM, Gallardo-Fuentes L, Neto A, Acemel RD, and Tena JJ. Pioneer and repressive functions of p63 during zebrafish embryonic ectoderm specification. *Nature communications.* 2019;10(1):3049.
15. Kouwenhoven EN, Oti M, Niehues H, van Heeringen SJ, Schalkwijk J, Stunnenberg HG, et al. Transcription factor p63 bookmarks and regulates dynamic enhancers during epidermal differentiation. *EMBO reports.* 2015;16(7):863-78.
16. Yang A, Schweitzer R, Sun D, Kaghad M, Walker N, Bronson RT, et al. p63 is essential for regenerative proliferation in limb, craniofacial and epithelial development. *Nature.* 1999;398(6729):714-8.
17. Mills AA, Zheng B, Wang XJ, Vogel H, Roop DR, and Bradley A. p63 is a p53 homologue required for limb and epidermal morphogenesis. *Nature.* 1999;398(6729):708-13.
18. Mikkola ML. p63 in skin appendage development. *Cell cycle.* 2007;6(3):285-90.
19. Laurikkala J, Mikkola ML, James M, Tummers M, Mills AA, and Thesleff I. p63 regulates multiple signalling pathways required for ectodermal organogenesis and differentiation. *Development.* 2006;133(8):1553-63.

20. Moon AM, and Capecchi MR. Fgf8 is required for outgrowth and patterning of the limbs. *Nature genetics.* 2000;26(4):455-9.
21. Lewandoski M, Sun X, and Martin GR. Fgf8 signalling from the AER is essential for normal limb development. *Nature genetics.* 2000;26(4):460-3.
22. Kouwenhoven EN, van Heeringen SJ, Tena JJ, Oti M, Dutilh BE, Alonso ME, et al. Genome-wide profiling of p63 DNA-binding sites identifies an element that regulates gene expression during limb development in the 7q21 SHFM1 locus. *PLoS genetics.* 2010;6(8):e1001065.
23. Lo Iacono N, Mantero S, Chiarelli A, Garcia E, Mills AA, Morasso MI, et al. Regulation of Dlx5 and Dlx6 gene expression by p63 is involved in EEC and SHFM congenital limb defects. *Development.* 2008;135(7):1377-88.
24. Lizarraga G, Ferrari D, Kalinowski M, Ohuchi H, Noji S, Kosher RA, et al. FGFR2 signaling in normal and limbless chick limb buds. *Developmental genetics.* 1999;25(4):331-8.
25. Xu X, Weinstein M, Li C, Naski M, Cohen RI, Ornitz DM, et al. Fibroblast growth factor receptor 2 (FGFR2)-mediated reciprocal regulation loop between FGF8 and FGF10 is essential for limb induction. *Development.* 1998;125(4):753-65.
26. Gorivodsky M, and Lonai P. Novel roles of Fgfr2 in AER differentiation and positioning of the dorsoventral limb interface. *Development.* 2003;130(22):5471-9.
27. Ferone G, Thomason HA, Antonini D, De Rosa L, Hu B, Gemei M, et al. Mutant p63 causes defective expansion of ectodermal progenitor cells and impaired FGF signalling in AEC syndrome. *EMBO Mol Med.* 2012;4(3):192-205.
28. Kawata M, Taniguchi Y, Mori D, Yano F, Ohba S, Chung UI, et al. Different regulation of limb development by p63 transcript variants. *PloS one.* 2017;12(3):e0174122.
29. McDade SS, Henry AE, Pivato GP, Kozarewa I, Mitsopoulos C, Fenwick K, et al. Genome-wide analysis of p63 binding sites identifies AP-2 factors as co-regulators of epidermal differentiation. *Nucleic acids research.* 2012;40(15):7190-206.
30. Richardson RJ, Hammond NL, Coulombe PA, Saloranta C, Nousiainen HO, Salonen R, et al. Periderm prevents pathological epithelial adhesions during embryogenesis. *The Journal of clinical investigation.* 2014;124(9):3891-900.
31. Richardson R, Mitchell K, Hammond NL, Mollo MR, Kouwenhoven EN, Wyatt ND, et al. p63 exerts spatio-temporal control of palatal epithelial cell fate to prevent cleft palate. *PLoS genetics.* 2017;13(6):e1006828.
32. Hammond NL, Dixon J, and Dixon MJ. Periderm: Life-cycle and function during orofacial and epidermal development. *Seminars in cell & developmental biology.* 2019;91:75-83.
33. Thomason HA, Zhou H, Kouwenhoven EN, Dotto GP, Restivo G, Nguyen BC, et al. Cooperation between the transcription factors p63 and IRF6 is essential to prevent cleft palate in mice. *The Journal of clinical investigation.* 2010;120(5):1561-9.
34. Peyrard-Janvid M, Leslie EJ, Kousa YA, Smith TL, Dunnwald M, Magnusson M, et al. Dominant mutations in GRHL3 cause Van der Woude Syndrome and disrupt oral periderm development. *American journal of human genetics.* 2014;94(1):23-32.
35. Ingraham CR, Kinoshita A, Kondo S, Yang B, Sajan S, Trout KJ, et al. Abnormal skin, limb and craniofacial morphogenesis in mice deficient for interferon regulatory factor 6 (Irf6). *Nature genetics.* 2006;38(11):1335-40.
36. Thompson J, Mendoza F, Tan E, Bertol JW, Gaggar AS, Jun G, et al. A cleft lip and palate gene, Irf6, is involved in osteoblast differentiation of craniofacial bone. *Developmental dynamics : an official publication of the American Association of Anatomists.* 2019;248(3):221-32.
37. Richardson RJ, Dixon J, Jiang R, and Dixon MJ. Integration of IRF6 and Jagged2 signalling is essential for controlling palatal adhesion and fusion competence. *Human molecular genetics.* 2009;18(14):2632-42.
38. Shalom-Feuerstein R, Lena AM, Zhou H, De La Forest Divonne S, Van Bokhoven H, Candi E, et al. DeltaNp63 is an ectodermal gatekeeper of epidermal morphogenesis. *Cell death and differentiation.* 2011;18(5):887-96.

39. Fan X, Wang D, Burgmaier JE, Teng Y, Romano RA, Sinha S, et al. Single Cell and Open Chromatin Analysis Reveals Molecular Origin of Epidermal Cells of the Skin. *Developmental cell.* 2018;47(1):133.
40. De Rosa L, Antonini D, Ferone G, Russo MT, Yu PB, Han R, et al. p63 Suppresses non-epidermal lineage markers in a bone morphogenetic protein-dependent manner via repression of Smad7. *The Journal of biological chemistry.* 2009;284(44):30574-82.
41. Barton CE, Tahinci E, Barbieri CE, Johnson KN, Hanson AJ, Jernigan KK, et al. DeltaNp63 antagonizes p53 to regulate mesoderm induction in Xenopus laevis. *Developmental biology.* 2009;329(1):130-9.
42. Koster MI, Kim S, Mills AA, DeMayo FJ, and Roop DR. p63 is the molecular switch for initiation of an epithelial stratification program. *Genes & development.* 2004;18(2):126-31.
43. Truong AB, Kretz M, Ridky TW, Kimmel R, and Khavari PA. p63 regulates proliferation and differentiation of developmentally mature keratinocytes. *Genes & development.* 2006;20(22):3185-97.
44. Keyes WM, Wu Y, Vogel H, Guo X, Lowe SW, and Mills AA. p63 deficiency activates a program of cellular senescence and leads to accelerated aging. *Genes & development.* 2005;19(17):1986-99.
45. Ferone G, Mollo MR, Thomason HA, Antonini D, Zhou H, Ambrosio R, et al. p63 control of desmosome gene expression and adhesion is compromised in AEC syndrome. *Human molecular genetics.* 2013;22(3):531-43.
46. Ferone G, Mollo MR, and Missero C. Epidermal cell junctions and their regulation by p63 in health and disease. *Cell Tissue Res.* 2015;360(3):513-28.
47. Ortt K, and Sinha S. Derivation of the consensus DNA-binding sequence for p63 reveals unique requirements that are distinct from p53. *FEBS Lett.* 2006;580(18):4544-50.
48. Testoni B, Borrelli S, Tenedini E, Alotto D, Castagnoli C, Piccolo S, et al. Identification of new p63 targets in human keratinocytes. *Cell cycle.* 2006;5(23):2805-11.
49. Yu X, Singh PK, Tabrejee S, Sinha S, and Buck MJ. DeltaNp63 is a pioneer factor that binds inaccessible chromatin and elicits chromatin remodeling. *Epigenetics & chromatin.* 2021;14(1):20.
50. Qu J, Yi G, and Zhou H. p63 cooperates with CTCF to modulate chromatin architecture in skin keratinocytes. *Epigenetics & chromatin.* 2019;12(1):31.
51. Ferretti E, Li B, Zewdu R, Wells V, Hebert JM, Karner C, et al. A conserved Pbx-Wnt-p63-Irf6 regulatory module controls face morphogenesis by promoting epithelial apoptosis. *Developmental cell.* 2011;21(4):627-41.
52. Kent S, Hutchinson J, Balboni A, Decastro A, Cherukuri P, and Direnzo J. DeltaNp63alpha promotes cellular quiescence via induction and activation of Notch3. *Cell cycle.* 2011;10(18):3111-8.
53. Nguyen BC, Lefort K, Mandinova A, Antonini D, Devgan V, Della Gatta G, et al. Cross-regulation between Notch and p63 in keratinocyte commitment to differentiation. *Genes & development.* 2006;20(8):1028-42.
54. Melino G, Memmi EM, Pelicci PG, and Bernassola F. Maintaining epithelial stemness with p63. *Science signaling.* 2015;8(387):re9.
55. Suzuki D, and Senoo M. Expansion of epidermal progenitors with high p63 phosphorylation during wound healing of mouse epidermis. *Experimental dermatology.* 2013;22(5):374-6.
56. Senoo M, Pinto F, Crum CP, and McKeon F. p63 Is essential for the proliferative potential of stem cells in stratified epithelia. *Cell.* 2007;129(3):523-36.
57. Antonini D, Russo MT, De Rosa L, Gorrese M, Del Vecchio L, and Missero C. Transcriptional repression of miR-34 family contributes to p63-mediated cell cycle progression in epidermal cells. *The Journal of investigative dermatology.* 2010;130(5):1249-57.
58. Wu N, Rollin J, Masse I, Lamartine J, and Gidrol X. p63 regulates human keratinocyte proliferation via MYC-regulated gene network and differentiation commitment through cell adhesion-related gene network. *The Journal of biological chemistry.* 2012;287(8):5627-38.
59. Karimian A, Ahmadi Y, and Yousefi B. Multiple functions of p21 in cell cycle, apoptosis and transcriptional regulation after DNA damage. *DNA repair.* 2016;42:63-71.

60. McDade SS, Patel D, and McCance DJ. p63 maintains keratinocyte proliferative capacity through regulation of Skp2-p130 levels. *Journal of cell science.* 2011;124(Pt 10):1635-43.
61. Yang A, Zhu Z, Kapranov P, McKeon F, Church GM, Gingeras TR, et al. Relationships between p63 binding, DNA sequence, transcription activity, and biological function in human cells. *Molecular cell.* 2006;24(4):593-602.
62. Kurinna S, Seltmann K, Bachmann AL, Schwendimann A, Thiagarajan L, Hennig P, et al. Interaction of the NRF2 and p63 transcription factors promotes keratinocyte proliferation in the epidermis. *Nucleic acids research.* 2021;49(7):3748-63.
63. Rufini A, Weil M, McKeon F, Barlattani A, Melino G, and Candi E. p63 protein is essential for the embryonic development of vibrissae and teeth. *Biochemical and biophysical research communications.* 2006;340(3):737-41.
64. Crum CP, and McKeon FD. p63 in epithelial survival, germ cell surveillance, and neoplasia. *Annual review of pathology.* 2010;5:349-71.
65. Rizzo JM, Romano RA, Bard J, and Sinha S. RNA-seq studies reveal new insights into p63 and the transcriptomic landscape of the mouse skin. *The Journal of investigative dermatology.* 2015;135(2):629-32.
66. Marshall CB, Beeler JS, Lehmann BD, Gonzalez-Ericsson P, Sanchez V, Sanders ME, et al. Tissue-specific expression of p73 and p63 isoforms in human tissues. *Cell death & disease.* 2021;12(8):745.
67. Kurita T, Cunha GR, Robboy SJ, Mills AA, and Medina RT. Differential expression of p63 isoforms in female reproductive organs. *Mech Dev.* 2005;122(9):1043-55.
68. Lena AM, Rossi V, Osterburg S, Smirnov A, Osterburg C, Tuppi M, et al. The p63 C-terminus is essential for murine oocyte integrity. *Nature communications.* 2021;12(1):383.
69. Deutsch GB, Zielonka EM, Coutandin D, Weber TA, Schafer B, Hannewald J, et al. DNA damage in oocytes induces a switch of the quality control factor TAp63alpha from dimer to tetramer. *Cell.* 2011;144(4):566-76.
70. Beyer U, Moll-Rocek J, Moll UM, and Dobbelstein M. Endogenous retrovirus drives hitherto unknown proapoptotic p63 isoforms in the male germ line of humans and great apes. *Proceedings of the National Academy of Sciences of the United States of America.* 2011;108(9):3624-9.
71. Gressner O, Schilling T, Lorenz K, Schulze Schleithoff E, Koch A, Schulze-Bergkamen H, et al. TAp63alpha induces apoptosis by activating signaling via death receptors and mitochondria. *EMBO J.* 2005;24(13):2458-71.
72. Helton ES, Zhang J, and Chen X. The proline-rich domain in p63 is necessary for the transcriptional and apoptosis-inducing activities of TAp63. *Oncogene.* 2008;27(20):2843-50.
73. Su X, Paris M, Gi YJ, Tsai KY, Cho MS, Lin YL, et al. TAp63 prevents premature aging by promoting adult stem cell maintenance. *Cell Stem Cell.* 2009;5(1):64-75.
74. Birkaya B, Ortt K, and Sinha S. Novel in vivo targets of DeltaNp63 in keratinocytes identified by a modified chromatin immunoprecipitation approach. *BMC Mol Biol.* 2007;8:43.
75. Medawar A, Virolle T, Rostagno P, de la Forest-Divonne S, Gambaro K, Rouleau M, et al. DeltaNp63 is essential for epidermal commitment of embryonic stem cells. *PloS one.* 2008;3(10):e3441.
76. Romano RA, Ortt K, Birkaya B, Smalley K, and Sinha S. An active role of the DeltaN isoform of p63 in regulating basal keratin genes K5 and K14 and directing epidermal cell fate. *PloS one.* 2009;4(5):e5623.
77. Romano RA, Birkaya B, and Sinha S. Defining the regulatory elements in the proximal promoter of DeltaNp63 in keratinocytes: Potential roles for Sp1/Sp3, NF-Y, and p63. *The Journal of investigative dermatology.* 2006;126(7):1469-79.
78. Romano RA, Smalley K, Magraw C, Serna VA, Kurita T, Raghavan S, et al. DeltaNp63 knockout mice reveal its indispensable role as a master regulator of epithelial development and differentiation. *Development.* 2012;139(4):772-82.
79. Vigano MA, Lamartine J, Testoni B, Merico D, Alotto D, Castagnoli C, et al. New p63 targets in keratinocytes identified by a genome-wide approach. *EMBO J.* 2006;25(21):5105-16.

80. Koster MI, Dai D, Marinari B, Sano Y, Costanzo A, Karin M, et al. p63 induces key target genes required for epidermal morphogenesis. *Proceedings of the National Academy of Sciences of the United States of America.* 2007;104(9):3255-60.
81. Carroll DK, Carroll JS, Leong CO, Cheng F, Brown M, Mills AA, et al. p63 regulates an adhesion programme and cell survival in epithelial cells. *Nat Cell Biol.* 2006;8(6):551-61.
82. Cheng CC, Wang DY, Kao MH, and Chen JK. The growth-promoting effect of KGF on limbal epithelial cells is mediated by upregulation of DeltaNp63alpha through the p38 pathway. *Journal of cell science.* 2009;122(Pt 24):4473-80.
83. Hau PM, Yip YL, Huen MS, and Tsao SW. Loss of DeltaNp63alpha promotes mitotic exit in epithelial cells. *FEBS Lett.* 2011;585(17):2720-6.
84. Kim CA, and Bowie JU. SAM domains: uniform structure, diversity of function. *Trends in biochemical sciences.* 2003;28(12):625-8.
85. Qiao F, and Bowie JU. The many faces of SAM. *Sci STKE.* 2005;2005(286):re7.
86. Suzuki D, Sahu R, Leu NA, and Senoo M. The carboxy-terminus of p63 links cell cycle control and the proliferative potential of epidermal progenitor cells. *Development.* 2015;142(2):282-90.
87. Rinne T, Brunner HG, and van Bokhoven H. p63-associated disorders. *Cell cycle.* 2007;6(3):262-8.
88. van Bokhoven H, Hamel BC, Bamshad M, Sangiorgi E, Gurrieri F, Duijf PH, et al. p63 Gene mutations in eec syndrome, limb-mammary syndrome, and isolated split hand-split foot malformation suggest a genotype-phenotype correlation. *American journal of human genetics.* 2001;69(3):481-92.
89. Maillard A, Alby C, Gabison E, Doan S, Caux F, Bodemer C, et al. P63-related disorders: Dermatological characteristics in 22 patients. *Experimental dermatology.* 2019;28(10):1190-5.
90. Clements SE, Techanukul T, Coman D, Mellerio JE, and McGrath JA. Molecular basis of EEC (ectrodactyly, ectodermal dysplasia, clefting) syndrome: five new mutations in the DNA-binding domain of the TP63 gene and genotype-phenotype correlation. *The British journal of dermatology.* 2010;162(1):201-7.
91. Qu J, Tanis SEJ, Smits JPH, Kouwenhoven EN, Oti M, van den Bogaard EH, et al. Mutant p63 Affects Epidermal Cell Identity through Rewiring the Enhancer Landscape. *Cell Rep.* 2018;25(12):3490-503 e4.
92. Vacic V, Markwick PR, Oldfield CJ, Zhao X, Haynes C, Uversky VN, et al. Disease-associated mutations disrupt functionally important regions of intrinsic protein disorder. *PLoS computational biology.* 2012;8(10):e1002709.
93. Celli J, Duijf P, Hamel BC, Bamshad M, Kramer B, Smits AP, et al. Heterozygous germline mutations in the p53 homolog p63 are the cause of EEC syndrome. *Cell.* 1999;99(2):143-53.
94. McGrath JA, Duijf PH, Doetsch V, Irvine AD, de Waal R, Vanmolkot KR, et al. Hay-Wells syndrome is caused by heterozygous missense mutations in the SAM domain of p63. *Human molecular genetics.* 2001;10(3):221-9.
95. Browne G, Cipollone R, Lena AM, Serra V, Zhou H, van Bokhoven H, et al. Differential altered stability and transcriptional activity of DeltaNp63 mutants in distinct ectodermal dysplasias. *Journal of cell science.* 2011;124(Pt 13):2200-7.
96. Dianzani I, Garelli E, Gustavsson P, Carando A, Gustafsson B, Dahl N, et al. Rapp-Hodgkin and AEC syndromes due to a new frameshift mutation in the TP63 gene. *J Med Genet.* 2003;40(12):e133.
97. Kantaputra PN, Hamada T, Kumchai T, and McGrath JA. Heterozygous mutation in the SAM domain of p63 underlies Rapp-Hodgkin ectodermal dysplasia. *J Dent Res.* 2003;82(6):433-7.
98. Rinne T, Bolat E, Meijer R, Scheffer H, and van Bokhoven H. Spectrum of p63 mutations in a selected patient cohort affected with ankyloblepharon-ectodermal defects-cleft lip/palate syndrome (AEC). *Am J Med Genet A.* 2009;149A(9):1948-51.
99. Koster MI, Marinari B, Payne AS, Kantaputra PN, Costanzo A, and Roop DR. DeltaNp63 knockdown mice: A mouse model for AEC syndrome. *Am J Med Genet A.* 2009;149A(9):1942-7.

100. Russo C, Osterburg C, Sirico A, Antonini D, Ambrosio R, Wurz JM, et al. Protein aggregation of the p63 transcription factor underlies severe skin fragility in AEC syndrome. *Proceedings of the National Academy of Sciences of the United States of America.* 2018;115(5):E906-E15.
101. Chen Y, Mistry DS, and Sen GL. Highly rapid and efficient conversion of human fibroblasts to keratinocyte-like cells. *J Invest Dermatol.* 2014;134(2):335-44.
102. Thomason HA, Dixon MJ, and Dixon J. Facial clefting in Tp63 deficient mice results from altered Bmp4, Fgf8 and Shh signaling. *Developmental biology.* 2008;321(1):273-82.
103. Taya Y, O'Kane S, and Ferguson MW. Pathogenesis of cleft palate in TGF-beta3 knockout mice. *Development.* 1999;126(17):3869-79.
104. Wurst W, Auerbach AB, and Joyner AL. Multiple developmental defects in Engrailed-1 mutant mice: an early mid-hindbrain deletion and patterning defects in forelimbs and sternum. *Development.* 1994;120(7):2065-75.
105. Riddle RD, Ensini M, Nelson C, Tsuchida T, Jessell TM, and Tabin C. Induction of the LIM homeobox gene Lmx1 by WNT7a establishes dorsoventral pattern in the vertebrate limb. *Cell.* 1995;83(4):631-40.
106. Wolff S, Talos F, Palacios G, Beyer U, Dobbelstein M, and Moll UM. The alpha/beta carboxy-terminal domains of p63 are required for skin and limb development. New insights from the Brdm2 mouse which is not a complete p63 knockout but expresses p63 gamma-like proteins. *Cell death and differentiation.* 2009;16(8):1108-17.
107. Huelsken J, Vogel R, Erdmann B, Cotsarelis G, and Birchmeier W. beta-Catenin controls hair follicle morphogenesis and stem cell differentiation in the skin. *Cell.* 2001;105(4):533-45.
108. Lin-Shiao E, Lan Y, Welzenbach J, Alexander KA, Zhang Z, Knapp M, et al. p63 establishes epithelial enhancers at critical craniofacial development genes. *Sci Adv.* 2019;5(5):eaaw0946.
109. Cao J, Spielmann M, Qiu X, Huang X, Ibrahim DM, Hill AJ, et al. The single-cell transcriptional landscape of mammalian organogenesis. *Nature.* 2019;566(7745):496-502.
110. Loomis CA, Harris E, Michaud J, Wurst W, Hanks M, and Joyner AL. The mouse Engrailed-1 gene and ventral limb patterning. *Nature.* 1996;382(6589):360-3.
111. Huettl RE, Luxenhofer G, Bianchi E, Haupt C, Joshi R, Prochiantz A, et al. Engrailed 1 mediates correct formation of limb innervation through two distinct mechanisms. *PloS one.* 2015;10(2):e0118505.
112. Cygan JA, Johnson RL, and McMahon AP. Novel regulatory interactions revealed by studies of murine limb pattern in Wnt-7a and En-1 mutants. *Development.* 1997;124(24):5021-32.
113. Adamska M, MacDonald BT, Sarmast ZH, Oliver ER, and Meisler MH. En1 and Wnt7a interact with Dkk1 during limb development in the mouse. *Developmental biology.* 2004;272(1):134-44.
114. Satoh W, Gotoh T, Tsunematsu Y, Aizawa S, and Shimono A. Sfrp1 and Sfrp2 regulate anteroposterior axis elongation and somite segmentation during mouse embryogenesis. *Development.* 2006;133(6):989-99.
115. Bardhan A, Bruckner-Tuderman L, Chapple ILC, Fine JD, Harper N, Has C, et al. Epidermolysis bullosa. *Nature reviews Disease primers.* 2020;6(1):78.
116. Aberdam D, Galliano MF, Vailly J, Pulkkinen L, Bonifas J, Christiano AM, et al. Herlitz's junctional epidermolysis bullosa is linked to mutations in the gene (LAMC2) for the gamma 2 subunit of nicein/kalinin (LAMININ-5). *Nature genetics.* 1994;6(3):299-304.
117. Ablinger M, Lettner T, Friedl N, Potocki H, Palmetzhofer T, Koller U, et al. Personalized Development of Antisense Oligonucleotides for Exon Skipping Restores Type XVII Collagen Expression in Junctional Epidermolysis Bullosa. *International journal of molecular sciences.* 2021;22(7).
118. Miyazaki K, Kikkawa Y, Nakamura A, Yasumitsu H, and Umeda M. A large cell-adhesive scatter factor secreted by human gastric carcinoma cells. *Proceedings of the National Academy of Sciences of the United States of America.* 1993;90(24):11767-71.
119. McLean WH, Irvine AD, Hamill KJ, Whittock NV, Coleman-Campbell CM, Mellerio JE, et al. An unusual N-terminal deletion of the laminin alpha3a isoform leads to the chronic

granulation tissue disorder laryngo-onycho-cutaneous syndrome. *Human molecular genetics.* 2003;12(18):2395-409.
120. Kariya Y, Yasuda C, Nakashima Y, Ishida K, Tsubota Y, and Miyazaki K. Characterization of laminin 5B and NH2-terminal proteolytic fragment of its alpha3B chain: promotion of cellular adhesion, migration, and proliferation. *The Journal of biological chemistry.* 2004;279(23):24774-84.
121. Koster J, Geerts D, Favre B, Borradori L, and Sonnenberg A. Analysis of the interactions between BP180, BP230, plectin and the integrin alpha6beta4 important for hemidesmosome assembly. *Journal of cell science.* 2003;116(Pt 2):387-99.
122. Gatalica B, Pulkkinen L, Li K, Kuokkanen K, Ryynanen M, McGrath JA, et al. Cloning of the human type XVII collagen gene (COL17A1), and detection of novel mutations in generalized atrophic benign epidermolysis bullosa. *American journal of human genetics.* 1997;60(2):352-65.
123. Kashgari G, Meinecke L, Gordon W, Ruiz B, Yang J, Ma AL, et al. Epithelial Migration and Non-adhesive Periderm Are Required for Digit Separation during Mammalian Development. *Developmental cell.* 2020;52(6):764-78 e4.
124. Kashgari G, Venkatesh S, Refuerzo S, Pham B, Bayat A, Klein RH, et al. GRHL3 activates FSCN1 to relax cell-cell adhesions between migrating keratinocytes during wound reepithelialization. *JCI insight.* 2021;6(17).
125. Vo AH, Swaggart KA, Woo A, Gao QQ, Demonbreun AR, Fallon KS, et al. Dusp6 is a genetic modifier of growth through enhanced ERK activity. *Human molecular genetics.* 2019;28(2):279-89.
126. Hanks MC, Loomis CA, Harris E, Tong CX, Anson-Cartwright L, Auerbach A, et al. Drosophila engrailed can substitute for mouse Engrailed1 function in mid-hindbrain, but not limb development. *Development.* 1998;125(22):4521-30.
127. Allou L, Balzano S, Magg A, Quinodoz M, Royer-Bertrand B, Schopflin R, et al. Non-coding deletions identify Maenli lncRNA as a limb-specific En1 regulator. *Nature.* 2021;592(7852):93-8.